Design of a Cardiovascular Blood Flow Simulator and Utilization in Hemodynamic Evaluation of Mechanical Circulatory Support Devices

Mohammad Amin Rezaienia
School of Engineering and Material Sciences
Queen Mary University of London

Supervisor: Professor Theodosios Korakianitis
(a.k.a. Theodosios Alexander)

A thesis submitted in conformity with the requirements
for the degree of Doctor of Philosophy
University of London

Abstract

Increasing numbers of old and sick patients who are no longer eligible for prolonged invasive implantation surgery have encouraged many researchers to investigate the development of a Mechanical Circulatory Support (MCS) device with more reliability and less possible invasive complications, which would benefit the majority of patients. This thesis will test experimentally and numerically the feasibility of installing an MCS device, as a bridge to destination, in the descending aorta, in a series configuration with the heart. To this end, a multi-chamber Simulator of the Cardio-Vascular blood-flow Loop (SCVL) was designed to simulate the in-vitro flow rates, pressures and other parameters representing normal and diseased conditions of the human cardiovascular system. The multi-chamber SCVL includes models for all four chambers of the heart, and the systemic as well as the pulmonic circulations. Next, a comprehensive study was conducted using the SCVL system to compare the novel in-series placement of the pump, in the descending aorta, with traditional in-parallel placements. Then, a comprehensive numerical study was conducted using the modified Concentrated Lumped Parameter (CLP) model developed by the same team. The numerical results are compared and verified by the experimental results under various conditions. The results for the pump installed in the descending aorta show that the pressure drop, upstream of the pump, facilitates the cardiac output as a result of after-load reduction. However, at the same time the generated pressure drop at the proximal part of the descending aorta induces a slight drop in the carotid perfusion which will be autoregulated by the brain in a native system. Further, the pressure rise downstream of the pump improves the blood perfusion in the renal artery. The pulse wave analysis show that the placement of the pump in the descending aorta leads to improved pulsatility which is beneficial for end-organ functionality in the native cardiovascular system.

Acknowledgements

First and foremost I thank my parents; Mr. Khosrow Rezaienia and Mrs. Jaleh Rahmati for their constant love, efforts and guidance. I also thank my uncles, Mr.Parviz Rezainia, Mr.Shahryar Rahmati and their families for their continuous support, care and love during my stay in the UK. I thank my supervisor, Professor Theodosios Alexander, Sc.D. (aka T. Korakianitis) for his instruction and understanding during this project. I thank my colleagues Dr.Akbar Rahideh and Dr. Paula Ruiz without their support and guidance I would not have been able to finish the project. I thank many people in the QMUL support staff; in particular Mr. Dennis Ife for their expertise, professionalism and patience. Finally, I thank all my friends and colleagues I have made over the course of this work for the useful discussions. Special thanks go to Miss Ghazal Hosseini, Miss Ann Louise Anderson, Mr. Sahand Mozaffari and Dr. Shahid Imran for helping me with the edition of my thesis.

Dedications

I would like to dedicate this thesis to my loving parents.

Nomenclature

Subscripts

ac	atrium compression
af	atrium filling
ao	aortic
arao	aortic arch artery
asc	ascending
ca	carotid
cereb	cerebral system
des	descending
dia	diastolic
f	frictional action
kid	kidneys
la	left atrium
lol	lower limb
lv	left ventricle
lv_0	initial left ventricle
mc	mean circulatory
mean	mean
mi	mitral
p	effect of pressure force
pas	pulmonary artery sinus
pat	pulmonary arteries
par	pulmonary arteriole
pcp	pulmonary capillary
pvn	pulmonary vein
po	pulmonary
ra	right atrium
ren	renal artery
rv	right ventricle
rv_0	initial right ventricle
s	systemic

sas	systemic artery sinus
sar	systemic arteriole
sat	systemic arteries
scp	systemic capillary
ivn	inferior vena cava
svn	superior vena cava
sys	systolic
ti	tricuspid
vc	ventricular compression
vf	ventricular filling

Greek

μ	first viscosity coefficient
ρ	density

Abbreviations

AoP	aortic pressure
Ax	axial rotary pump
bpm	beats per minute
BLDC	brushless direct current motor
C	compliance
CaP	carotid pressure
Ce	centrifugal rotary pump
CHF	congestive heart failure
CVD	cardiovascular disease
CO	cardiac output
D	displacement
DA	descending aorta
EDP	end-diastolic pressure
ESP	end systolic pressure
EDP	end diastolic pressure
F	flow-meter
He	helical rotary pump
Hyd	hydrolic bearing
HR	heart rate

L	intertance
LA	left atrium
LAP	left atrium pressure
LM	linear motor
LOS	low output syndrome
LV	left ventricle
LVAD	left ventricular assist device
LVP	left ventricular pressure
LVV	left ventricular volume
Ma	magnetic bearing
MCS	mechanical circulatory support
Me	mechanical bearing
PaP	pulmonary artery pressure
PM	permanent magnet
POP	pump operation point
PT	pressure transducer
PV	pressure-volume
Q	flow-rate
QI	flow index
R	resistance
RA	right atrium
RaP	radial aortic pressure
RAP	right atrium pressure
rpm	revolution per minute
RV	right ventricle
RVP	right ventricular pressure
RVV	right ventricular volume

Contents

List of Figures

List of Tables

Chapter 1

Introduction

Cardiovascular System Physiology

As shown in Figure 1.1, the human cardiovascular system consists of the following components: heart, systemic circulation and pulmonary circulation.

1.1 The Heart

The heart is the main component of the cardiovascular system. Its key role is to pump the oxygenated blood into the systemic circulation and de-oxygenated blood into the pulmonary circulation. The heart in the human body has a cone-shape and it is divided into left and right sections each representing an individual pump. Both left and right sections are further separated through a common wall and a valve into two sections. The upper sections are called the atria and the lower sections are called the ventricles. The right atrium and the left atrium are acting as active conduits of ventricles whereas the right ventricle and the left ventricle are acting as the major pumping activators. As shown in Figure 1.2, the right atrium is located in the top right part of the heart and receives de-oxygenated blood from the superior vena cava, inferior vena cava and coronary veins. The

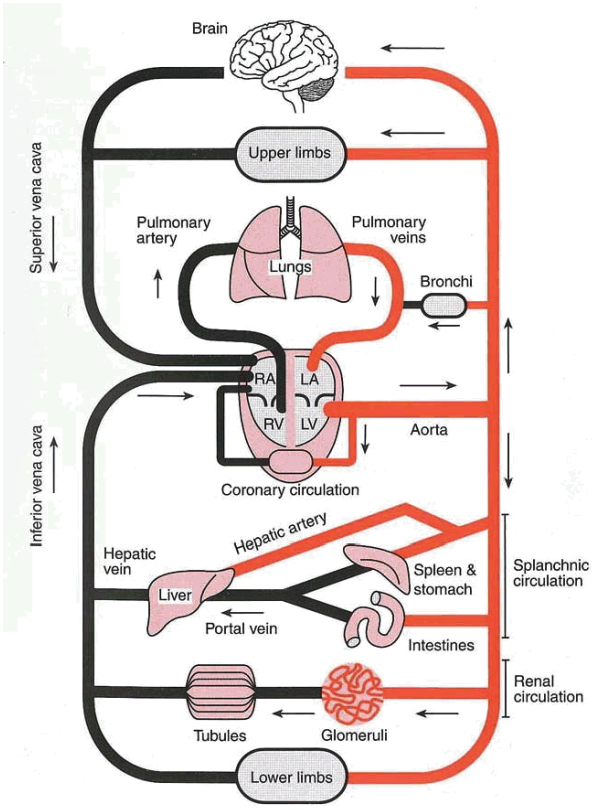

Figure 1.1: Schematic diagram of cardiovascular system. *From: R.J. Levick [1]. An Introduction to Cardiovascular Physiology, 2003.*

right atrium is provided with a very thin wall and it is highly distensible, so it can accommodate a substantial level of de-oxygenated blood from the entire cardiovascular system.

The right atrium chamber is connected to the right ventricle chamber through the tricuspid valve. The right ventricle in contrast to the right atrium has a thick wall which is around 0.5 cm in thickness. The de-oxygenated blood from the right ventricle is pumped into the pulmonary loop through the pulmonary valve for a refinement process inside the lungs. Fresh oxygenated blood enters the left atrium and then through the mitral valve is directed into the left ventricle. Due to the high level of resistance in the systemic circulation, the left ventricle is required to provide a higher level of energy to expel the oxygenated blood into

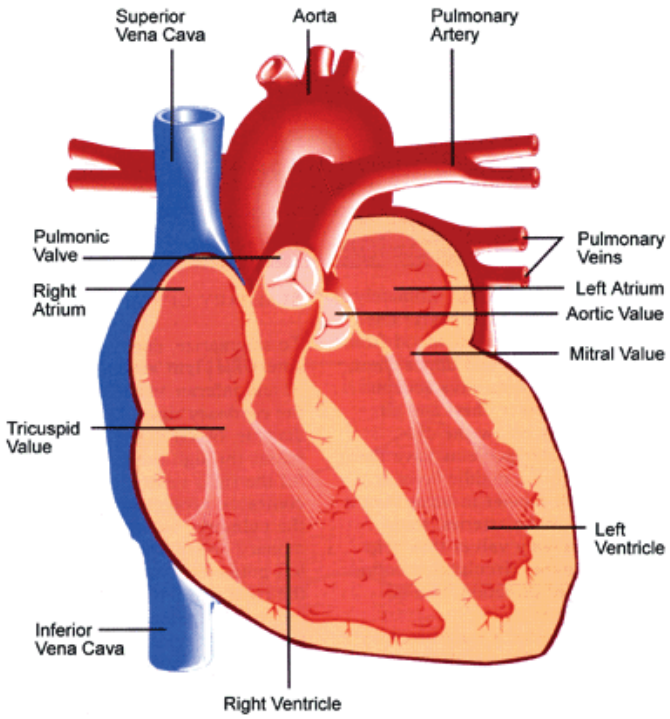

Figure 1.2: Structure of human's heart. *From: R.J. Levick [1]. An Introduction to Cardiovascular Physiology, 2003.*

the systemic circulation. As a result, the left ventricle is provided a wall that is about three times thicker than the right ventricle, as shown in Figure 1.2. The pressure generated during the systolic phase in the left ventricle (120 mmHg) is about 5-7 times higher than that of the right ventricle (15-20 mmHg). The oxygenated blood from the left ventricle is pumped into the systemic circulation and the coronary branches through the aortic valve.

The expansion (diastolic phase) and contraction (systolic phase) of the atrium and ventricular chambers in the alternating phases of filling and ejection are regarded as the cardiac cycle. In one cardiac cycle, both ventricles work in a series configuration. As a result, the same amount of blood passes through both of the ventricles unless there is a leakage through the ventricle or atrium chambers. Each cardiac cycle, for an average human in resting condition, lasts

approximately 0.9 sec which is equivalent to 67 beats per minute (bpm). Each cardiac cycle is divided into four phases:

- Filling phases (Diastole)
- Isovolumetric contraction phase
- Pumping phase (Systole)
- Isovolumetric relaxation phase

1.1.1 Filling Phase (Diastole)

The filling phase in a resting condition lasts about 0.5 sec and is subdivided into passive and active phases. During the passive phase, the tricuspid and the mitral valves are open, whereas the pulmonary and the aortic valves are closed. During the passive phase, the blood through the tricuspid and the mitral valves is directed into the right and left ventricles respectively. During the active phase, the atriums are contracted. The artruim contraction contributes about 20% of the filling phase and is reflected as a small bump just before the ascending limb of the left ventricle and the right ventricle pressure waveform. Figure 1.3 presents the left ventricular pressure waveform in a clinical setting for an adult human in a resting condition [2]. Left ventricular end-diastolic pressure (LVP_{dia}) and right ventricular end-diastolic pressure (RVP_{dia}) are measured upon the closure of the mitral and the tricuspid valves respectively. Left ventricular end-diastolic volume (LVV_{dia}) and right ventricular end-diastolic pressure (RVV_{dia}) are measured when ventricles reach their maximum volumes at the end of the filling phase.

1.1.2 Isovolumetric Contraction Phase

The isovolumetric contraction phase follows the atrium contraction phase. When the pressure in the ventricles is above the atrium internal pressure, the tricuspid and the mitral valves are closed to avoid any backflow into the atriums. At

this stage, due to the existing high tension in the ventricles, the pressure in the ventricles starts rising, whereas the volume remains constant for a few seconds. The maximum pressure in the left and right ventricles before the beginning of the ejection phase are called the left ventricular end-systolic pressure (LVP_{sys}) and the right ventricular end-systolic pressure (RVP_{sys}).

1.1.3 Pumping Phase (Systole)

The pumping phase triggers when the internal pressures of the right ventricle and the left ventricle exceed the pulmonary and the aortic pressures respectively. At this point, both the pulmonary and the aortic valves are forced to open leading to trigger the ejection phase. Upon the ejection, the internal right ventricle and left ventricle pressures begin to drop and become lower than the pulmonary and the aortic artery pressures respectively. However, due to the high energy level of the ejected flow, the aortic and pulmonary valves are not closed instantly. By increasing the adverse pressure, the flow momentum begins to fall causing retrograde flow into the ventricles and ultimately the closure of the aortic and pulmonary valves.

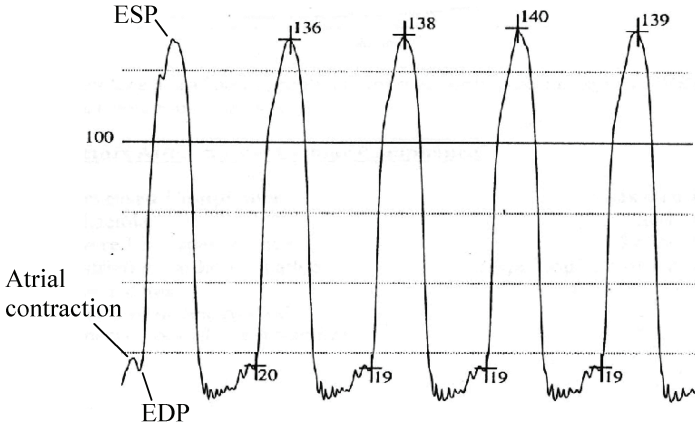

Figure 1.3: Clinical LVP waveform in controlled condition, *From: E. I. Cabrera Fischer et al. [2]. Endothelium-dependent arterial wall tone elasticity modulated by blood viscosity, 2002.*

1.1.4 Isovolumetric Relaxation Phase

The isovolumetric relaxation phase occurs after the ejection phase. During this phase all four valves are closed and the pressure falls down sharply due to the elastic recoil of the heart chambers. This continues until the pressure in the ventricles becomes lower than the pressure in the atriums. At this point, the new cardiac cycle begins again by opening the mitral and the tricuspid valves refilling the atriums.

1.1.5 Frank-Starling Law

The Frank-Starling law states that the contactile energy of an intact heart is proportional to the pre load pressure in the ventricle chambers. It is shown in Figure 1.4, for an intact heart, whereby an increase in Central Venous Pressure (CVP) or Right Atrial Pressure (RAP) results in a higher level of stroke volume. This can be explained as follows, an increase in the CVP leads to a subsequent rise in the left ventricular pressure, causing an increase in the distension of the left ventricle myocardial cell. Starling demonstrated that the contractile energy of the myocardial cell is proportional to the initial length of the myocardial cell [3]. Therefore, any variation occurring in the CVP level results in different levels of Cardiac Output (CO) and Stroke Volume (SV).

1.2 Systemic and Pulmonary Circulation

As shown in Figure 1.1, the objective of the systemic circulation is to distribute the oxygenated blood from the heart to the whole human body and collect the de-oxygenated blood from the body and send it back to the heart. The systemic circulation starts from the left ventricle chamber and it continues to the ascending aorta until it reaches the aortic arch. The aortic arch splits into the upper arteries and lower arteries. The upper arteries are divided further into arteriole and capillaries branching toward the cerebral system as well as the arms. The

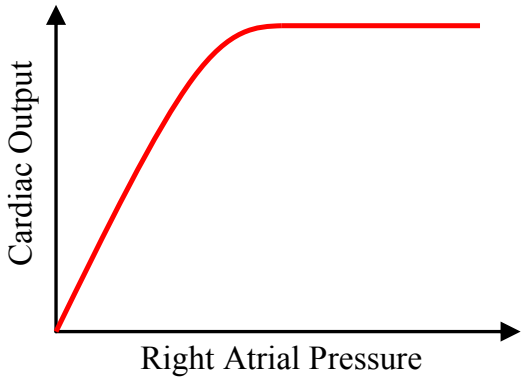

Figure 1.4: Cardiac output against right atrial pressure representing the Frank-Starling law.

lower arteries are divided further into arterioles and capillaries branching toward abdominal organs such as the kidneys, liver and the legs. The pulmonary circulation starts from the right ventricle where de-oxygenated blood is sent through the pulmonary valve to the pulmonary system for blood refinement. Next, the oxygenated blood from the pulmonary system is sent back to the left atrium.

Both the systemic and the pulmonary circulation systems consist of various types of vessels with variable characteristics. In the systemic loop, the sinus aortic artery is connected directly to the left ventricle and its task is to transfer the oxygenated blood from the heart to the coronary arteries and the ascending aortic artery. The sinus artery is more distensive and less resistive than the other arteries. As proximal arteries, including the sinus aorta and the ascending aorta, progress distally away from the heart, they branch into smaller vessels called arterioles. Arterioles are less distensive and more resistive. The arterioles are subdivided into very small and narrow vessels called capillaries. The capillary's task is to transfer the oxygenated blood into vital cells and collect the de oxygenated blood from them. Capillaries are highly resistive and the blood flow in them is much slower than the arterioles. Slow blood flow makes substance exchange with cells more efficient. Capillaries are eventually connected together

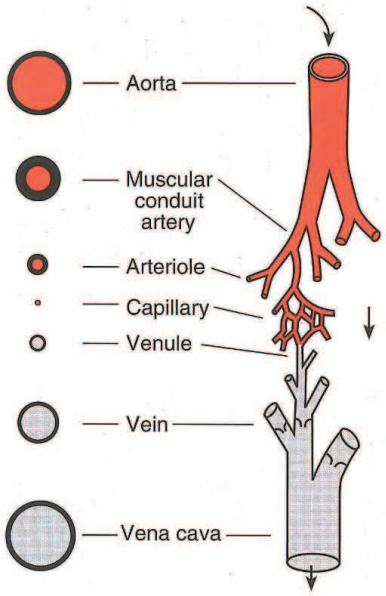

Figure 1.5: Different types of blood vessel branches present in a native cardiovascular system. *From: R.J. Levick [1]. An Introduction to Cardiovascular Physiology, 2003.*

and create venules. As venules progress toward the heart, they turn into highly distensive veins. Vein vessels from the abdominal part and upper part of the body converge together and make the inferior vena cava and the superior vena cava respectively. Figure 1.5 shows the schematic representation of different types of blood vessel branches present in a native cardiovascular system. There are two characteristics in vessels that can considerably influence the hemodynamic behavior of the blood:

- **Compliance**
- **Resistance**

1.2.1 Compliance

As indicated in Equation 1.1, arterial compliance is proportional to the change in blood volume and inversely proportional to the change in arterial pressure.

$$\text{Arterial compliance (C)} = \frac{\text{Change in blood volume } (\Delta V)}{\text{Change in arterial pressure } (\Delta P)} \tag{1.1}$$

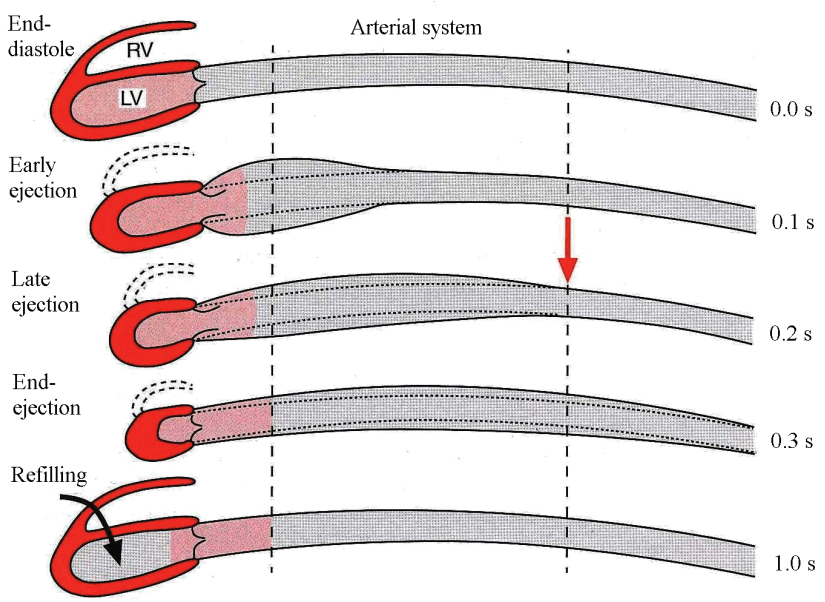

Figure 1.6: Change in the aortic sinus artery during the cardiac cycle of one second. *From: R.J. Levick [1]. An Introduction to Cardiovascular Physiology, 2003.*

Compliance is not a fixed parameter throughout the cardiovascular system. Larger arteries adjacent to the heart are very compliant in size compared to distal arterioles and capillaries. In a native cardiovascular system, the largest arteries like the aorta and the iliac have very distensible walls since they are rich in Elastin. Elastin is an extracellular protein that is six times more extensible than rubber. The aortic artery and the iliac are able to expand by 10% during systolic phase and hence accommodate nearly 70 to 80% of the cardiac output. During diastolic phase elastic vessels shrink back (contraction, recoil) to the normal size and expel the remaining blood to the peripheral system. As

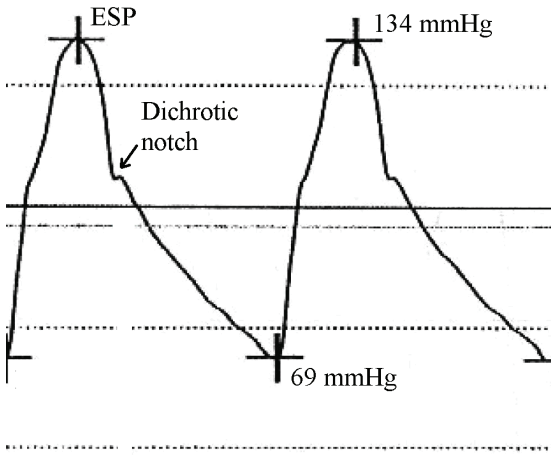

Figure 1.7: Clinical aortic pressure (AoP) waveform.*From: E. I. Cabrera Fischer et al. [2]. Endothelium-dependent arterial wall tone elasticity modulated by blood viscosity, 2002.*

a result of distensibility of native vessels the on-off cardiac output is converted to the continuous pulsatile flow. Vasculature compliance is not a constant value and is varying through out the cardiovascular systems. Besides, the other factors discussed earlier such as the age and the pathological condition have significant effect on vasculature compliance in a native system [1]. During the diastolic phase, elastically expanded vessels recoil to the normal size leading to the ejection of the rest of the accommodated blood into the peripheral resistances. Figure 1.7 shows the clinical aortic pressure waveform of an average human in resting condition [2]. The difference between the gradient of the aortic pressure waveform of the ascending and the descending limbs is evident. A slight oscillation on the descending limb of the aortic pressure is due to the slight back-flow into the left ventricle occurring at the onset of the diastolic phase which is regarded as dicrotic notch (incisura).

As the blood travels distally away from the proximal arteries toward the peripheral system, the arterial compliance decreases considerably. A decrease in compliance level of arterioles and capillaries result in a sharp rise in pressure gradient during the diastolic phase. Figure 1.8 compares the simultaneous clinical radial artery prssure and the sinus aortic artery pressure waveform at resting condition. It is shown that radial pressure has a sharper gradient during the

systolic and diastolic phase compared to the sinus aortic pressure. As shown in Figure 1.8, the end systolic radial pressure (RaP_{sys}) is higher than the AoP_{sys} , whereas the end diastolic radial pressure (RaP_{dia}) is slightly lower than the AoP_{dia}.

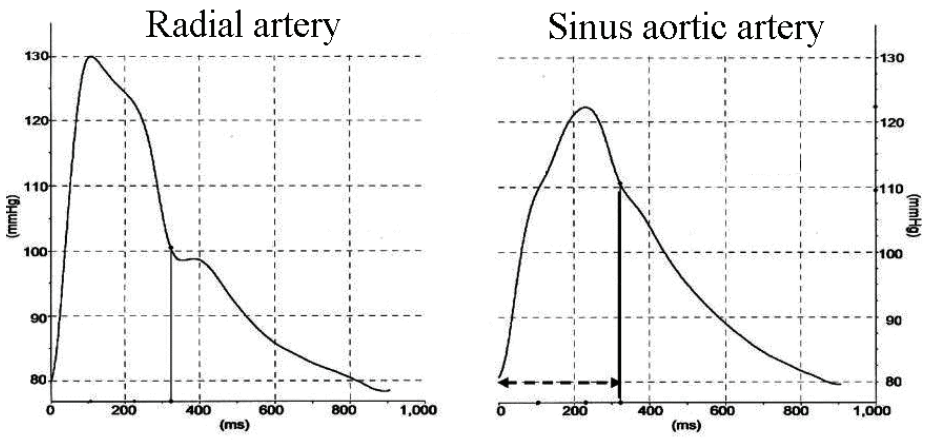

Figure 1.8: Clinical radial pressure (left panel) and sinus aortic pressure (right panel) waveform in controlled condition. *From: S. J. Denardo, et al. [4]. Pulse wave analysis of the aortic pressure waveform in severe left ventricular systolic dysfunction, 2010.*

Another factor is the patient's age. Arterial compliance declines with advancing age. In elderly people, due to the physiological change in the body, the wall vessels become stiffer which subsequently increases the heart work. Also, arterial compliance changes with various pathological conditions.

1.2.2 Resistance

Vessels in a native cardiovascular system resemble a tube with a circular cross section. According to Poiseuille's law [1], the resistance in a tube is directly proportional to L and inversely proportional to r^4, where L and r are the length and the radius of the tube, respectively. Also, in Equation 1.2, η represents the

viscosity of the working liquid.

$$\text{Resistance} = \frac{8\eta \mathrm{L}}{\pi \mathrm{r}^4} \tag{1.2}$$

Proximal arteries adjacent to the heart are highly dominated by the compliance and they are less resistive than the other arteries. As the blood travels distally away from the proximal arteries toward the arterioles, capillaries and terminal arteries, the size of the arteries become significantly smaller. This leads to a considerable rise in vascular resistance. In the capillaries, an increase in the resistance leads to a rise in the pressure gradient and subsequently a fall in the blood flow. As a result, the blood flow in the capillaries is more continuous compared to the proximal arteries.

In addition, the resistance level in the native cardiovascular system is outo-regulated and it changes under various physiological and pathological conditions. So, when the resistance level, in any local vessel, is increased (vasoconstriction), the blood perfusion drops down and, in contrast when the resistance level is decreased (vasodilation), the blood perfusion rises up.

1.3 Cardio-Vascular Disease

Cardio-Vascular Diseases (CVD) including coronary heart disease, cerebro-vascular disease, high blood pressure, peripheral artery disease, rheumatic heart disease, congenital heart disease and heart failure lead to the highest rate of death in the western countries. Approximately about 17.3 million people died from CVD in 2005, representing 30% of all global deaths [5]. Approximately 10 million in Europe and five million people in America are suffering from end-stage heart failure [6]. Cardiogenic shock and acute myocardial infarction are the most pronounced forms of heart failure conditions occurring in 4-7% of patients [7].

1.3.1 Congenital Heart Disease

Congenital heart disease occurs when the heart of an infant is not developed thoroughly during pregnancy. This can result in various complications. For instance, in some rare cases just one single ventricle might be developed, which pumps the blood simultaneously into the systemic and the pulmonary system in an abnormal pattern. This abnormality can be detected at different stages. In some cases, congenital heart defects can be diagnosed before child birth. In other cases the disease is diagnosed a couple of years after birth. In fortunate cases, the heart can be remodeled through a surgery and the heart can gain its normal functionality. In cases with small defects, the heart might gain the functionality in a natural process. There is a substantial number of patients suffering from congenital heart defects who are normally aided with pediatric cardiac assist devices.

1.3.2 Valve Abnormality

Valve disease occurs when one or more heart valves are not operating efficiently. Valve abnormality can be divided into two categories; valve stenosis where the valve is not opening appropriately and may result in high resistance and valve regurgitant where the valve closure incompetence results in a back flow into the heart. The main treatment for valve abnormality disease is to replace the impaired valve with an artificial valve. The two main types of artificial heart valves are mechanical and biological valves. Mechanical valves are stronger and more fault tolerant than biological valves but at the same time they cause some unwanted impulses due to their inflexible structure. Biological valves normally consist of two or three leaflets made of animal tissues and they are more expensive than mechanical valves.

1.3.3 Coronary Disease

Coronary disease occurs when the coronary arteries are obstructed by a blood clot or fatty substances. As a result the myocardium cells suffer from the shortage of oxygenated blood, which in the long term leads to a gradual depression of cardiac function. There are various approaches to treat coronary disease including atherectomy (grinding the plaque), angioplasty (short balloon inflation in the arteries) or bypass surgery.

1.3.4 Cardiomyopathy Disease

Cardiomyopathy disease occurs when the myocardium cell becomes too weak to eject the blood out. The main cause of cardiomyopathy is not known (idiopathic). However, it has been shown that the alcohol or drug abuse can deteriorate the condition [5]. Cardiomyopathy can be divided further into three categories:

- A **dilated condition** where the heart wall becomes thin causing further deterioration of ejection power.
- A **stiff condition** where the heart wall becomes too thick and the chamber volume becomes smaller causing deterioration of the compliant characteristics.
- A **hyperterophic condition** where the myocardium becomes thick thereby causing alternation of blood into the myocardium cells.

1.3.5 Low Output Syndrome

Low Output Syndrome (LOS) is considered as a post-operative complication where the heart temporarily loses its normal cardiac function. The LOS is most often attributed to open heart surgery shock and can be fixed by using an assistant blood pump to take over part of the cardiac output temporarily. Centrifugal

pumps and in some complex cases pulsatile pumps are being used as assistant devices during the LOS state. Normally, in three days time the patient will recover and be weaned from the assistant blood pump.

1.3.6 Congestive Heart Failure

Congestive heart failure (CHF) as a result of different heart diseases is one of the leading cause of death in men and women alike. Patients with severe heart failure are breathless at rest and treatment is palliative. More than seven million people in both continents of North America and Europe are diagnosed with heart failure condition, among whom nearly 6% are categorized as CHF stage IV [8]. In Germany less than 2% of the population are diagnosed with the sever heart failure with almost 80,000 new cases annually [9].

The heart consists of two separate sides, each activating as an individual pump. Thereby, the specific heart failure is associated with either the right or the left side. CHF condition can be identified whereby the left or the right side of the heart becomes severely weakened, as a product of other prior cardiovascular disorders, mainly hyepertension, valve abnormality, coronary disease or cardiomyopathy.

Right heart failure occurs when the right ventricle fails to expel enough blood through the pulmonary artery into the left ventricle. If this is the case, the venous return continues to direct the blood into the right atrium and in a long term, it will probably cause a blood congestion and edema in the legs. Since both ventricles are working in a series, a low output from the right ventricle has a subsequent effect on the cardiac output. If this is the case, the right ventricle filling pressure becomes high, whereas the left ventricle pressure remains low. Left heart failure is the most common CHF condition in which the left ventricle is too weak to expel the blood coming from the pulmonary loop to the systemic loop. Since again both ventricles are working in series, left ventricle failure results in a blood congestion in the pulmonary artery and subsequent high filling pressure in the left ventricle. This makes breathing action very difficult for a patient suffering

from end-stage left heart failure [10]. In this study CHF is associated only with the left heart failure condition.

Patients with severe heart failures suffer from renal impairment and pulmonary hyepertension [11]. The kidneys are one of the crucial organs of the body and they consume about 6% of the total oxygen and also account for nearly 20% of the cardiac output. If the heart failure condition is not diagnosed and treated in the earlier stage of the disease, multiple organ failure may occur leading to early mortality [1]. Since the heart failure condition is accompanied by symptoms of variable internal organ disorder, it is difficult to classify the severity of CHF. One of the best CHF classifications was conducted by the New York Heart Association (NYHA). It suggested that the CHF condition can be divided into four categories known as Class I, Class II ,Class III and Class IV [12].

Class I CHF accounts for patients with cardiac disease but without restriction to physical activity. Class II accounts for patients with cardiac disease with slight limitation to physical activity. Patients with Class II CHF are comfortable at rest, however, normal physical activity results in a pain in the chest area. Class III CHF accounts for patients with cardiac disease with significant limitations to physical activity, and they are only comfortable at rest. However, even slight physical activity results in pain in the chest area. Class IV CHF accounts for patients not able to do any physical activity. In clinical practice, class IV CHF is considered as the most dangerous state, in which a patient is not able to undertake any physical activity comfortably and so she/he is bed bound.

1.4 Treatment of Heart Failure

Depending on the level of the heart failure condition, there are various therapies. In early-stage CHF, traditional pharmacological treatment can to some degree prevent the disease. In end-stage CHF, when the patient does not respond to the pharmacological treatment, surgical intervention including heart transplantation, total artificial heart implantation, Intra-Aortic Balloon Pump (IABP) and MCS devices can be suggested.

1.4.1 Drugs

Depending on the type and severity of heart disease, different pharmological treatments are suggested. Drugs prescribed for early-stage CHF may help cardiac improvement via a reduction of after-load pressure. As mentioned, the after-load pressure is attributed to the pulmonary and the aortic artery pressure against which the right and the left ventricle ejection occur respectively. Therefore, to expel the blood from the heart into the cardiovascular system, the pressure in the ventricles needs to exceed the corresponding after-load pressure. The higher the after-load pressure, the greater the force is required for ejection. Vasolidator drugs work by reducing peripheral resistance in the pulmonary or the systemic circulation and result in after-load reduction leading to cardiac improvement [1]. Furthermore, there are other types of drugs such as Nitroprusside or Prostacyclin which are commonly used for the treatment of myocardial infarction as well as hypertension condition [13]. In addition, there are inotropic drugs including Dopamine and Dobutamine, which are being used to support the failing myocardial muscle [14].

1.4.2 Heart Transplantation

When the patient does not respond to pharmacological treatment, other types of treatments are suggested. Heart transplantation is the most reliable and well-

established surgical treatment. At the beginning, due to a wide number of unknown complications, the rate of survival was limited to some days or weeks. However right now nearly 85% of recipients are alive at least one year after surgery [15]. Recently, the first infant recipient in the UK celebrated her 25th birthday [16]. However, the demand for heart transplantation is more than the supply, as a result, many of the patients who are on the waiting list to receive a donor heart may not survive. Among 4,200,000 patients with end-stage heart failure in both North America and Europe, only small minority of young patients ($\leq$50 year old) are eligible for the heart transplantation surgery and the rest are not included in this category. Donor hearts supply meets less than 2% of the demand of eligible patients and leaves nearly great majority of end-stage CHF patients under palliative treatment [17]. Further it must be noted that the heart transplantation is a significantly invasive and prolonged surgery needing the recipient's median sternotomy to be cracked and opened. As a result, those patients who are not in a suitable physical condition may not survive.

1.4.3 Total Artificial Heart

Before heart transplant surgery became the most reliable treatment for end-stage CHF, considerable efforts were made by many researchers and cardiologists for the development of a Total Artificial Heart (TAH). The first TAH implant surgery in the human body was conducted on an end-stage CHF patient in 1968. The device was in the body of a patient for 64 days before heart transplant surgery [18].

Older versions of TAH such as Jarvik 7 [18] and SynCardia [19] are mainly pneumatically actuated devices. They are, to some extent, large, heavy and less efficient. Many of these devices are still under development in various medical centers. New versions of TAH, such as AbioCor [20] are electrically actuated devices which are normally implemented as a bridge to transplant. They are smaller in size compared to the pneumatically actuated types and are more efficient. Use of TAH as a replaced support device in various heart failure cases has shown a lot of complications, such as bleeding, valve failure and blood clotting. These complications are generally attributed to the large size of the TAH. Therefore, the

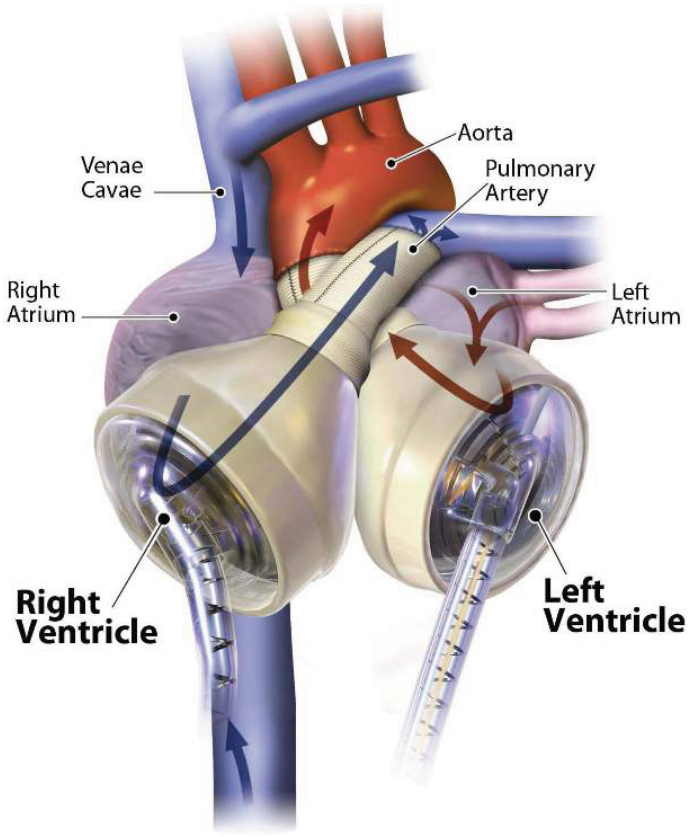

Figure 1.9: Schematic diagram of the SynCardia TAH. *From: M. J Slepian, et al. [19]. The syncardia (tm) total artificial heart: in vivo, in-vitro, and computational modeling studies, 2013.*

development of a smaller and more efficient support device capable of improving the action of an impaired heart has been pursued.

1.4.4 Intra-Aortic Baloon Pump

The Intra-Aortic Baloon Pump (IABP) is recognized as one of the established treatments for end-stage CHF patients. The concept of the IABP was introduced first by Kolff and Moulopoulos in 1962 [21]. The IABP incorporates a pulsatile balloon which is normally inserted through the femoral artery and is placed in the proximal descending aorta. During the systolic phase the balloon deflates

and lets the blood travel to the peripheral system. During the diastolic phase the balloon inflates leading to a rise in after-load pressure favoring coronary perfusion. The balloon is connected to a console by means of a thin catheter. The console controls the inflate-deflate action synchronously with the heart beat. Although the IABP is not categorized as mechanical assistance device, it helps the heart function to improve while the patient is waiting for a donor heart. Immobility is the main drawback of the device, so the patient needs to be hospitalised to be put on a IABP during the treatment.

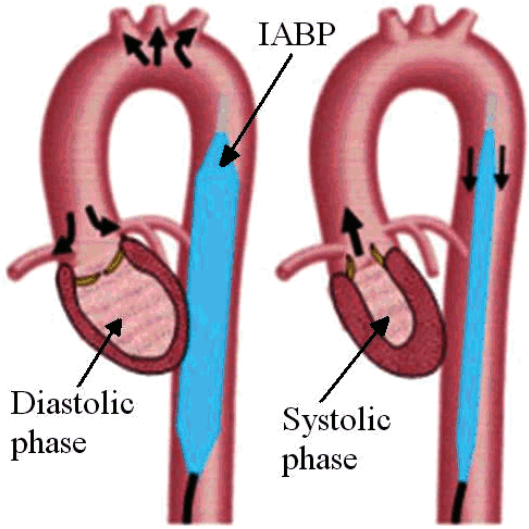

Figure 1.10: Schematic representation of IABP.

1.4.5 Mechanical Circulatory Support

In the USA, the supply of donor hearts only meets about 2% of the demand. The numbers are similar in percentage for the population of the western world. This shortfall in supply has resulted in the development of MCS devices as a reliable transplant alternative. In the past, 80% of CHF cases would have ultimately died. However, in recent years the increasing the use of MCS devices have significantly reduced the mortalities [22].

MCS devices mainly consist of a pump that is connected from the heart to

either the systemic or the pulmonary blood circulation through one graft [23] or two grafts [24]. The pump directs the blood from the heart to the blood circulation system by extracting kinetic energy from the electrical source. In contrast to the TAH device which is implanted as an alternative to the heart, the MCS device is implanted next to the heart and is intended to take over part of the cardiac function. Normally, this device is assisting one impaired heart chamber. However, in many cases, if two heart chambers such as the left and the right ventricles are malfunctioning, two MCS devices operating simultaneously are required. Depending on the severity of heart failure and also the type of MCS device used, the end goal of the application of the MCS device can be different. The application of an MCS device can be classified into three sub-categories including:

- As a bridge to transplant [25].
- As a bridge to recovery [26].
- As a bridge to destination [27].

The application of an MCS device as a bridge to heart transplant has been crucial in recent years [25]. Only a small number of patients with end-stage CHF can have heart transplant surgery. Owing to an insufficient number of heart donors, many patients with end-stage CHF conditions have to wait for cardiac transplant surgery for more than six months. It is also reported [28] that patients supported with MCS devices, while on the heart transplant waiting list, have a higher chance to survive after the heart transplant operation. It is demonstrated that patients on MCS support have better physical conditions compared to the ones treated pharmacologically.

The application of MCS devices as a bridge to recovery has been reported in the study conducted by Frazier et al. [26]. It is demonstrated that using the MCS device in a number of patients can help them regain the cardiac function during the support period, therefore the device can be removed without a need to implant a donor heart. Depending on the age of the patient and the severity of the disease, the recovery time prior to explantation may vary.

The application of MCS devices as a bridge to destination has also been reported [27]. Currently, the only alternative solution for heart transplantation in patients suffering from chronic irreversible heart failure is to implant a permanent MCS device with minimum complications. Permanent implantation of an MCS device as a destination therapy has helped a significant number of patients who could not benefit from a suitable donor heart [27]. An MCS device developed for prolonged application must satisfy three crucial criteria; long term safety, efficiency and durability. Meeting the above criteria can help to decrease the probability of morbidity and mortality. It is reported [29, 30, 31] that the new generation of continuous MCS devices [23, 32] are more reliable for long term use due to their simplicity, high efficiency and in particular they are very compact and their usage results in less morbidity and mortality.

In general, MCS devices are categorized on the basis of their dynamic motion into Pulsatile [33] and Continuous (rotary) [32, 34]. The latter can be further categorized on the basis of the rotor structure into axial [32] and centrifugal [34]. The efficiency of an MCS device is determined by its aerodynamic design and also by the biocompatibility of the inner components.

1.4.6 Pulsatile MCS Devices

Pulsatile MCS devices, regarded as the first generation of MCS devices, can mimic the native left ventricle and provide pulsatile flow by taking over the function of the patients own left ventricle. The first pulsatile MCS device implantation was conducted in 1968. In this operation, a pulsatile MCS device was implanted, through the left thoracotomy, next to the heart and was bypassed between the apex of the left ventricle and the descending aorta [35]. Pulsatile pumps normally employ a flexible diaphragm which is displaced either pneumatically or electrically to produce the pulsatile flow. Use of a displacement mechanism inevitably increases the volume of the device. Also, the pump consists of two unidirectional valves to direct the blood from the heart to the aorta and to stop back flow to the pump.

The most widely used pulsatile MCS devices have been extracorporeal devices such as the BVS 5000 VAD produced by Abiomed, Inc. (Danvers, MA, USA) [36] and the Thoratec VAD produced by Thoratec Corporation (Pleasanton, CA, USA) [37]. The rest are intracoporeal devices such as the Novacor LVA System produced by WorldHeart, Inc. (Oakland, CA, USA) [38]. Newer Pulsatile MCS devices such as the LionHeart VAD produced by Arrow International, Inc. (Reading, PA, USA) [39] are totally implantable. Figure 1.11 shows the Thoratec pulsatile pump from the Thoratec Corporation.

Previoues studies [40, 41, 42] have demonstrated that the pulsatile flow has an enormous influence on flow circulation physiology of the cardiovascular system. The pulsatile flow stimulates the blood perfusion as well as oxygenation in vital organs such as the kidneys and the liver. It can also improve the micro-circulation in diseased myocardium cells that ultimately leads the cardiac function being regained. However, the concept of a pulsatile MCS device suffers from serious drawbacks such as device weight, size, noise and drive line infection. Furthermore, as a result of the contribution to the number of moving mechanical components in one unique pulsatile device, the durability of these types of devices is limited to a few years. The repetitive displacement of the diaphragm in the long term results in tremendous stress on the moving components. This reduces the distensiblity of the diaphragm and ultimately leads to the development of some physiological consequences such as thrombosis formation in the blood system [43].

1.4.7 Centrifugal MCS Devices

Complexity, inefficiency and the large size of pulsatile MCS devices has encouraged researchers towards the development of an assistant device with higher efficiency, smaller size and less moving elements. Centrifugal MCS devices are regarded as the first generation of non-pulsatile pumps. Centrifugal pumps have been used for Cardio-Pulmonary Bypass (CPB) and also Extra-Corporeal Membrane Oxygenation (ECMO) Since 1980. The first centrifugal pump used as a bridge to transplant MCS device was developed in the early 1980s by Golding et al. [44].

Figure 1.11: Implantable, intracorporeal version of the Thoratec (IVAD). *From: D. J. Farrar et al. [37], Long-term follow-up of thoratec ventricular assist device bridge-to-recovery patients successfully removed from support after recovery of ventricular function, 2002.*

Figure 1.12: HeartWare centrifugal pump. *From: M. S. Slaughter et al. [45], Heartware miniature axial-flow ventricular assist device design and initial feasibility test, 2009.*

In general, centrifugal pumps are employed in various applications to produce pressure build up rather than flow rate. The centrifugal MCS device has a titanium impeller driven by magnetic coupling. The inlet flow is in parallel with the rotational axis and the outlet flow is perpendicular to it. The impeller is made

of a number of vanes that convert the axial velocity into the radial velocity. The impeller rotating speed in the centrifugal MCS is lower (2000 rpm-6000 rpm) than the axial MCS (3000 rpm-25000 rpm) [46]. The lower the rotational speed, the smaller the shear stress on the interacting components of the pump and thereby the lesser the physiological consequences. Thus, centrifugal pumps are regarded as highly efficient MCS devices compared to other types of MCS devices. One of the drawbacks of the centrifugal MCS device is its large size. Implantation of a large mechanical device into the patient's body is usually followed by some complications. In particular, very ill patients can develop severe organ infections, cancer or neurologic damages which may result in morbidity and mortality [47]. The second generation of centrifugal MCS devices, such as the NEDO PI-601 pump (evolved GyroC1E3) [34] consist of two contacting bearings for holding the impeller. Use of contacting bearings increases the risk of clotting and thrombus formation at the contact bearing and thus reduces the reliability of the device for long term use.

The third generation of centrifugal MCS devices includes DuraHeart [48], HeartMate III [49] and HeartWare [45], which are more desirable to be used as a bridge to destination. The third generation of centrifugal MCS devices employs magnetic and hemodynamic bearings instead of using contacting bearings. Employment of the magnetic bearing reduces the stagnant spots and hence the risk of thrombus formation as well as component wear.

In order to reduce the risk of infection inside the recipient's body, it is preferred to implant a fully sealed device, with less interaction with blood circulation [50]. As a result, looking for a pump with a smaller size and smaller interacting surface is preferable. Axial MCS devices are smaller in size compared to centrifugal MCS devices.

1.4.8 Axial MCS Devices

In general, axial pumps are used for generating low pressure gradients and high flow rate conditions. This will make the axial MCS devices suitable for many

pathological conditions with low cardiac output. Axial MCS devices are smaller in size compared to centrifugal MCS devices. The smaller the size of an MCS device in the body, the lesser the risk of infection and subsequent post-operative complications. Figure 1.13 shows the schematic diagram of the DeBakey pump [24]. It is indicated that the pump consists of an axial impeller rotating inside a concentric cylindrical housing. The impeller is normally made of titanium and includes a couple of helical guided vains to lead the flow forward. As shown in Figure 1.13, a number of small rare earth magnet cylinders are embedded into each blade of the impeller. The brushless magnet has been developed and used around the flow tube where the moving part is located. As a result of an inductive magnetic field between the magnetized blades and the brushless magnet, the impeller spins and makes the flow move forward. Normally, the impeller rotates at a speed of 8000 -12000 rpm, producing average blood perfusion from 3-6 lt/min against the physiological resistance. As shown in Figure 1.13, a diffuser is set downstream of the impeller to convert the swirl velocity produced by the impeller to axial flow which eventually leads to the conversion of the kinetic energy to static pressure.

The second generation of axial MCS devices integrate two contacting bearings to hold the impeller. Major off-the-shelf second generation axial pumps include the Jarvik 2000 (25 ml in volume) [32], the HeartMateII (124 ml in volume) [27] and the Micromed (30 ml in volume) [51]. Employment of contact bearings increases the risk of thrombus formation at the bearings and thus reduces the reliability of the MCS device for long-term use [52].

This problem has been solved by third generation axial MCS devices by implementing a magnetically levitated impeller. Major third generation axial pumps such as the Incore1 [24] that employ magnetic bearings avoid tremendous friction force between the impeller and the housing leading to significant noise reduction.

1.4.9 MCS Device Complications

In general, introducing an MCS device into a native cardiovascular system is followed by a number of physiological variations in the blood circulation which

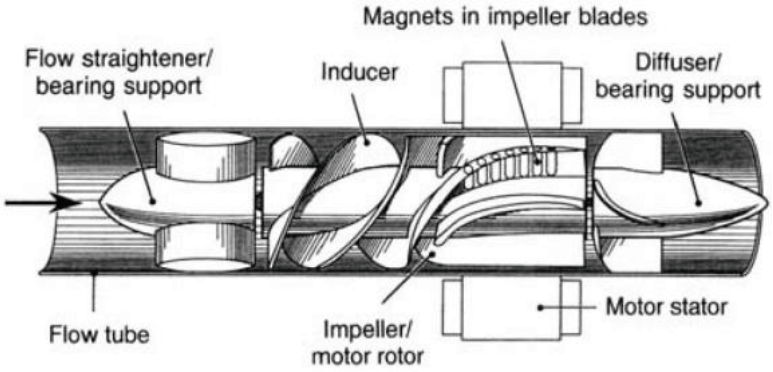

Figure 1.13: Debakey axial rotary pump. *From: R. Hetzer et al. [24], First experiences with a novel magnetically suspended axial flow left ventricular assist device, 2004.*

may lead to some subsequent complications such as flow-induced haemolysis, bleeding, infection and thrombus formation in the long-term period [31].

Haemolysis, in medical terminology, is defined as the destruction of red blood cells. Blood haemolysis levels are attributed with the shear stress and the exposure time of interacting components of an MCS device. Measuring the level of blood haemolysis induced by the shear stress of mechanical devices is one of the common approaches for evaluating the effect of MCS devices on physiological alteration of the blood.

Induced haemolysis can potentially exist for both pulsatile and continuous MCS devices. However the level of blood haemolysis, depending on the pump characteristic, may vary. Pulsatile MCS devices, due to their inherent dynamic mechanism, tend to generate considerable turbulent flow. Particularly, severe turbulent flow is generated in the vicinity of moving components, such as flexing diaphragm and the mechanical unidirectional valve. Presence of the turbulent regime leads to the creation of extra shear stress (Reynolds shear stress) in these areas and therefore causes an increase to the blood haemolysis level in these devices [43]. For the continuous MCS devices, increasing the rotational speed results in an increased shear stress in vicinity of the propeller which may lead to a significant haemolysis [53].

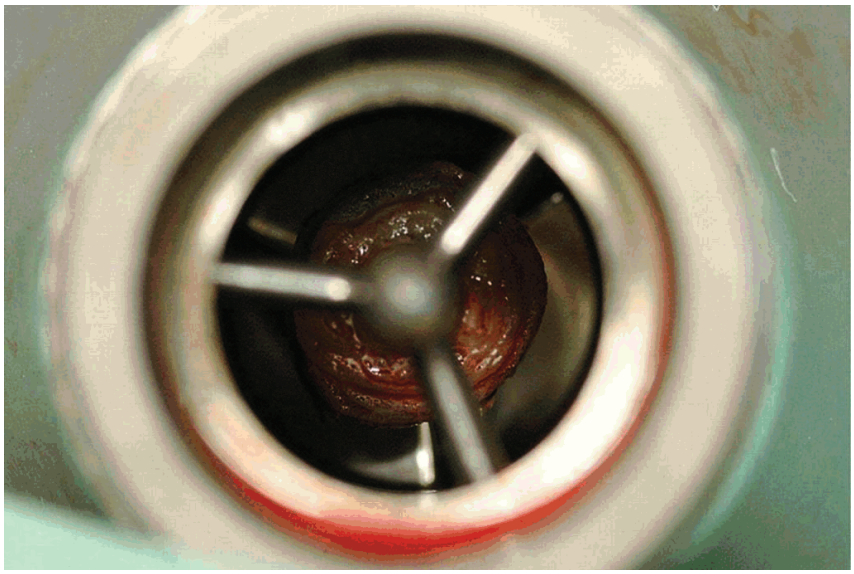

Figure 1.14: Thrombus formation in the axial pump after explantation. *From: G. S. Allen et al. [43], The importance of pulsatile and nonpulsatile flow in the design of blood pumps, 1997.*

Thrombus formation inside the continuous and pulsatile MCS devices is highly life threatening. This, in the worst case scenario, may cause thromboembolic complications in the recipient's cerebral system. In general, the natural blood system is laminar unless an artificial device is introduced into the blood circulation system. Thrombus formation is more likely to develop in association with turbulent flow than laminar flow. As stated earlier, pulsatile MCS devices due to their inherent dynamic mechanism, tend to generate a considerable turbulent flow. Development of turbulent flow causes thrombus formation in the pump chamber, which may gradually accumulate and in some cases may affect the inflow and outflow valves [43]. Turbulent flow formation in a continuous MCS device is highly dependent on the aerodynamic design of the impeller. Normally, thrombus formation develops downstream from the impeller at the diffuser where the blood flow is turbulent as shown in Figure 1.14.

The bleeding is one of the more frequent postoperative complications. The bleeding complications are normally caused after a prolonged invasive implantation surgery in patients with advanced ages. As a result, looking for a less invasive implantation technique which can be utilized in a variety of patients has

become a recent area of interest. The use of various anticoagulants in patients supported with MCS device is another factor that may cause bleeding. Anticoagulations are used in recipient's blood system to avoid the thromboembolic complications. However, there is a difficulty in choosing the right anticoagulation protocol which not only can prevent the thrombus formation but also can avoid the bleeding complications [9].

Infection rate is another MCS device complications occurring normally just after implantation and may increase with the length of the MCS usage. The infection complication are caused by various sources mainly wire infection and MCS pocket infection. The wire infection is due to the skin perforation which let the microbe and bacteria into the body. The use of Transcutaneous Energy Transmission (TET) may prevent this problem significantly. The pocket infection is caused mainly by implantation of large sized MCS devices. This requires highly invasive tissue dissection surgery which increases the risk of infection. The use of miniatured MCS device and the implementation of novel implantation techniques with less invasive surgery may reduce the infection [9].

Technical failure is another highly risk factor complication which is not predictable and may lead to the death of the patient. Motor and bearing failures are the most frequent technical complications. Further research is required to overcome these problems. Inflow graft occlusion can be another technical complication that normally develops in dehydrated patients after MCS implantation. This is due to the high level of suction in the absence of blood inside the left ventricle where a lot of myocardial tissue is sucked and accumulated [52].

1.5 Implantation Techniques

Surgical deployment of an MCS device in the native cardiovascular system causes a variety of hemodynamical alterations to the natural system. There are two typical techniques for MCS devices implantation:

- Median sternotomy

- Left thoracotomy

In the median sternotomy technique, the sternum is cracked, opened and the device is implanted next to the heart. In the left thoracotomy technique, the device is implanted through a small incision in the left thoracotomy without breaking the sternum. Both of these techniques are considerably invasive and require CPB for critically ill patients. It is demonstrated [54] that a prolonged invasive operation in critically ill patients results in considerable post-operative complications such as infection, bleeding and renal failure. Development of less invasive techniques has become a subject of interest recently. There are currently no cardiac support devices for permanent implantation that can be installed with minimally invasive surgery, and therefore there is a need for a viable alternative.

1.5.1 In-Parallel Configuration from Left Ventricle to Ascending Aorta

The most traditional implantation technique for pulsatile and continuous MCS devices is to implant the device between the apex of the Left Ventricle (LV) and the Ascending Aorta (AA), in-parallel with the heart, by conducting sternotomy surgery. Figure 1.15 shows the HeartWare pump [45] in the LV-AA configuration. Studies on the in-parallel LV-AA technique [48, 55, 56] indicated that the insertion of an MCS device between the left ventricle and the ascending aorta resulted in a promising hemodynamic improvement in blood circulation system. However in this technique, the dissection process is prolonged which necessitates the use of Cardio-Pulmonary Bypass (CPB) during the operation. Having a prolonged surgery in seriously ill patients results in some considerable complications post-surgery such as right ventricular dysfunction, end-organ injury and internal bleeding [56]. Moreover, long hospitalization after surgery increases the risk of contacting infectious diseases.

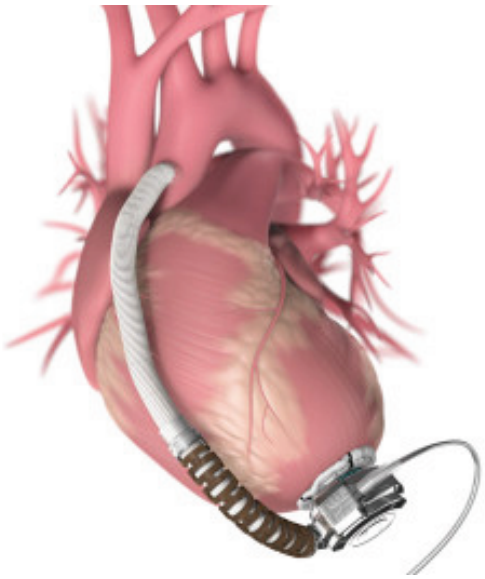

Figure 1.15: Heartware pump in the LV-AA configuration. *From: M. S. Slaughter et al. [45], Heartware miniature axial-flow ventricular assist device design and initial feasibility test, 2009.*

1.5.2 In-parallel Configuration from Left Ventricle to Descending Aorta

When compared to the older generation of MCS devices [32, 34] and the pulsatile VADs [33], the third generation of MCS devices such as Jarvik 2000 [32], MicroMed Debakey [51] and Incor [24] are more desirable for implantation through the left thoracotomy. This is due to minimal size, weight and low energy demand. Figure 1.16 shows the Jarvik pump which is surgically configured in a transcardial arrangement within the apex of the left ventricle [23].

In this technique, the device is implanted through a small incision into the left thoracotomy without breaking the sternum. Then the inflow graft is sewn to the apex of the left ventricle and the outflow graft is anostomised to the descending aorta (DA), adjacent to the left atrium, in parallel with the heart [24, 56, 57, 58]. In many cases the MCS implantation procedure through thoracotomy surgery could be conducted without CPB [56].

The implantation procedure without CPB shortens the time of the operation

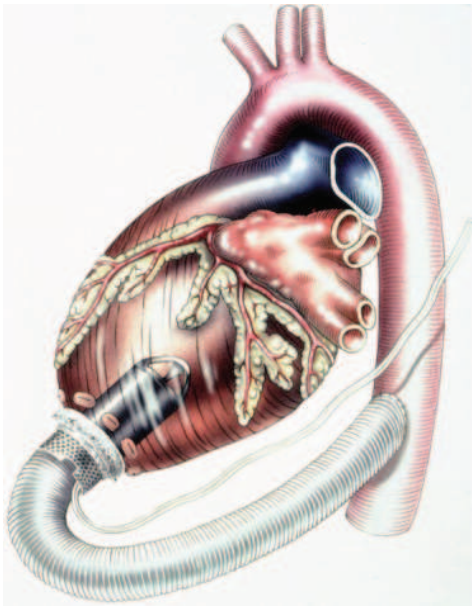

Figure 1.16: Jarvik pump in LV-DA configuration. *From: O. H. Frazier [23], Research and development of an implantable, axial-flow left ventricular assist device: the jarvik 2000 heart, 2001.*

considerably and hence reduces the probability of post-operative complications such as bleeding and infection. Nevertheless recent findings on LV-DA suggest that this technique may not be hemodynamically optimal in various degrees of the pump support. It is reported [54, 58, 59] that the outflow graft connection to the descending aorta results in a reduction in the mean aortic arch flow as the level of MCS support is increased. This will result in formation of stagnant and then retrograde flow in the aortic arch which may lead to aortic valve stenosis [46].

1.5.3 In-Series Configuration in Descending Aorta

In both LV-AA and LV-DA in-parallel techniques, the pump operates as a competitor to the left ventricle. A parallel working system improves the cardiac output by reducing the pre-load. In this approach, the pump can take over part or the entire heart load. In a series configuration, the entire cardiac output is delivered through the aortic valve and the device. Negative pressure upstream of

the pump reduces the after-load pressure to facilitate cardiac output.

In clinical practice, pharmacological treatments such as vasolidators are the best approach to reduce the after-load pressure in high filling failure condition. Although the use of vasodilators leads to an improvement to the cardiac output, in a critically low blood pressure situation, such as cardiogenic shock or post-cardiac operation, it may lead to the creation of extreme perfusion disturbances in the abdominal organs.

Recent studies on two temporary paracorporeal MCS devices, inserted percutaneously into the descending aorta to prevent cardiogenic shock, suggests that the descending aorta can be a promising location to install a long-term implantable MCS device with minimally invasive surgery [46, 53, 60, 61].

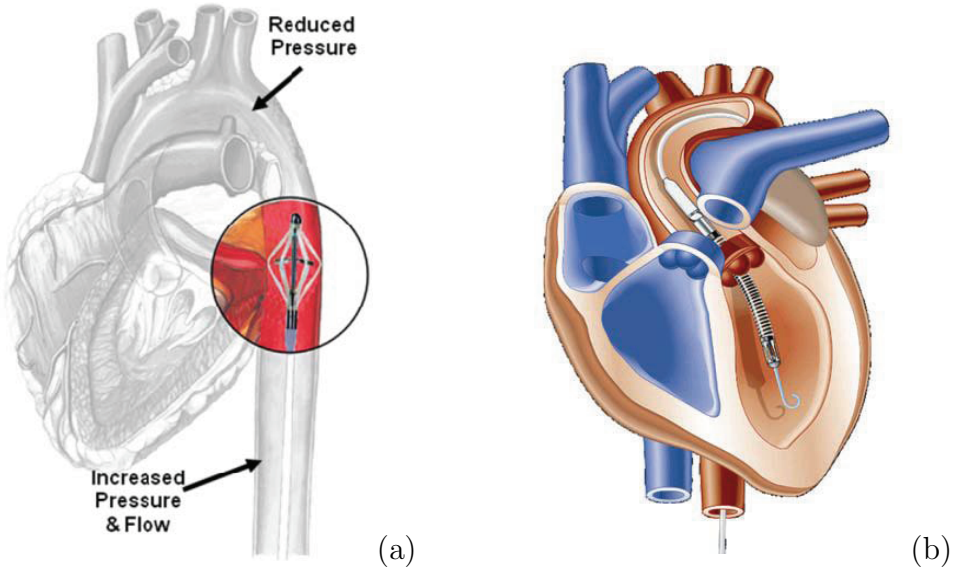

Figure 1.17: (a) Reitan Catheter Pump (RCP) in the descending aorta. *From: O. Reitan et al. [53], Hemodynamic effects of a new percutaneous circulatory support device in a left ventricular failure model, 2003* (b) Impella axial rotary pump crossing the aortic valve. *From: A. G. Rose et al. [46], Partial aortic valve fusion induced by left ventricular assist device, 2000.*

The Reitan Catheter Pump (RCP) is a novel approach among other mechanical circulatory systems. The RCP consists of two foldable blades embedded inside a surrounding umbrella-like mechanism cage and an external DC motor (paracorporeal MCS). The RCP blades are connected to a DC motor through a rotating

wire placed inside a flexible catheter. Similar to the IABP, the RCP rotor is inserted through a small incision in the femoral artery and is advanced towards the proximal descending aorta. Once the rotor is placed at the right position, the cage is expanded and the rotor is unfolded. Figure 1.17(a) shows the schematic diagram of the RCP placed in-series configuration with the heart. The pressure difference produced across the RCP rotor at 14000 rpm rotational speed is about 24 ± 10 mmHg. The pressure drop generated at the upstream of the pump results in a reduction of the after-load pressure and subsequent improvement of CO without the risk of kidney failure that would have occurred by using vasodilators.

Impella Recover is an intra-cardiac axial pump which is being used to provide short-term assistance for patients with end-stage cardiac failure. The pump consists of a propeller with a diameter of 4.5 mm. The propeller is driven by a micro-engine through a flexible cable. The propeller and the electronic driver are placed inside the inflow cannula, which guides the flow into the ascending aorta. The pump is inserted through a small incision in the femoral artery and is advanced into the left ventricle, by crossing the aortic valve, as shown in Figure 1.17(b). At a propeller speed of 30000 rpm, the maximum flow rate produced by the Impella is 4.5 lt/min [46]. Clinical findings on an Impella recipient with hypotensive condition (75/61 mmHg) show that the cardiac output has improved by up to 2.5 lt/min. When compared to the standard IABP, the Impella pump exhibits higher hemodynamic performance [46].

Table 1.1 presents the specifications of the available rotary heart assistance devices as well as their implant configurations in the human body.

Table 1.1: Specification of available rotary MCS devices

Device	ΔP	Q	D	ω	Power	Dimension	Mass	Bearing	Configuration
Debakey (He)	100-120	5-10	12	7500-12000	10	86×25	95	Me	In-parallel LV-(AA&DA)
HeartAssist5(He)	100-120	1-10	12	8500-10600	10	71×30	92	Me	In-parallel LV-DA
Jarvik(He)	100	2-7	11	8000-12000	≥ 12	55×25	85	Me	In-parallel LV-DA
Theoratec(He)	100	6.5	-	8000-12000	3-7	55×25	85	Me	In-parallel LV-AA
IncorLVAD(He)	100	6	13	5000-10000	≥ 5	123×30	200	Mag	In-parallel LV-(AA&DA)
MicroVAD(He)	80	4	7	30000	-	50×12	-	Me	In-parallel LV-DA
MagneVAD(He)	100	6	14	12500	5	60×30	89	Mag	In-parallel LV-DA
HeartMateII(He)	80-100	10	11	6000-15000	10-12	81×43	281	Me	In-parallel LV-AA
Impella 2.5(Ax,Pe,Te)	-	4.5	-	30000	10	65×4.5	-	Me	In-series AA
Reitan(Ax,Pe,Te)	14-34	5	15	10000-15000	1.11	21×25	-	Me	In-series DA
GyroCiE3(Ce)	110-150	5-8	68	2000-2500	-	53×65	305	Me	In-parallel LV-DA
EvaHeart(Ce)	100	5-9	40	2600	9-10	55×64	370	Me	In-parallel LV-DA
VentrAssist(Ce)	100	5	16-40	1800-3000	7-8	60	298	Hyd	In-parallel LV-AA
DuraHeart(Ce)	150	2-10	50	1200-2600	8-13	72×45	540	Mag	In-parallel LV-DA
Heartmate III(Ce)	135	7	44	2000-5500	≥ 10	30×69	535	Mag	In-parallel LV-AA
MiTi(Ce)	100	2-7	34.5	2500-3500	6.5	80×50	300	Mag	In-parallel LV-DA

ΔP: maximum pressure gradient of pump (mmHg), Q: maximum flow-rate (lt/min), D: diameter (mm), ω: rotor speed (rpm), Power (watt), Dimension ($mm \times mm$), Mass (g), Ax: axial, Ce: centrifugal, He: helical, Pe: percutaneous, Me: mechanical, Mag: Magnetic, Hyd: Hydrolic, Te: temporary usage LV: left ventricle, RV: right ventricle, AA: ascending aorta, DA: descending aorta.

1.6 Simulators of the Cardio-Vascular Blood-flow Loop

The design and development of a Simulators of the Cardio-Vascular blood-flow Loop (SCVL) which is capable of emulating the characteristics of the cardiovascular system not only can provide one with the required hemodynamic response but it also avoids number of complications that one may come across in an in-vivo test. In order to dynamically model a cardiovascular system (whether computationally or experimentally), the physiological characteristics of each component of the native cardiovascular system should be investigated at different pathological conditions. Each part of the cardiovascular system has its own characteristics and dynamic behavior. As a result, broad knowledge of the hemodynamic behavior of cardiovascular system in various physiological and pathological states is a major pre-requisite for developing an SCVL system.

The design and implementation of an SCVL system is motivated by the necessity and significance of in-vitro tests of various artificial devices such as heart valves, Ventricular Assist Devices (VAD) and Mechanical Circulatory Support (MCS) devices prior to in-vivo testing. Earlier versions of SCVL systems were mostly pulsatile and were driven by stepping motor. These SCVL systems were mainly developed for the investigation of various heart valves [62, 63, 64]. The next generation of SCVL systems were developed in order to conduct hydrodynamic, hemodynamic and haemolysis investigations on cardiac assistance devices as well as on prosthetic vessels [65, 66, 67, 68, 69, 70]. Moreover, there are a number of SCVL systems developed to simulate some specific physiological parameters of a native cardiovascular system [71, 72, 73, 74, 75, 76]. In a recent study a hybrid (numerical-experimental) model of the native cardiovascular system has been developed to overcome the problem of inflexibility in SCVL systems [59, 77]. SCVL systems can be classified into various categories in terms of the number of chambers, type of actuators, type of heart valves, type of resistance and compliance components, control techniques, measurement devices and objectives. In this study, SCVL systems are classified into three main categories

based on the number of actuators implemented to simulate the heart chambers:

- Single-Chamber SCVL
- Twin-Chamber SCVL
- Multi-Chamber SCVL

If the left ventricle and aorta are under investigation, the system has only one chamber which is the left ventricle, one drive to excite the chamber and one or two valves. If the systemic or the pulmonary circulation needs to be replicated, two chambers, two drives and two or three valves are required. In the case of recreating a complete circulation loop consisting of the systemic and pulmonary loops, four chambers, four drives and four or five valves need to be employed.

1.6.1 Single-Chamber SCVL

The simplest SCVL system includes one chamber normally activated by a pneumatic or DC motor actuator. The objective of these devices would be, in general, to evaluate the performance of newly developed time-varying elastance models simulating dynamic mechanism of the heart. This type of SCVL system is easy to set up and is also cost effective.

Colacino et al. [78] developed a single-chamber SCVL for simulation of the left ventricle of the heart as shown in Figure 1.18. For the experimental model a screw-driven piston cylinder mechanism actuated by a DC motor is employed to drive the left ventricle chamber. In this model, the modified version of the classical Suga-Sagawa elastance model [79] was employed to simulate the correct ventricular pressure-volume relationship.

The experimental results show that the modified elastance function is able to successfully reproduce the elastance mechanism of the native left ventricle according to the Frank-Starling law [80]. However, as shown in Figure 1.19, the Left Ventricle Pressure (LVP) waveforms in controlled and diseased conditions

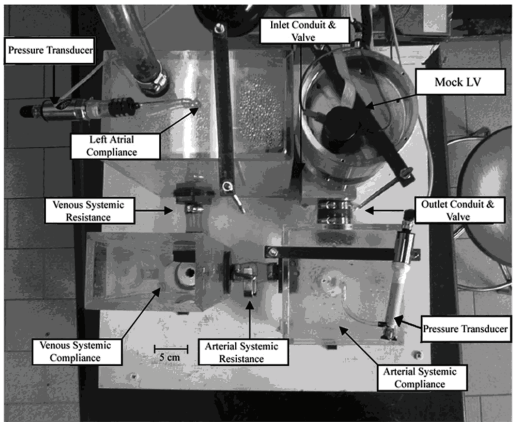

Figure 1.18: The photograph of the single-chamber SCVL system. *From F. M. Colacino et al. [78], A modified elastance model to control mock ventricles in real-time: Numerical and experimental validation, 2008.*

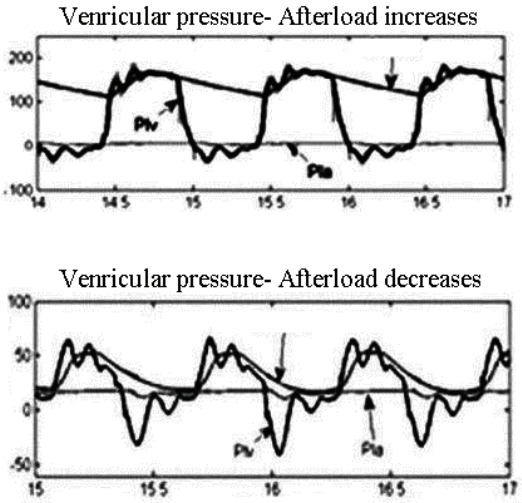

Figure 1.19: The LVP waveform for the diseased condition when the afterload pressure increases and decreases, respectively from the SCVL system. *From F. M. Colacino et al. [78], A modified elastance model to control mock ventricles in real-time: Numerical and experimental validation, 2008.*

are not in close agreement with the left ventricle conceptual feature [80]. The inherent rigidity of the tubing system combined with the DC motor vibration results in significant transient oscillations appearing on the left ventricle pressure waveforms and hence reduces the accuracy of the results.

In another study, a hybrid one-chamber SCVL system was proposed by Ferrari et al. [81] to reproduce the Frank-Starling law of the left ventricle using another newly developed variable elastance function developed by the same team. In general, a hybrid model combines the numerical model and the experimental model. Therefore, a hybrid model shows better flexibility and performance compared to a purely numerical or an experimental model. In a hybrid model, both numerical and experimental models are connected together through an electro-hydraulic interface. This study employs an electro-hydraulic actuator. Depending on the objective of the experiment, some part of the test can be implemented hydraulically and the rest numerically. Considering the electro-hydraulic analogy, the hydraulic parameters including the pressure and the flow-rate are converted to numerical parameters of the voltage and the current respectively. Figure 1.20 corresponds to the measured Aortic Pressure (AoP) from the test rig and the computed LVP from the numerical model in a control condition, pathologic condition and IABP assistance condition. Both numerical and experimental pressure waveforms are within the physiologic levels. However, it can be observed that the pressure waveform features are not predicted clearly.

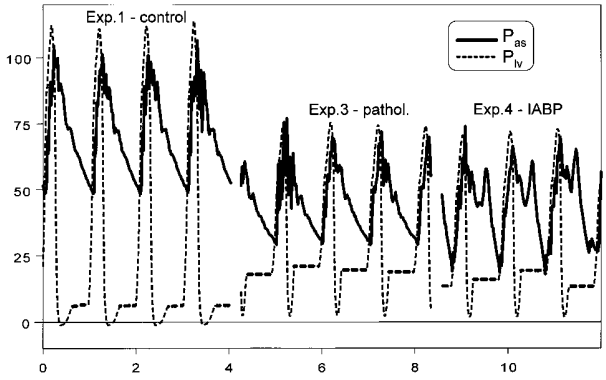

Figure 1.20: The numerical LVP and experimental AoP waveforms from the SCVL system. *From G. Ferrari et al. [81], A hybrid mock circulatory system: Testing a prototype under physiologic and pathological conditions, 2002.*

1.6.2 Twin-Chamber SCVL

In a twin-chamber SCVL, the ventricle is generally actuated by a pneumatic pump and the atrium is simulated by an open-to-atmosphere water header tank. Therefore, the atrium pressure is simulated by the constant static pressure from the head of water in the tank throughout the cardiac cycle. To reproduce the systemic or the pulmonary circulation in a twin-chamber SCVL system, a combination of resistance and compliance components similar to the Windkessel model [82] have been employed in previous studies [78, 81, 83].

Garcia et al. [84] describes a twin-chamber SCVL including the left ventricle, left atrium and the systemic circulation. The objective of this study was to investigate the effect of the aortic valve abnormality on the hemodynamic response of a left-side VAD device. As shown in Figure 1.21(a), the left ventricle chamber was made of silicon rubber which is embedded inside the pressurised water tank. The level of water pressure in the tank is controlled by the pump connected to a stepper motor and it is driven according to the ventricular volume change. The left atrium is simulated by an open-to-atmosphere water header tank. The systemic compliance unit is simulated by a pressurized air tank. The total peripheral resistance is modelled with a single metal clamp. Both the mitral and the aortic valves are modelled with two tricuspid bio-prosthetic valves. In this study, the left ventricle pressure as well as the aortic pressure were measured at four different levels of VAD support. Experimental results show that the twin-chamber SCVL in this study can provide a reasonably controlled environment for testing the characteristics of VADs. Figure 1.21(b) shows that both the left ventricle and the aortic pressure waveforms are in a good agreement with the clinical data [80]. However it is evident that due to the high level of transient pressure oscillation, the main features of pressure waveforms are not predicted clearly. This can be due to the inherent rigidity of the tubing system employed for the systemic circulation. Another drawback of this SCVL is that the left ventricle is not following the Frank-Starling law precisely in response to various levels of pre-load and after-load changes. This can be justified as a result of not using a more precise actuator for the left ventricle and using an inappropriate

variable-elastance model for the left ventricle.

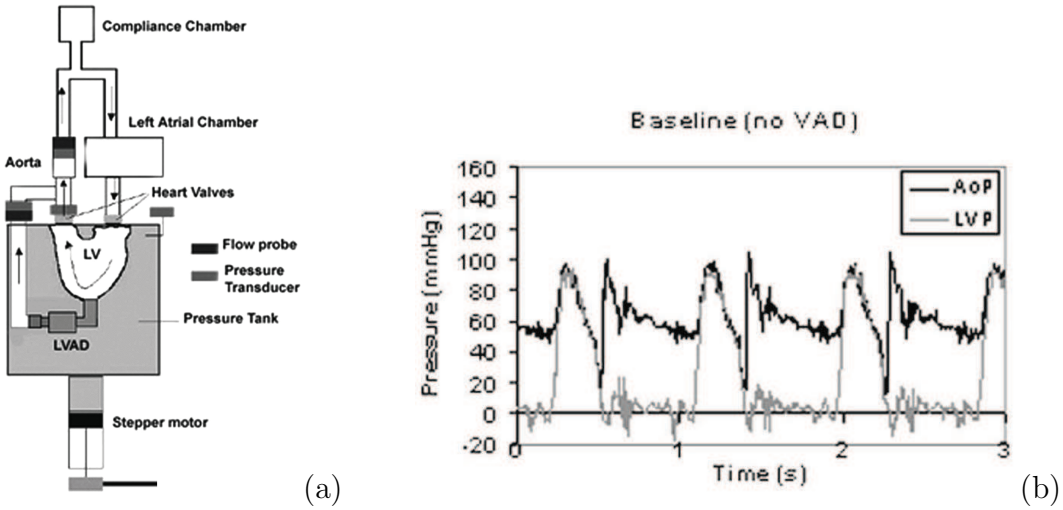

Figure 1.21: (a) Schematic diagram of the twine-chamber SCVL system. (b) The LVP and AoP waveforms for the diseased condition, *From: M. A. Z. Garcia et al. [84], The effect of aortic valve incompetence on the hemodynamics of a continuous flow, ventricular assist device in a mock circulation, 2008.*

In another study by Legendre et al. [85], a twin-chamber SCVL, as shown in Figure 1.6.2(a), was developed to study the hemodynamic parameters of the left ventricle and the aortic artery in various physiological and pathological conditions. In this study, the left ventricle displacement is modeled through a diaphragm actuated by a piston. A connecting rod is used to convert the linear displacement of the piston into the rotary motion of a DC motor. The left atrium is modeled by an open to atmosphere tank. Alternation of the height of the atrium tank results in a change of pressure inside the left ventricle. This leads to a simulation of various physiological or pathological conditions in the system. In addition to the pressure and the flow-rate, in this study, the temperature was being measured constantly and kept stable, very close to the physiological temperature of a native body. To simulate the characteristics of natural blood, a mixture of 63% water and 37% glycerol was used as the working fluid [85].

Figure 1.6.2(b) shows the aortic pressure and the corresponding flow waveform in a control condition. It is evident that the measured aortic pressure waveform is in good agreement with the clinical data [80]. However the main features of a

pressure waveform such as dicrotic notch, appearing normally in the clinical aortic pressure, was not predicted clearly. Another drawback of this system is that due to the use of the DC motor as an actuator of the left ventricle, the left ventricle chamber is getting activated at a fixed rate. Therefore, the cardiac iso-volumetric phases cannot be predicted precisely. This is similar to the study conducted by Colacino et al. [78]. It is concluded that the DC motor as an actuator is not an appropriate option to actuate the left ventricle.

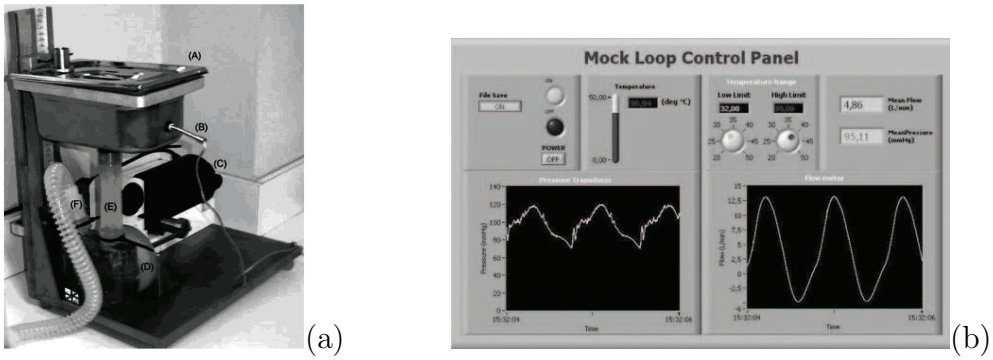

(a) (b)

Figure 1.22: (a) Photograph of the twin-chamber SCVL system, (b) Control panel shows the AoP and aortic flow waveform for the controlled condition. *From: D. Legendre, et al. [85], Mock circulatory system for the evaluation of left ventricular assist devices, endoluminal prostheses, and vascular diseases, 2008.*

Another study on a twin-chamber SCVL was conducted by Sharp et al. [86]. The objective of this SCVL was to simulate the Frank-Starling response of a native body in different physiological and pathological conditions. The test rig simulates the systemic circulation and includes two chambers of the left atrium and the left ventricle. The left atrium chamber is made of a flexible polymer and the left ventricle chamber is made of a polymer sac embedded inside another pressurized chamber. The required air for compressing the ventricular chamber during the systolic phase to deliver the cardiac stroke volume is provided by a pneumatic actuator connected to a control system. The mitral valve is modeled by polyurethane trileaflet valve and the aortic valve is modeled by a rigid tilting disk. Figure 1.23 shows the schematic diagram of the SCVL system developed by Sharp et al. [86]. The compliance unit in this system was modelled by using a coil spring-loaded bellows and the resistance unit was modeled by using a compressible folded fibre-sheet. The whole vasculature system is connected through tygon tubing. To

control the effect of impedance on the system, the tubing system length has been optimised and the input impedance of the system has been measured in terms of different levels of resistance and compliance units.

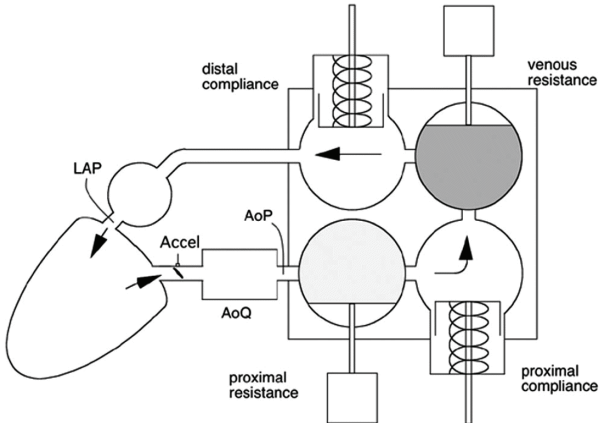

Figure 1.23: Schematic diagram of the twin-chamber SCVL. *From M. K. Sharp et al. [86], The influence of mock circulation input impedance on valve acceleration during in-vitro cardiac device testing, 2008.*

Figure 1.24 shows the AoP and LVP waveforms for a controlled condition. Final results show that the SCVL system was able to reproduce the Frank-Starling response reported clinically and the simulated native pressure and flow waveforms were in good agreement with the native system. It is evident from Figure 1.24 that the main features of the aortic pressure waveforms include a sharp rise of the systolic pressure, gradual fall of the diastolic pressure and the dicrotic notch, which are predicted fairly similar to the clinical data. In comparison with the other studies [78, 84, 85] on twine-chamber SCVL systems, it is evident that the measured pressure trace carries the least transient oscillations which is mainly due to the use of an appropriate compliance unit.

Studies such as [78, 84, 85, 86, 87] on twin-chambers SCVL systems show that these emulators are able to replicate the action of a native system at various physiological and pathological conditions. However, they have inherent limitations in emulating the atrium-to-ventricle and the ventricle-to-artery interactions of both the systemic as well as pulmonary circulations. Moreover, the hemodynamic assessment of bi-VADs or the effect of the left-side VADs on the pulmonary cir-

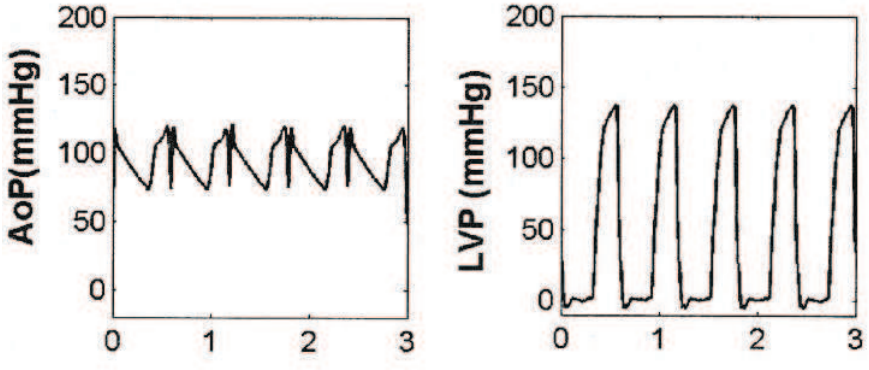

Figure 1.24: The experimental AoP and LVP for the controlled condition from the SCVL system. *From M. K. Sharp et al. [86], The influence of mock circulation input impedance on valve acceleration during in-vitro cardiac device testing, 2008.*

culation is required to have additional features. In order to investigate the central and peripheral hemodynamic variables of the systemic and the pulmonary circulations simultaneously, a cardiovascular simulator needs more additional features. Therefore, there is a need for the development of a cardiovascular simulator which behaves similar to a native cardiovascular system.

1.6.3 Multi-Chamber SCVL

Multi-chamber SCVL systems consist of four chambers including two ventricles and two atriums. In previous studies [78, 81, 83], the ventricle chambers were generally actuated by pneumatic pumps and the atriums were simulated by two open-to-atmosphere water header tanks. To reproduce the systemic as well as the pulmonary circulation in a multi-chamber SCVL, a combination of resistance, compliance and up to five mechanical or biological valves were used.

Timms et al. [83] developed a multi-chamber SCVL system to evaluate the effect of left-side VAD, right-side VAD or both on the systemic as well as the pulmonary circulation. The test rig includes four chambers of the heart. The right and the left ventricle chambers were controlled by two pneumatic actuators. The contraction and expansion of the ventricle chambers are controlled

by compressing and ventilating air through a 3/2″ solenoid valve into the corresponding chambers using a regulated compressor. Two air/water header tanks for each of the atriums were employed as shown in Figure 1.25. Any change in the volume of water in the atriums determines the pre-load pressure in the ventricle chambers. The pathological conditions were modelled by changing a number of vasculature parameter characteristics, such as mean circulatory pressure, heart rate, ventricle elasticity, systemic and pulmonary resistances and compliance. Figure 1.26 shows that the measured left ventricle and the aortic pressures are in

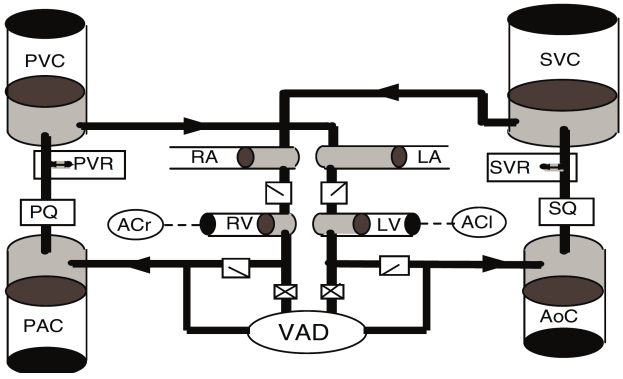

Figure 1.25: Schematic diagram of the multi-chamber SCVL system. *From: D. Timms et al. [83], A complete mock circulation loop for the evaluation of left, right, and biventricular assist devices, 2005.*

good agreement with the clinical data [80]. The results show that the test rig is thoroughly adherent to the Frank-Starling law, however due to the inherent rigid nature of the vasculature system and rapid closure of the swing check valves, the pressure waveforms carry significant transient pressure oscillations. As a result, similar to previous studies [78, 85], some features of the clinical pressure waveform, such as dicrotic notch appearing on the aortic pressure waveform were not predicted. In addition, it is evident from Figure 1.26 that there is a phase difference between the aortic pressure and the left ventricle pressure which can be attributed to the inherent rigidity of the vasculature system and the use of an inappropriate compliance unit in the system.

Figure 1.28 shows another multi-chamber SCVL system developed by Pantalos et al. [88]. The objective of the system was to investigate the hemodynamic

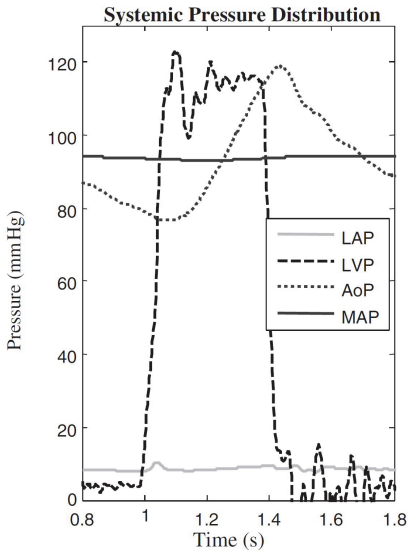

Figure 1.26: LVP and AoP waveform for a controlled condition from the SCVL system. *From: D. Timms et al. [83], A complete mock circulation loop for the evaluation of left, right, and biventricular assist devices, 2005.*

response of a pediatric cardiovascular system in the presence of a pediatric cardiopulmonary assistance device. In this study, the ventricles are made of polymer sac embedded inside pressurised chambers. Each chamber was actuated individually by a separate pneumatic pump. The atriums were made of silicon rubber. The polyvinyl tubing with an inner diameter of 3/8″ were incorporated to mimick the systemic as well as the pulmonary vasculature. A number of pinch clamps were used to control the pulmonary and the systemic resistances. The systemic and pulmonary compliances are modelled using the latex tubing. The results show that the SCVL system is capable of mimicking the hemodymamic pressures and flows reasonably close to a native pediatric system. However, similar to previous studies [78, 83, 85], the system is not capable of predicting the crucial features of the clinical pressure waveforms. For instance, comparison of the measured aortic pressure and the corresponding clinical data in Figure 1.28 indicates that the sharp rise of the aortic pressure waveform during the systolic phase is not close to the corresponding clinical waveform. It is apparent that the use of a pneumatic driver to actuate the ventricles is not an accurate technique to simulate full phases of cardiac function.

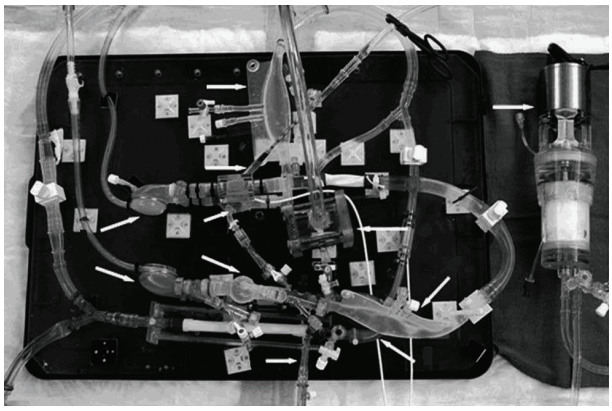

Figure 1.27: Photograph of the pediatric multi-chamber SCVL system. *From: G. M. Panatalos et al. [88], Expanded pediatric cardiovascular simulator for research and training, 2010.*

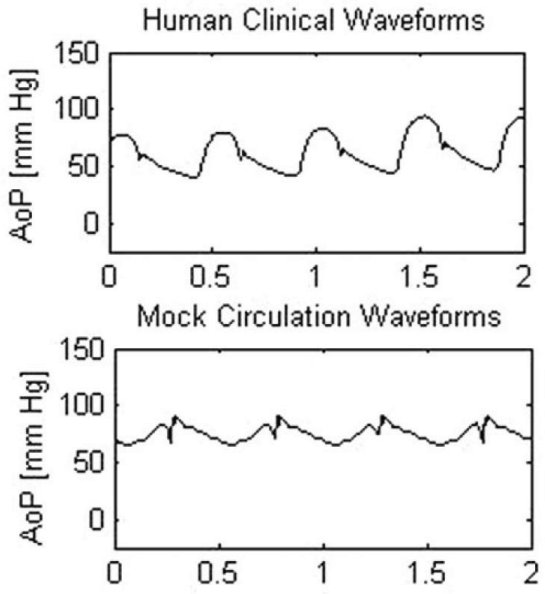

Figure 1.28: Comparison of the clinical and the experimental AoP for a controlled condition from the SCVL system. *From: G. M. Panatalos et al. [88], Expanded pediatric cardiovascular simulator for research and training, 2010.*

Another multi-chamber SCVL system was developed by Liu et al. [89] to investigate the hemodynamic response of the cardiovascular system to a left-side VAD. As shown in Figure 1.29, the ventricles are modelled by two silicon diaphragms which were embedded inside the corresponding pressurized air chambers. The expansion and the contraction of each of the chambers were controlled

by a pneumatic system. Air/water header tanks were used to model the venous chamber, the artiums and the pulmonary compliance. Clear tygon tubes were used to model the vasculature circulation and a number of tuning clamps were used to control the systemic and pulmonary resistances.

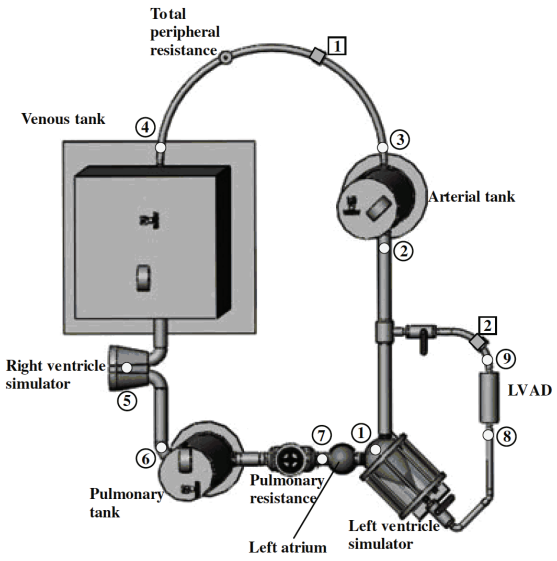

Figure 1.29: Schematic diagram of the multi-chamber SCVL system. *From: Y. Liu et al. [89], Mechanical simulator of the cardiovascular system, 2009.*

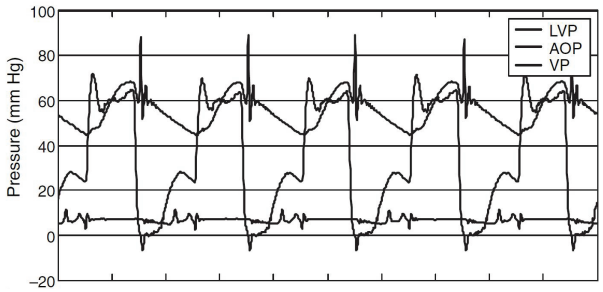

Figure 1.30: Experimental LVP and AoP for a diseased condition measured from the SCVL system. *From: Y. Liu et al. [89], Mechanical simulator of the cardiovascular system, 2009.*

Figure 1.30 shows that although the aortic and the left ventricle pressure are in reasonable agreement with the clinical data, similar to previous studies [78,

83, 85, 88], the SCVL system cannot predict the crucial feature of the clinical pressure waveform. Moreover, due to the limited displacement of the diaphragm in the ventricle chambers, the system has not adhered to the Frank-Starling law of the native heart. Thus, the system' response to the left-side VAD device is not reliable.

In a nutshell, the results from previous studies [78, 83, 85, 88, 89] show that although the measured hemodynamic findings from SCVL systems are in reasonable agreement with the clinical data, these cardiovascular emulators cannot predict the crucial clinical features as found in a native cardiovascular system. For instance, due to the inherent rigidity of the tubing system and the use of inappropriate compliance units, the original measured pressure waveforms carried significant levels of transient oscillations [83, 88]. Therefore, some features of the clinical aortic pressure waveforms such as the dicrotic notch were not captured. Further, it was observed that the implementation of the conventional pneumatic driver to actuate the ventricles produces better results compared to the use of a DC motor. However, the application of a pneumatic actuator has a drawback. For simulating the diastolic phase, the solenoid valve needs to be vented to the atmosphere resulting in an immediate vacuum. Therefore, the rapid and slow filling phases of the native system are not simulated properly. Another drawback of the previous SCVL systems is the lack of a full simulation of the atriums instantaneous activation function. In all previous studies [83, 88, 89, 90] including single-chamber, twin-chamber and multi-chamber SCVL systems, the atrium chambers are represented by an open to atmosphere header tank. Changing the height of the tank leads to a change of pre-load pressure in the ventricle chambers. However, in an intact heart, the atrium muscles are active and the pressure inside the atrium is not constant and varies instantaneously.

Considering the deficiencies of the existing SCVL systems, there has been a need to develop a multi-chamber SCVL system fully capable of simulating the hemodynamic features of a native cardiovascular system in different physiological and pathological conditions. The new cardiovascular simulator should replicate the whole cardiovascular system including the heart and the systemic as well as the pulmonic circulations. To avoid hemodynamic complications, as indicated in

the existing SCVL systems, an appropriate compliance unit for both the systemic as well as the pulmonary circulation needs to be incorporated. In addition, new sets of actuators which are able to model all four phases in one cardiac cycle need to be employed.

1.7 Aims and Objectives

It is demonstrated that the descending aorta can be a promising location to install a long-term implantable MCS device with minimally invasive surgery. However there is a theoretical concern that as the pump is operating in the descending aorta, there may be a steal phenomenon of blood from the brain and the upper extremities. In addition, there is a question associated with the effect of the pressure rise on renal perfusion.

The aim of this thesis is to conduct numerical and experimental investigations on the hemodynamics responses of the cardiovascular system aided with an MCS device operating in the descending aorta. The numerical and experimental simulations of the cardiovascular system allow investigation into the hemodynamic parameters of the whole circulatory system which is not feasible in a native human body due to the complexity of the system.

The objectives of this study are met by using our in-house multi-chamber SCVL system as well as the Concentrated Lumped Parameter (CLP) model developed by our team. In each case, different pathological conditions were simulated numerically as well as experimentally according to the clinical data.

1.8 Outline of the Thesis

A brief outline of the thesis is presented below.

Chapter 2 evaluates the performance of the multi-chamber SCVL system by simulating three physiological and pathological conditions; control, congestive heart failure (CHF) and left ventricular diastolic disfunction in hypertension (LVDDH). Using four tubular permanent magnet linear motors and working according to the prescribed elastance function of the native ventricles and atria shows the high success of this technique in emulating the contraction phase filling phases as found in the native cardiac muscle. In addition, in this chapter two rotary pumps, pump A and B, are introduced and the characteristics of each are evaluated at various rotor speeds.

Chapter 3 presents an experimental investigation on the novel approach of placement of the pump in the descending aorta, in-series with the heart, and its comparison with the traditional approaches of the Left Ventricle to Ascending Aorta (LV-AA) and the Left Ventricle to Descending Aorta (LV-DA), in-parallel with the heart. Tests were conducted by using the in-house multi-chamber SCVL system. The results indicate that the use of in-parallel LV-AA configuration leads to a significant improvement in the systemic and the pulmonic flow as the level of continuous flow is increased. The use of LV-DA in-parallel technique leads to an improvement in the systemic and pulmonic flow at lower level of continuous flow but at higher level of support leads to a flow retrogradation. In both in-parallel approaches (LV-AA and LV-DA), increasing the level of MCS continuous flow leads to a decrease in the aortic and the carotid pulse pressures to a certain extent. The results of the in-series configuration show that the pressure drop upstream of the pump facilitates the cardiac output as a result of the after-load reduction. Also the pressure rise downstream of the pump may assist with the renal perfusion. At the same time the generated pressure drop at the proximal part of the descending aorta induces a slight drop in the carotid perfusion which will be autoregulated by the brain in a native cardiovascular system. The pulse wave analysis show that the placement of the pump in the descending aorta, in

series with the heart, leads to improved pulsatility which is beneficial for end-organ functionality in the native cardiovascular system.

Chapter 4 presents a comprehensive numerical and experimental study on the novel approach of placement of the pump in the descending aorta, in-series with the heart, using the modified concentrated lumped parameter (CLP) model as well as the multi-chamber SCVL system respectively. The numerical results are compared and verified by experimental results under various conditions. Both experimental and numerical studies show that the generated pressure gradient in the descending aorta can lead to an increase in cardiac output and abdominal organs perfusion (e.g. liver, kidneys). Also, it causes a substantial improvement in the flow and pressure pulsatility. However, at the same time, depending on the level of pump support, it induces a slight drop in carotid perfusion, whom in a native cardiovascular system may be compensated through the auto-regulation system of the brain.

Chapter 2

Design and Development of Simulator of the Cardio-Vascular Blood-Flow Loop

2.1 Motivation

The design and development of a mechanical cardiovascular system simulator is motivated by the necessity and significance of in-vitro tests of various artificial devices such as heart valves, ventricular assist devices (VAD), mechanical circulatory support (MCS) devices etc. In order to model the whole cardiovascular system correctly, the characteristics of each part of the system should be modelled accurately. Although, it is practically impossible to accurately model every part of the cardiovascular system with in-vitro models, an approximate model in which all the key flow elements are represented is achievable.

The Simulator of cardiovascular loops (SCVL) systems are classified into three main categories based on the number of actuators implemented to simulate the heart chambers; single-chamber SCVL, twin-chamber SCVL and multi-chamber SCVL. The simplest SCVL system includes one chamber normally activated by a pneumatic actuator. This is easy to set up and cost effective. The objective of these devices would be, in general, to simulate the pressure-volume relation of the native heart [91, 92, 93, 94, 95, 96]. For instance Colacino et al. [78] and Ferrari et al. [81] separately developed a single-chamber SCVL system to emulate

ventricular function. The results show that single-chamber SCVL systems are able to successfully reproduce the time varying elastance of the native ventricle, thus achieving a good representation of Frank Starling's law of the heart, but they have limitations in reproducing the effects of pulmonary circulation in the system.

In a twin-chamber SCVL system the ventricle is normally actuated by a pneumatic pump and the atrium is simulated by an open-to-atmosphere water header tank which simulates the atrial pressure by the constant pressure from the head of water in the tank throughout the cardiac cycle. Two heart chambers (i.e. one atrium and one ventricle, or two ventricles), with two actuators, and up to three heart valves in addition to the resistances (R) and compliances (C) inherent to the system are required to closely emulate additional aspects of the circulation loops. For instance Garcia et al. [84] describes a twin-chamber SCVL system to investigate the effect of opening and closing the aortic valve on the hemodynamic response to the continuous flow produced by a left-side VAD. Other work conducted by Sharp et al. [86] describes a twin-chamber SCVL to study the effect of arterial impedance on the closing dynamics of prosthetic heart valves. These devices have good ability to replicate the action of the native system at physiological and pathological conditions, but they have inherent limitations in emulating the atrium-to-ventricle and ventricle-to-artery interactions of both systemic and pulmonary circulations. In order to investigate the central and peripheral hemodynamic variables of the systemic and pulmonary circulations simultaneously SCVLs need additional features.

The increasing number of patients using VADs and MCS devices requires more elaborate methods to study the hemodynamic impact of these devices (for instance to simulate the effect of the addition of continuous flow devices on the resultant overall pulsatile flow from the combination of the native heart and VAD/MCS).

In general a multi-chamber SCVL consists of four chambers of the heart, both systemic and pulmonary circulations, and up to five mechanical or biological valves. The results for all previous studies on multi-chambers represent accurately

diastolic and systolic pressure and flow rate; however, the features of the pressure waveform are not well captured, particularly at the interface between the cardiac chamber and the valve where there seems to be a large pressure gradient across the valve [83, 88, 90, 97]. Another aspect of multi-chambers SCVL system, which has not been appropriately addressed, is the simulation of the full atrial instantaneous activation function, particularly the representation of the filling phase of the chamber [83, 88, 89, 90]. One of the purposes of this SCVL system is to simulate the arterial pressure waveforms, closer to a control condition as that found in the clinical setting, including a steep rise of the pulse pressure, dicrotic notch which is due to the closure of the aortic valve, and a gradual decline of pressure to the end-aortic diastolic pressure.

This chapter evaluates the performance of the multi-chamber SCVL system by simulating three physiological and pathological conditions; control, congestive heart failure (CHF) and left ventricular diastolic disfunction in hypertension (LVDDH). The experimental measurements are compared with the numerical data obtained with adaptations of programs described in different studies conducted by Korakianitis et al. [98, 99, 100, 101, 102, 103], where in addition to the previous work, we have added the upper limb and the lower limb segments. A comprehensive description of the modified numerical model will be presented in **Chapter 4**.

It is worth mentioning that Dr. Akbar Rahideh and Dr. Paula Ruiz have a had a significant collaboration in development of the multi-chamber SCVL system.

2.2 Methodology

Figure 2.1 and Figure 2.2 show a photograph and schematic representation of the multi-chamber SCVL system respectively. The multi-chamber SCVL system can be classified into three main parts:

- Heart model

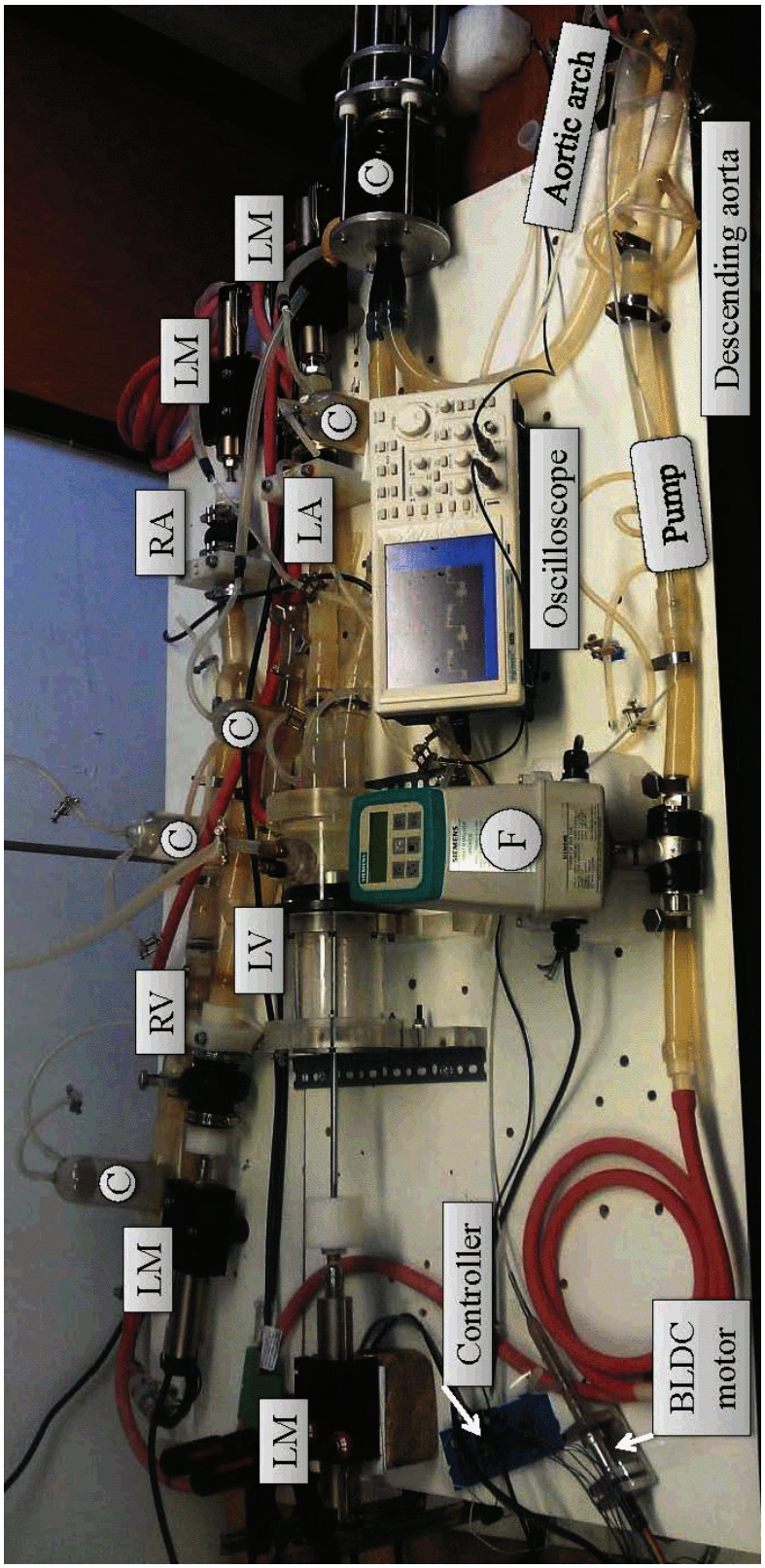

Figure 2.1: Photograph of the multi-chamber SCVL test-rig, LM: Linear Motor, LA: Left Atrium, LV: Left Ventricle, RA: Right Atrium, RV: Right Ventricle, C: Compliance, F: Flow meter.

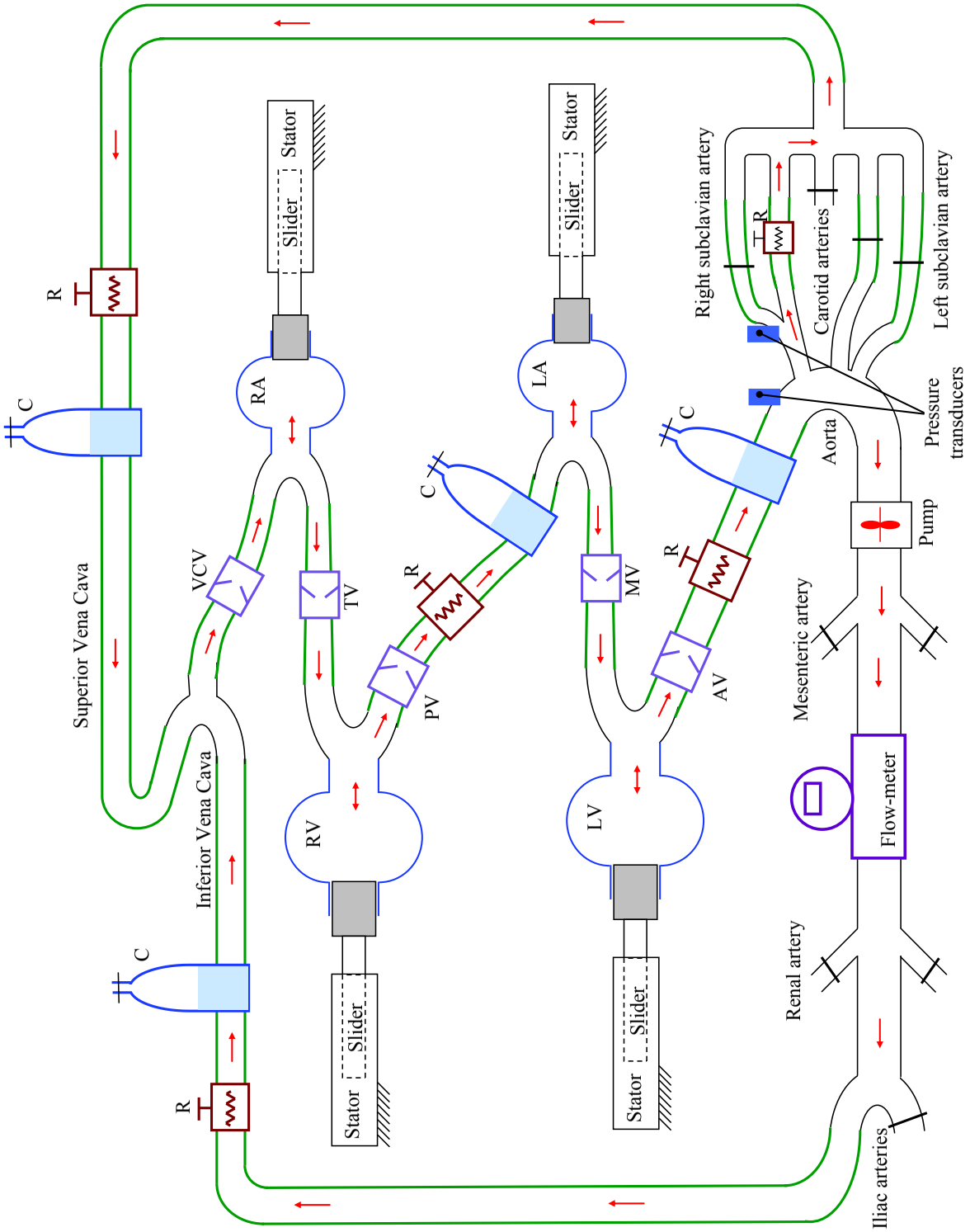

Figure 2.2: Schematic diagram of the SCVL system.

- Pulmonary and systemic circulations
- Control, measurement and monitoring systems

The heart model consists of four chambers, four actuators and four heart valves.

2.2.1 Chambers

The SCVL system consists of four chambers each representing an individual chamber of the native heart. Figure 2.4 shows the photograph of the left ventricle chamber. The left ventricle chamber was designed and manufactured separately based on the diaphragm pump mechanism with an internal size of 200 ml. The chamber consists of an acrylic cylinder and the inner diaphragm disk made of elastic rubber, as shown in Figures 2.3. The diaphragm disk is connected to a linear motor. Changing the position of the linear motor, according to the time varying elastance function of the left ventricle, leads to a change in position of the diaphragm inside the chamber.

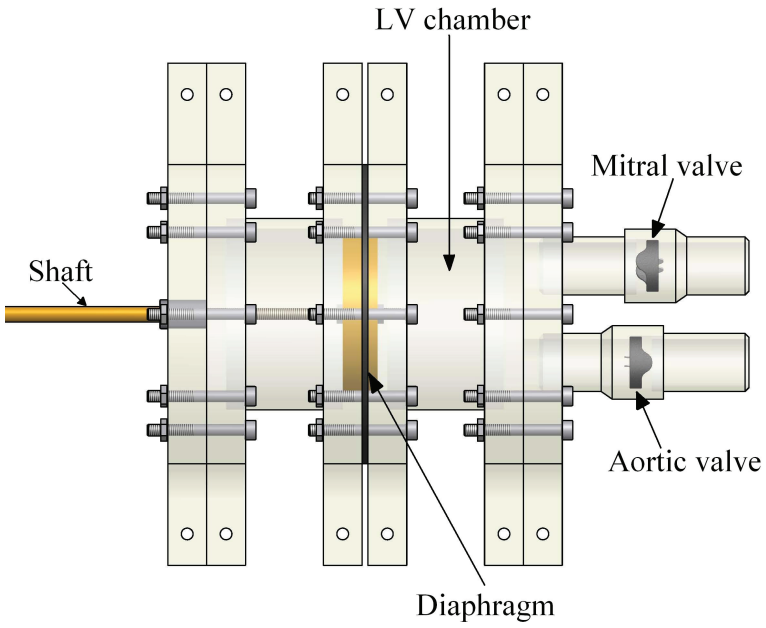

Figure 2.3: Schematic diagram of the left ventricle chamber.

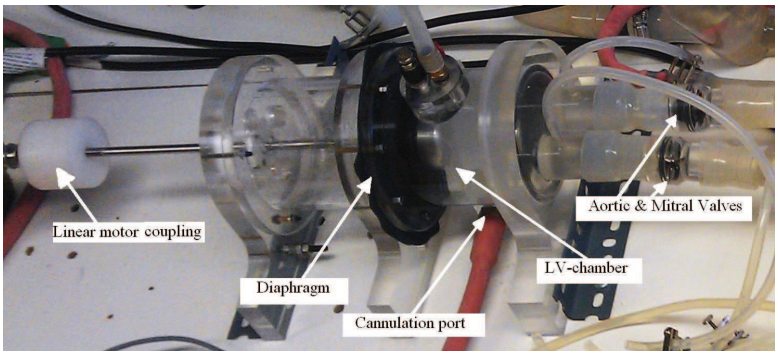

Figure 2.4: Photograph of the left ventricle chamber.

For modeling three other chambers, including the right ventricle, right atrium and left atrium, three rubber gaiters with proper sizes (right ventricle with a volume of 120 ml; left atrium and right atrium with a volume of 50 ml) are used to represent the three native heart chambers, as shown in Figure 2.5. Each rubber gaiter is connected to an individual linear motor. Driving each rubber gaiter back and forth, according to the corresponding time varying elastance function, simulates the diastolic and systolic phases of the native heart chambers.

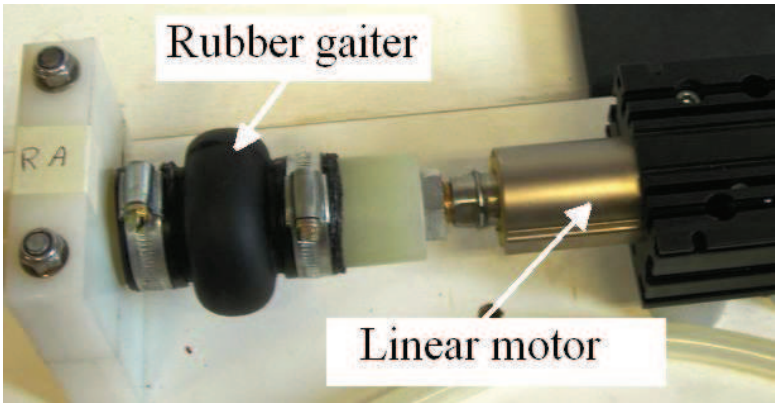

Figure 2.5: Photograph of the right atrium chamber.

2.2.2 Actuators

In previous studies, stepper motors [97] or pneumatic actuators [83, 88, 89, 90] have been used to actuate the heart chambers. Stepper motors are not the obvious

choice when a system is required to emulate pathophysiological conditions as there would be a need to change the mechanism.

Conventional pneumatic actuators accurately simulate the contraction phase of the cardiac muscle by injecting compressed air into a flexible membrane. A downside of the pneumatic actuator is that for simulating the diastole, the solenoid valve needs to be vented to atmosphere resulting in an immediate vacuum; consequently, the rapid and slow filling phases of the native system are not simulated.

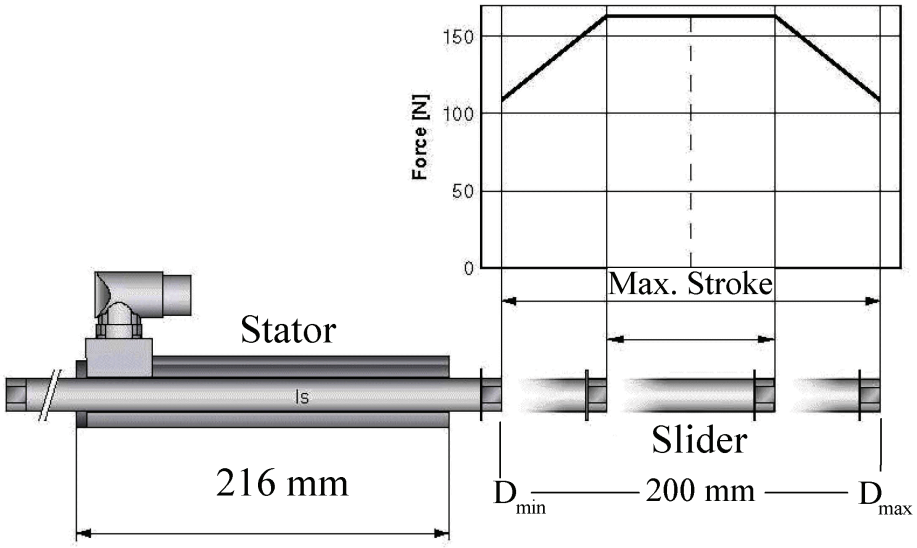

Figure 2.6: Schematic representation of the linear motor.

In our study four identical tubular permanent magnet linear motors (P01-37x120 from LinMot, Switzerland) have been employed to drive the four chambers of the heart. As shown in Figure 2.6, each linear motor consists of a cylindrical slider which moves linearly inside a stator. The maximum stroke displacement is 1460 mm. Each linear motor produces the peak force of 163 N with a maximum velocity of 3.2 m/s.

2.2.3 Heart Valves

A heart valve is a unidirectional valve which operates on the basis of the pressure difference on either side of the valve. The best option for heart valves to be used in SCVL systems is off-the-shelf artificial heart valves. Two main types of artificial heart valves are the mechanical and biological valves. The mechanical valves are divided further into ball and cage valves, tilting disc valves, bi-leaflet valves and polymeric valves. The mechanical valves are stronger and more fault tolerant than biological valves. The drawback of mechanical valves is that their inflexible structure may cause some unwanted hemodynamic oscillations [46].

Biological valves normally consist of two or three leaflets made of animal tissues. Similar to natural valves in a native body, the opening-closing mechanism of biological valves is based on the pressure gradient across the valves. If the upstream pressure is greater than the downstream pressure, leaflets are pushed outward to let the flow pass whereas if the downstream pressure is greater than the upstream pressure then the leaflets overlap in the center and do not allow the retrograde flow. Biological valves show better functionality compared to mechanical valves and they cause less biological complications such as thrombology. However they are more expensive and their long-term durability is lower than the mechanical valves [104]. Figure 2.7 (a-b) show two types of off-the-shelf mechanical valves and biological valves respectively.

In previous studies on SCVL systems, both the mechanical and the biological valves have been employed. For instance, Timms et al. [83] implemented a couple of swing check valves to simulate the four heart valves. In another study conducted by Sharp et al. [86], the mitral valve was modeled by a polyurethane tri-leaflet valve and the aortic valve was modeled by a rigid tilting disk. Hemodynamic results showed significant transient oscillations on the pressure and flow traces. This is regarded as the hammer effect and it is due to the sudden opening-closing mechanism of the rigid tilting disk. In another study conducted by Garcia et al. [84] both the mitral and the aortic valves are modeled with two tricuspid porcine-bio-prosthetic valves. Hemodynamic results showed less transient harmonic effects on the pressure and flow waveforms.

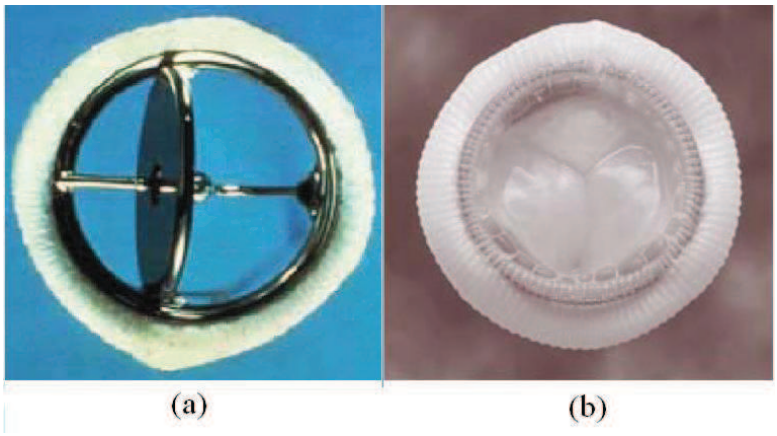

Figure 2.7: Photograph of (a) Mechanical valve, (b) Biological valve. *From: H. Mohammadi [104], Prosthetic aortic heart valves: Modeling and design, 2011.*

In our study as illustrated in Figure 2.2, four tilting disc heart valves corresponding to the mitral, pulmonary, tricuspid and the aortic valve have been used in the vicinity of each chamber to control the unidirectional flow. In addition, another mechanical valve is set at the end of the vena cava before the right atrium to help venous return and prevent backflow of blood. These five mechanical heart valves are Medtronic's 29 mm diameter Hall Easy-Fit mechanical valves (Minneapolis, Minnesota, USA).

2.2.4 Resistance Units

Vascular resistance is the key factor to control the blood perfusion in different parts of a native cardiovascular system. The level of resistance in each local vessel is variable. The resistance level in any local vessel changes inversely with the flow rate. In large arteries, due to the low level of resistance, the pressure drop is small, whereas in arterioles and terminal arteries, due to the high level of resistance, the pressure drop is more pronounced [1]. Variable resistances can be introduced into a mock cardiovascular system to mimic different conditions and diseases. Two major concepts for introducing resistances into the system is to implement the proportional multi-turn pinch or globe valves which can be controlled manually or automatically using stepper motors.

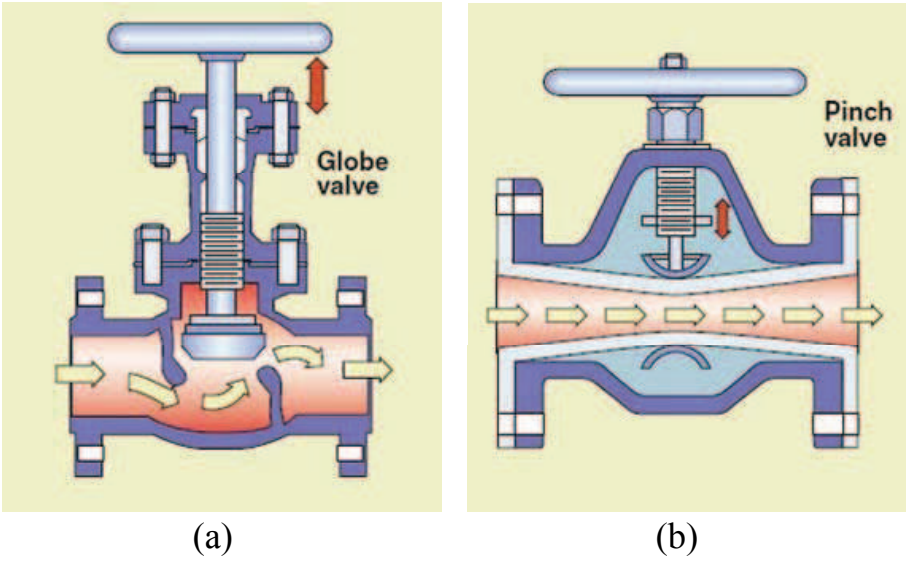

Figure 2.8: (a) Globe resistance, (b) Pinch resistance.

In the study by Timms et al. [83], the vascular resistance of arteries, capillaries and veins of the systemic as well as the pulmonic circulations were combined into two lumped resistance units using two control pinch valves which are adjusted by the input voltage. In the studies by Colacino et al. [78] and Legendre et al. [85], a screw clamp was placed in the aorta to change the ventricular after-load pressure for different pathological conditions. The after-load pressure can be increased or decreased by tightening or loosening of the resistance. In another study by Pantalos et al. [88], the total systemic as well as pulmonary resistance were modelled using a tuning clamp and a gate valve respectively.

In our study total systemic and pulmonary resistances have been modelled by using a set of adjustable resistors (Hoffman clips screw-type occluder). Figure 2.9 shows a photograph of the Hoffman clips. The resistance level can be increased or decreased by tightening or loosening of the screw. As it is evident in Figure 2.2, a set of clips have been distributed proportionally in different parts of the SCVL system. The level of resistance at various parts of the systemic and pulmonary loops has been manually adjusted to mimic different pathological states.

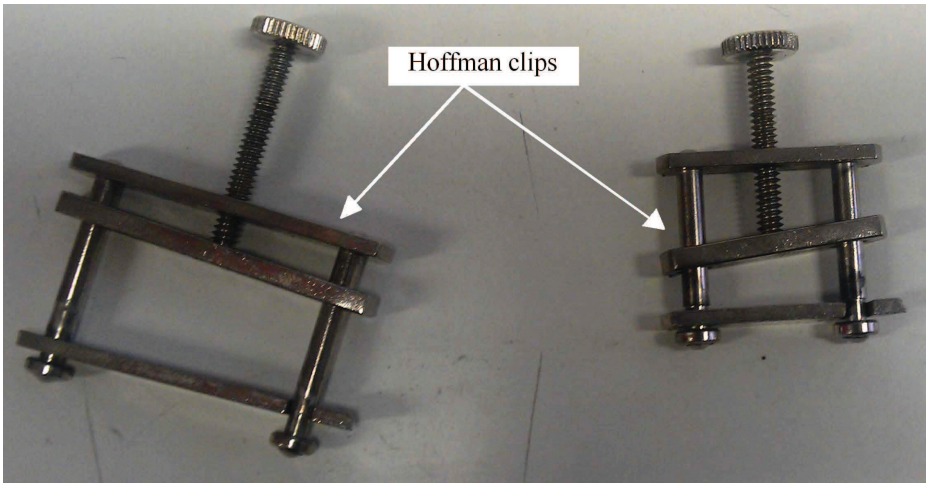

Figure 2.9: Hoffman clips resistances.

2.2.5 Compliance Units

One of the most influential characteristics of an SCVL system is the compliance unit. The compliance unit should preferably be adjustable to provide the opportunity to mimic different conditions and diseases. In prior studies [83, 85, 87, 88, 89], to simulate the compliance of a native vascular system, different ideas have been implemented.

A simple idea is to use a highly compliant balloon placed in a bucket of water, as shown in Figure 2.10(a). Any change in the level of water in the bucket changes the compliance level. Another concept, as shown in Figure 2.10(b), is a cylinder and piston concept. In this concept, the piston is connected to a fixed plate through a number of springs. Use of a different spring constant or a change in the number of springs changes the compliance level. The latter concept which has been employed in this investigation, as shown in Figure 2.10(c), consists of a chamber partially filled with liquid, with compressed air above the water column. Any change in air pressure results in a change in the compliance level.

Timms et al. [83] have employed a couple of tunable pressurised air-water chambers. In the other studies conducted by Pantalos et al. [88] and Legendre et al. [85], both the systemic and venous compliances have been modelled by a

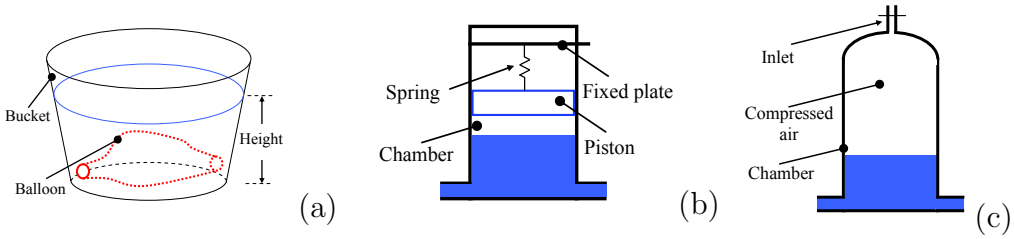

Figure 2.10: (a) balloon and bucket concept, (b) piston and cylinder concept, and (c) pressurized air-water concept.

piston cylinder mechanism loaded through a spring. Liu et al. [89] have employed three pressurised air tanks for simulating the systemic as well as pulmonary compliances. The level of air pressure inside each tank is adjusted by a valve provided on the top and it is measured by a pressure gage.

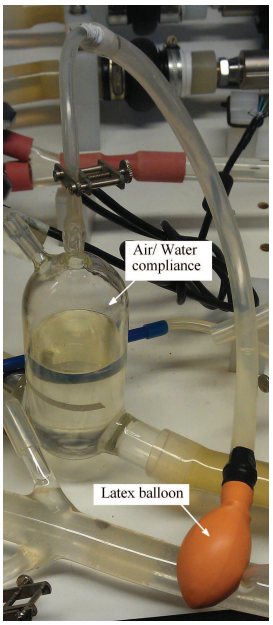

Figure 2.11: Photograph of the air/water compliance unit connected to a latex balloon.

In our study two different compliance units have been employed:

- Air/water compliance
- Rubber-bellows compliance

The air/water compliance units have been modelled by using four air capacitors which consist of a chamber partially filled with both water and compressed air, with one located in the ascending aorta, one in the pulmonary circulation, and two in the vena cava artery, as shown in Figure 2.2. The level of air pressure in each compliance has been adjusted via a sphygmomanometer for various physiological conditions. Any change in air pressure changes the level of compliance in the system. In order to increase the compliance characteristics of each unit, a latex balloon with particular specifications has been connected to each compliance unit, as shown in Figure 2.11.

In addition, due to the importance of the sinus aortic artery compliant characteristics, in various physiological and pathological conditions, in a native cardiovascular system, an individual compliance unit has been added to the ascending aorta. This compliance unit, as shown in Figure 2.12 has different specifications than the compressed air/water tank units. It consists of a rubber-bellow unit which is adjustable through a knob. Turning the knob clockwise and anticlockwise results in various levels of compliance into the system.

2.2.6 Systemic and Pulmonic Circulation

The model of the systemic and pulmonic vasculature was conducted with the intention of accurately distributing the cardiac output to the upper body, lower body and the heart. The replicated systemic and pulmonary vasculature are presented in Figure 2.2.

The aortic artery and abdominal artery segments are made of glass and the rest of the systemic and pulmonary vasculature are reproduced using 24 mm diameter rubber tubing, according to the anatomical features similar to a study conducted by Pantalos et al. [88].

Figure 2.2.6(a) and Figure 2.2.6(b) show the schematic diagrams of the aortic artery segment and the abdominal artery segment respectively. The aortic artery segment consists of the ascending aorta and its branches, right and left subclavian

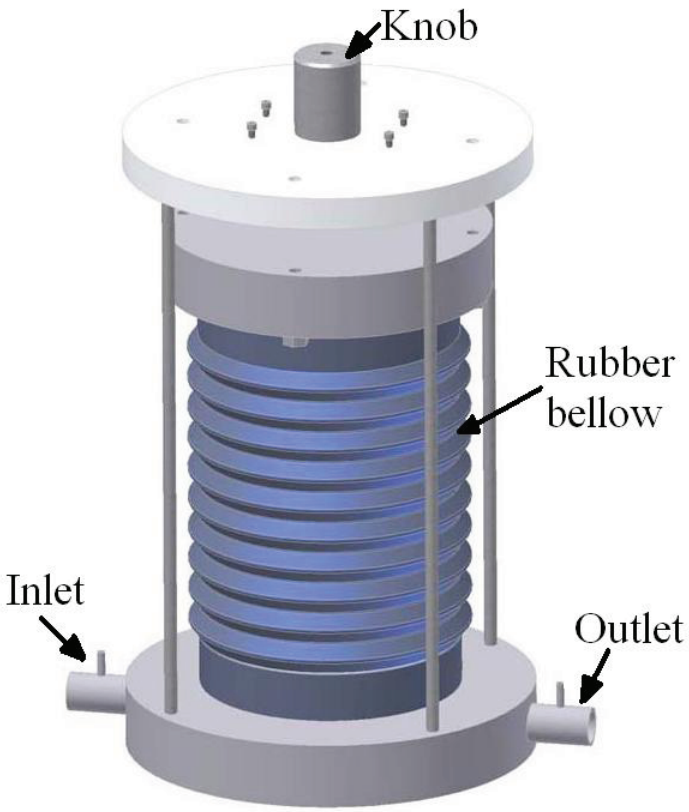

Figure 2.12: Schematic diagram of the rubber-bellow compliance.

arteries, right and left common carotid arteries and the brachiocephalic trunk. The abdominal artery segment consists of the right and left renal arteries and common iliac branches.

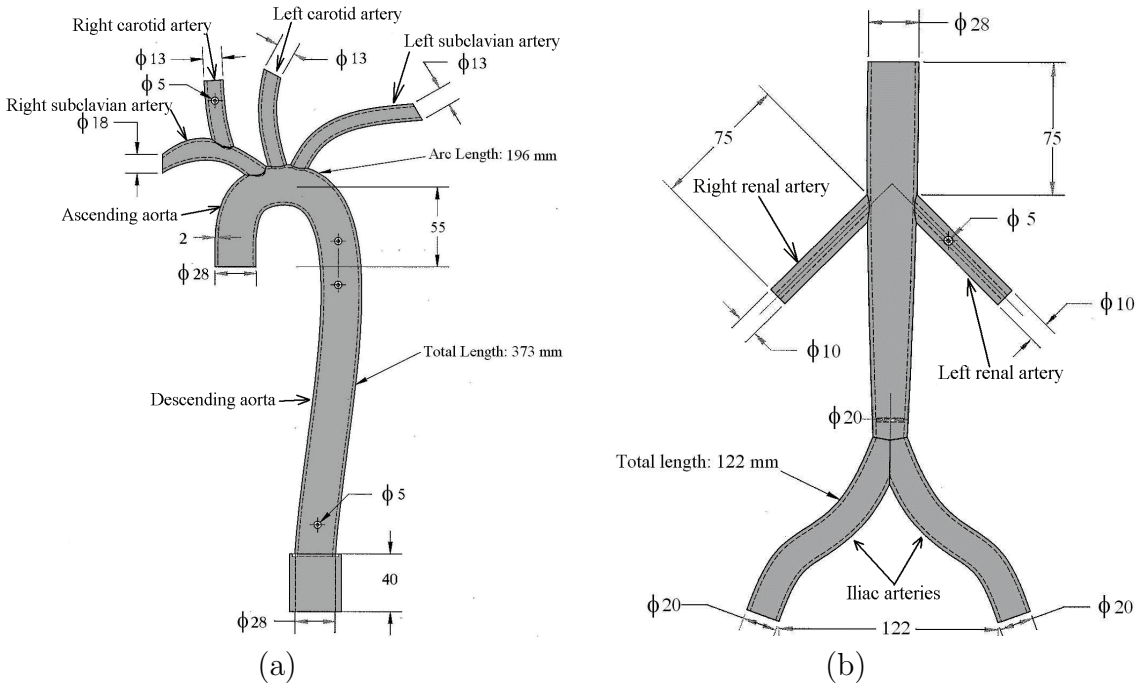

Figure 2.13: (a) Schematic diagram of the aortic artery section, (b) Schematic diagram of the abdominal artery section.

2.2.7 Control System

A control system, integrated in an SCVL system, can either be open-loop or closed-loop. Figure 2.14 shows the schematic diagram of the open-loop control system. The open-loop control systems do not use the measured signals in the control process and the desired trajectory signals to the actuators are predefined, so there is no need for a sensor. The advantage of an open-loop system is that it is low cost and easy to set up. However, in an open-loop system, producing a desired signal is not an easy task and it can be done manually through a trial and error process. Moreover,an open-loop control system cannot compensate for any disturbance or fault in the system. Owing to the simplicity and low cost, the open-loop control systems have been integrated into a number of prior studies on SCVL systems [85, 86].

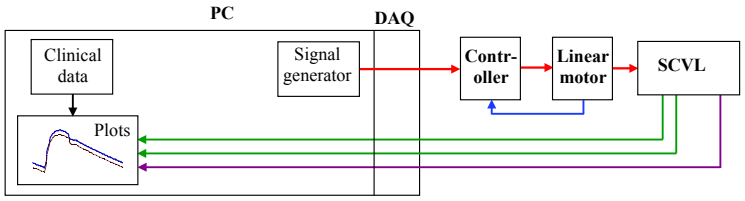

Figure 2.14: Schematic diagram of an open-loop control system.

Figure 2.15 shows the schematic diagram of the closed-loop system. In a closed-loop control system, the measured signals are fed back to the controller to change the desired trajectory signals based upon the instantaneous error between the desired and the measured signals. Sensors are necessary compartments of the closed-loop-control system. A closed-loop proportional-integral control system is more accurate, complex and expensive than the open-loop control system but it performs well for a multi-variable system. However the drawback of using a closed loop system for a multi variable system is that if one of the variables are not well-tuned, due to the disturbances in feedback signals, the system may become unstable.

Colacino et al. [78] employed the closed-loop system to control the displacement of the left ventricle actuator. In their study, the left ventricle pressure is chosen

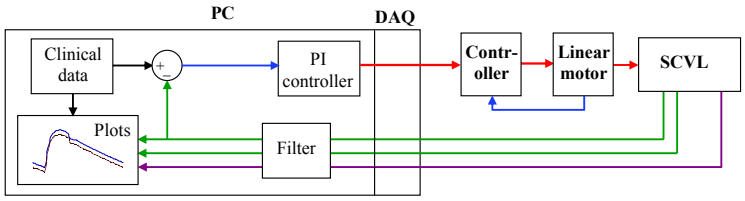

Figure 2.15: Closed-loop control system diagram.

as a control variable. So, in each cardiac cycle the pressure inside the ventricular chamber is measured by a pressure transducer and is fed back to the controller. The actuator displacement is adjusted in accordance with instantaneous error between the desired and real measured pressure signals.

In our study, due to the simplicity and low cost, the open-loop control system has been integrated into our multi-chamber SCVL system. Figure 2.16 shows the schematic diagram of the open-loop control system employed in the multi-chamber SCVL system. To control the position of the motors, a controller (E400 from LinMot, Switzerland) with 4 control channels is employed which is able to accurately and independently control the displacement of each slider according to a predefined time-varying function as shown in Figure 2.17.

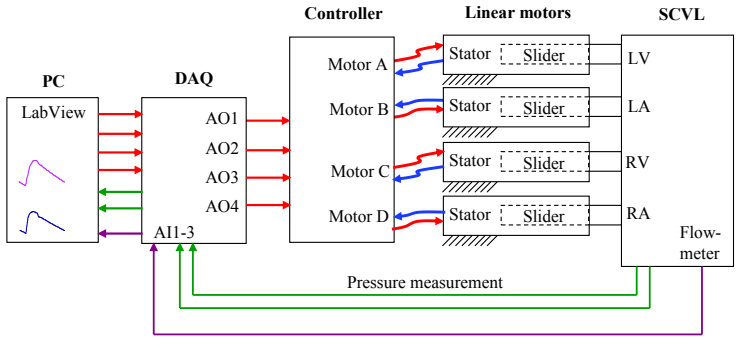

Figure 2.16: Schematic diagram of the open-loop control system, employed in the multi-chamber SCVL system.

A high speed, high performance Data AcQuisition card (DAQ) with four analogue outputs, 16 analogue inputs and 48 digital input/outputs (NI PXIe-6368 from National Instrument, Hungary) has been used. DAQ sends the desired

displacement trajectories from the PC to the linear motor controller as well as it reading the measurement signals from the pressure transducers and the flow meter into the PC.

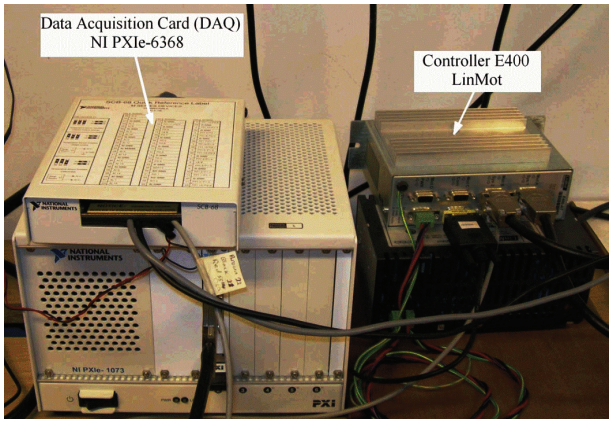

Figure 2.17: Photograph of the DAQ card and the linear motors controller.

The desired trajectory generation and monitoring tasks have been achieved using the NI LabView program. Figure 2.18 shows the NI LabView program on the computer screen monitoring the measured signals in red and desired trajectories in green. The upper panel and the lower panel show the measured aortic pressure waveform before and after tuning the SCVL system respectively.

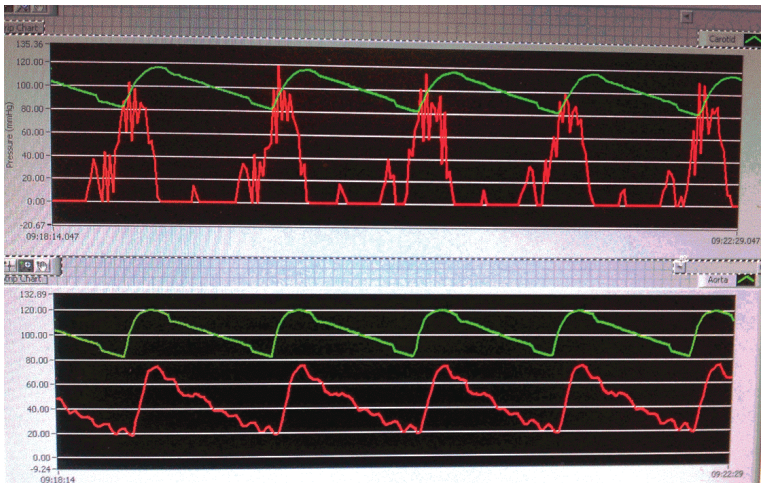

Figure 2.18: Monitoring the measured signals and desired trajectories on computer screen using NI LabView program.

2.2.8 Time-Varying Elastance Function

The dynamic action of the heart is governed by the Frank-Starling law [80] which can be functionalized in the ventricular and the atrial chambers in response to the pre-load variation in order to simulate the physiological and pathological conditions.

A wide number of variable elastance functions have been developed in order to reproduce the Starling's law of heart [91, 92, 93, 94]. Suga et al. [93, 94] in 1973 developed the first numerical elastance function of the left ventricle which reproduces the Starling's law of a native heart. They concluded that the pressure-volume ratio (Elastance) is independent of the end-diastolic volume (pre-load) as well as the arterial pressure (after-load) and hence could be used to characterize the ventricular contractility. The classical Suga-Sagawa model utilizes linear relation between simultaneous intraventricular pressure and volume. Since then, many researchers in various studies [78, 81, 95, 96, 105] have improved and optimised the classical Suga-Sagawa model to achieve closer agreement with the complex and time-varying mechanism of the native heart in various physiological and pathological conditions.

In our study, each linear motor slider is displaced, according to the well established time-varying elastance model as used in different studies conducted by Korakianitis et al. [98, 99, 100, 101, 102, 103] to individually activate the four chambers. Considering the left ventricle for instance:

$$\mathrm{D_{lv}(t)} = \mathrm{D_{lv_{min}}} + \frac{\mathrm{D_{lv_{max}}} - \mathrm{D_{lv_{min}}}}{2} e(t) \tag{2.1}$$

where $\mathrm{D_{lv}}(t)$ represents the time-varying displacement of the left ventricle linear motor as a function of the maximum and minimum position of the slider ($\mathrm{D_{max}}$ and $\mathrm{D_{min}}$) and e(t) represents the activation function as adopted from studies conducted by Korakianitis et al. [98, 99, 100, 101, 102, 103]. Equation (2.2)

presents the activation function of the left ventricle in a single cardiac cycle:

$$e_{\mathrm{lv}}(t) = \begin{cases} 1 - \cos\left(\dfrac{t}{\mathrm{T_{vc}}}\pi\right) & : \quad 0 \leq t < \mathrm{T_{vc}} \\ 1 + \cos\left(\dfrac{t - \mathrm{T_{vc}}}{\mathrm{T_{vf}} - \mathrm{T_{vc}}}\pi\right) & : \quad \mathrm{T_{vc}} \leq t < \mathrm{T_{vf}} \\ 0 & : \quad \mathrm{T_{vf}} \leq t < \mathrm{T} \end{cases} \tag{2.2}$$

where $\mathrm{T_{vc}}$ and $\mathrm{T_{vf}}$ are related to the time to reach the maximum contraction and that to initiate chamber filling of the left ventricle respectively. The model for the right ventricle is similar to that for the left atrium, apart from the parameters. Equation (2.3) presents the activation function of the left atrium in a single cardiac cycle:

$$e_{\mathrm{la}}(t) = \begin{cases} 0 & : \quad 0 \leq t < \mathrm{T_{ac}} \\ 1 - \cos\left(\dfrac{t - \mathrm{T_{ac}}}{\mathrm{T_{af}} - \mathrm{T_{ac}}}2\pi\right) & : \quad \mathrm{T_{ac}} \leq t < \mathrm{T_{af}} \\ 0 & : \quad \mathrm{T_{af}} \leq t < \mathrm{T} \end{cases} \tag{2.3}$$

where $\mathrm{T_{ac}}$ and $\mathrm{T_{af}}$ are related to the time to reach the maximum contraction and that to initiate chamber filling of the atrium respectively. The model for the right atrium is similar to that for the left atrium, apart from the parameters. The time parameters are listed in Table 2.1.

Table 2.1: List of time parameters.

Parameter	Value	Unit
HR	60	bpm
T	1.0	s
$\mathrm{T_{vc}}$	0.3	s
$\mathrm{T_{vf}}$	0.45	s
$\mathrm{T_{ac}}$	0.85	s
$\mathrm{T_{af}}$	1.0	s

2.2.9 Measurement Devices

Several measurement devices are employed to evaluate the performance of an SCVL system as well as to provide necessary feedback signals in the case of closed-loop control systems. Flow and pressure are the most important parameters to be measured. The volume measurement, additionally, can assist to further evaluate the performance of the test rig. The number of flow-meters, pressure transducers and volume sensors employed depend on the application, accuracy and the required outcome of the SCVL system.

Among various flow-meters such as nutating disk, oval gear, pressure-based, optical, thermal mass, vortex, magnetic, coriolis, ultrasonic and laser doppler flowmeters, the electro magnetic and the ultrasonic ones have been commonly used. An electromagnetic flowmeter integrates a couple of magnetic poles on either side of the flow stream. As semi-conductor flow cuts through the magnetic field it produces electric potential which is proportional to the flow velocity. Then, the diameter of the tube can be used to measure the flow rate [1]. In this study, as shown in Figure 2.19(a), an electromagnetic flow meter of SITRANS F M MAG 1100 F from Siemens, Germany has been employed to measure the flow rate of the ascending and the descending aorta.

Different pressure transducers are available including piezoresistive strain gauge, capacitive, electromagnetic, piezoelectric and optical variations types. The pressure transducers employed in the SCVL system should have the ability to measure the pressure in a range of 1-200 mmHg. This study employs a couple of pressure transducers of PMP1400 Druck from General Electric Company, as shown in Figure 2.19(b), to simultaneously measure the pressures at the key points in the system as shown in Figure 2.19(b). The operating pressure of the PMP 1400 pressure transducer ranges from 0 to 250 mbar gauge. The supply voltage ranges from 9 to 30V d.c. The output voltage ranges between 0 to 5V and the operating temperature ranges from -200°C to +800°C.

(a) (b)

Figure 2.19: (a) Flow meter (SITRANS F M MAG 1100 F), (b) Pressure transducers (PMP1400 Druck).

2.3 Rotary Pumps Simulating MCS

In general, centrifugal pumps are used to produce high pressure gradient and low flow rate conditions, whereas axial pumps are used to produce low pressure gradient and high flow rate conditions. The selection of the pump to be used as an MCS device depends on the pathological condition. The rotational speed in centrifugal pumps is much lower (2000-6000 rpm) than axial pumps (3000-20000 rpm), whereas the size of centrifugal pumps is, to some degree, larger than the axial pumps. An axial pump requires less invasive implantation surgery because it is smaller, whereas centrifugal pumps are more efficient than axial pumps due to their lower rotational speed and consequently result in less physiological complications. The typical operating condition for an MCS device implanted in parallel with the heart is 100 mmHg against 5 lt/min [106], while an MCS device implanted in the descending aorta, in series with the heart, typically operates at 24 ± 10 mmHg against 5 lt/min [53, 60, 61, 107].

In this study, two rotary pumps are used to simulate MCS devices. One has a centrifugal impeller (pump A) and the other has an axial impeller (pump B). Since this project has been conducted under severe constraints imposed by intellectual property of the Queen Mary University of London, the hydrodynamic aspects of the rotary blood pumps A and B are beyond the scope of this thesis and our focus will be on the hemodynamic responses of the SCVL system with these pumps integrated and operating at various conditions. The detailed design aspects of the pumps A and B, including the hydrodynamic and haemocrit performance, have been published in various internal reports and will be published in relevant journals in the near future. However, to give the reader an understanding of the MCS device design process the physical aspects of blood and MCS design constraints, which are essential to consider for the design of any rotary blood pumps, are discussed in Sections 2.4 and 2.5, respectively.

2.4 Physical Aspects of Blood flow

In contrast to an industrial application of rotary pumps in which some hydrodynamic losses including high shear stress, local recirculation or local acceleration can be largely neglected, in a clinical application these hydrodynamic losses may have a remarkable adverse effect on the properties of the blood. As a result, prior to designing an MCS device, it is important to understand various aspects of blood properties which may have a direct impact on the design procedure of an MCS device.

Blood is a combination of different elements including the red blood cells (RBCs), white cells and platelets suspended in a liquid known as plasma. The density of blood (1.05 g/cm^3) is slightly greater than that of water. Its main duty in the body is to transfer oxygen as well as nutrients from the left ventricle to the vital organs and transfer CO_2 as well as metabolic waste to the pulmonic circulation.

RBCs are one of the the most essential elements of the blood. Each individual RBC has a biconcave disc shape and a diameter and thickness of approximately 8 μm and 2 μm, respectively. The shape of RBCs can deform significantly as they pass through small arteries and capillaries due to a high shear stress in these regions.

Problems with high shear stress in rotary blood pumps have stimulated a considerable amount of research on different aspects of blood complications, particularly RBC fragmentation [108, 109]. For instance, a controlled exam of shear-induced-haemolysis was conducted by Sutera et al. [108] using a concentric cylinder viscometer. This showed that high shear stress over a long exposure time can result in RBC fragmentation leading to the release of a certain level of haemoglobin into the plasma, which is known as haemolysis. Figure 2.20 shows the deformation and fragmentation of RBCs after four minutes under various level of induced shear stress in an experiment conducted by Sutera et al. [108].

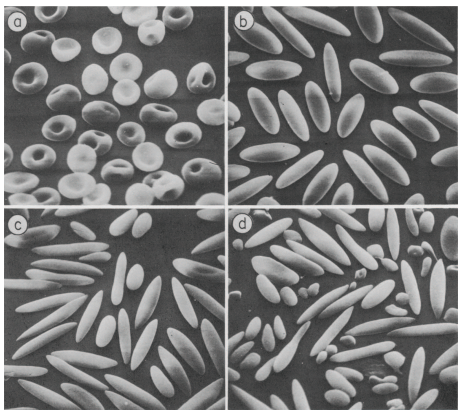

Figure 2.20: Photographs of RBCs at shear stress of (a) 10, (b) 200, (c) 250, (d) 400 Pascals over the exposure time of 4 min. *From: S. P. Sutera et al. [108], Deformation and fragmentation of human red blood cells in turbulent shear flow, 1975.*

Platelets are the other important elements of the blood to be considered for the design procedure of an MCS device. Platelet activation is the main cause of thrombus formation in the vicinity of mechanical heart valves or MCS devices. Platelet activation is more likely to develop in association with stagnant and recirculating flow or under high shear stress [110]. Once the platelets are activated they gradually accumulate on the surface and form thrombi at a rate determined by local flow conditions.

Another important element of the blood which can have a remarkable impact on an MCS design procedure is the blood viscosity. In a native cardiovascular system, the blood viscosity in large arteries is independent of the blood shear rate, thus it behaves as a Newtonian fluid. In small arteries the viscosity varies with the blood shear rate, thus the blood flow exhibits non-Newtonian behavior. Also, the viscosity of the blood is highly dependent on the haematocrit level. The haematocrit level is defined as the fraction of RBC volume to total blood volume. For instance, for a normal physiological condition where the haematocrit is about 45%, the blood viscosity is about 0.0036 pa.s [111]. This is about four times greater than the viscosity of water at room temperature. So any changes occurring on the haematocrit level due to some blood abnormalities such as haemolyis may have an impact on the blood viscosity.

2.5 MCS Design Constraints

2.5.1 Pump Size

One of the drawbacks of most first and second generation MCS devices is their large size. Implantation of a large mechanical device into the patients body is usually followed by some complications. In particular, very ill patients can develop severe organ infections, cancer or neurologic damage which may result in morbidity and mortality [47]. This is mainly due to the highly invasive tissue dissection surgery which increases the risk of infection [54]. Although the use of miniatured MCS devices with less invasive surgery may reduce the infection substantially, it must be noted that in order to meet the required parameters of the operating condition, the pump needs to be operated at a higher rotor speed which could potentially increase the risk of blood complications. As a result, it is highly important to optimise the hydrodynamic performance of the impeller and casing to minimise the shear stress, exposure time of the blood to contacting surfaces, local recirculation and stagnation.

2.5.2 Shear Stress and Exposure Time

As indicated in Section 2.4, blood impelled through an MCS device may experience a significantly higher degree of shear stress compared to a native arterial system. For smaller MCS devices with a higher rotational speed, the high levels of shear stress between the rotating impeller and casing increases the risk of blood complications. As a result significant attention should be paid to the hydrodynamic design of MCS device components. In many studies the maximum shear stress of 250 Pa has been used as the threshold for haemolysis formation, however it has been identified that the haemolysis is determined by both shear stress and exposure time [108]. In general, the RBCs that are exposed for very short periods can withstand very high level of stress, whereas prolonged exposure at much lower shear stress may result in some blood complications, particularly haemolysis and thrombosis. The effect of the shear stress and exposure time on

the haemolysis has been examined in previous studies [108, 114]. Many investigators have attempted to develop different empirical formulas for evaluation of the haemolysis level. For instance Giersiepen et al. [115] relates the shear stress and exposure time to the level of haemolysis, using Equation 2.4.

$$D = C^{\alpha}\tau^{\beta} \tag{2.4}$$

where D represents the damage fraction, t represents the time and τ represents the shear stress. C, α and β are constant values defined in empirical tests.

A wide number of computational fluid dynamic simulations have been conducted to investigate the haemolysis level of a number of MCS devices operating at various conditions [116, 117, 118, 112]. For instance, Song et al. [117] used a computational approach to estimate the level of haemolysis of a rotary blood pump by considering the shear stress histories of a number of particles traveling across the pump using the Lagrangian tracking method. Taskin et al. [116] performed a study on evaluation of Eulerian and Lagrangian models for haemolysis estimation. Zhang et al. [112] conducted a computational study on the level of shear stress in the secondary flow path of a newly developed centrifugal MCS device.

In order to validate the computational results, it is necessary to conduct in-vitro haemolysis testing. The experimental haemolysis test involves running the MCS device in a single loop for a certain period of time with animal blood as the working fluid. Different studies have been conducted on experimental evaluation of haemolysis level for a number of MCS devices operating over a certain range of rotational speeds [119, 112]. For instance, as shown in Figure 2.21 Zhang et al. [112] conducted an in-vitro test on a newly developed pump, CentriMag, to validate their computational results on the haemolysis level.

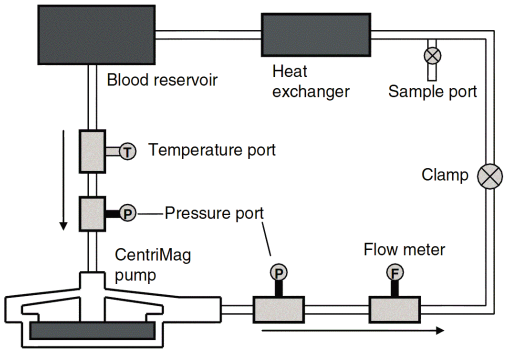

Figure 2.21: Schematic Diagram of the in-vitro Haemolysis test. *From: J. Zhang et al. [112], Computational and experimental evaluation of the fluid dynamics and hemocompatibility of the centrimag blood pump, 2006.*

2.5.3 Stagnant and Recirculation

Another crucial design constraint for an MCS device is to avoid thrombus formation. In the worst case scenario, thrombus formation may lead to embolism in the patients cerebral system which may result in morbidity and mortality. Two local flow conditions which may increase the risk of thrombus formation are re-circulating flow and stagnant regions. The incidence of both these conditions is highly dependent on the hydrodynamic design of the impeller passages. There are a number of geometrical parameters which can potentially minimise these local flow conditions. For instance in a centrifugal pump, the selection of number of blades greatly influences the hydrodynamic and hemolytic performance. A large number of blade sets reduces recirculation by making the impeller vane passages become narrower. However, for blood with viscosity four times higher than water, the larger surface area leads to greater friction and hydraulic losses which may result in a drop in efficiency and increase the blood temperature. A wide number of computational and experimental studies have been conducted on the effect of the impeller geometry on hydrodynamic and hemolytic performance of a rotary pump [120, 121].

2.5.4 Secondary Flow Path

Another design constraint which may have a crucial impact on the hydrodynamic efficiency as well as hemolytic performance of an MCS device is the size of the clearance gap between the impeller and the casing. For an MCS device there are two paths for the blood to travel. The primary path is the path through which the flow travels from the inlet to the outlet of the pump in order to generate the required flow and pressure. The secondary path exists to separate the rotating impeller from the stationary casing. The secondary flow path is more important in centrifugal than in axial pumps because centrifugal pumps generally have much longer secondary flow paths. Due to the small size and low flow rate of the secondary flow, there is a risk of haemolysis complications and platelet activation. Although increasing the size of the secondary flow path may improve the hemolytic performance, it may compromise the hydraulic efficiency of the pump. Computational Fluid Dynamic (CFD) simulation has been employed by a number of researchers [122, 123, 124, 112] to optimise the secondary flow path sizes leading to a lower risk of blood complications without sacrificing the pump's hydraulic efficiency. Figure 2.23 shows a schematic diagram of a centrifugal pump in which the secondary flow paths are represented by blue arrows.

2.5.5 Active and Passive Bearings

One of the major drawbacks of the second generation MCS devices incorporating mechanical bearings is the high risk of wear and thrombus formation in vicinity of the mechanical bearing and sealing due to blood stagnation. The life span of the second generation MCS device is around five years [125], so they can not be used for destination therapy. Exclusion of the mechanical bearing can minimise the shear stress level as well as the chance of stagnant flow formation around the mechanical bearings, thus eliminating the risk of wear and thrombus formation. For the third generation MCS devices the mechanical bearings have been replaced by magnetic bearings [123], hydrodynamic bearings [126], or combinations of both techniques [127]. Both magnetic and hydrodynamic bearings have their

own advantages and disadvantages.

The magnetic bearings are categorised into two classifications known as passive and active. The passive magnetic bearings operate based on the attraction and repulsion force between two permanent magnets where one is integrated into the impeller and the other into the casing. The passive magnetic bearing can create a high clearance gap between the impeller and casing with less complexity and lower energy consumption. However, from the physical point of view, the passive magnetic bearings can not be used independently and hence should be combined with other types of bearings [128]. Similar to the passive magnetic bearings, the active magnetic bearings can operate at high clearance and thereby minimise the risk of blood complication. For instance, the UltraMag pump [123], incorporating an active magnetic bearing, allows the minimum clearance gap of 500 μm. However, the active magnetic bearing requires a complex feedback system to control the position of impeller, resulting in high energy consumption.

The passive hydrodynamic bearing system is less complex but requires a minimal clearance gap to operate. The passive hydrodynamic bearing systems use pressure built up between the impeller and casing to generate the thrust in a similar fashion to journal bearings. For instance, the VentrAssist pump [126], incorporating passive hydrodynamic bearings requires a clearance gap between 50 and 200 μm for suspension of the impeller. Although the passive magnetic bearings consume less energy than the active magnetic bearings, it must be noted that the small clearance gap required for the hydrodynamic bearing may increase the risk of blood complications over off-design operating conditions.

Figure 2.22 and Figure 2.23 show a schematic diagram of an axial and a centrifugal MCS device, respectively. It must be noted that these two figures are only to aid understanding and do not represent our MCS devices' configurations.

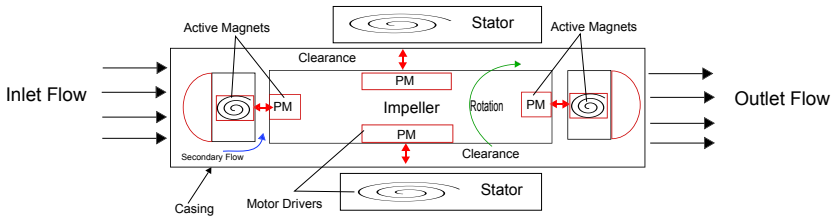

Figure 2.22: Schematic diagram of an axial MCS device implementing two axial active magnetic bearings.

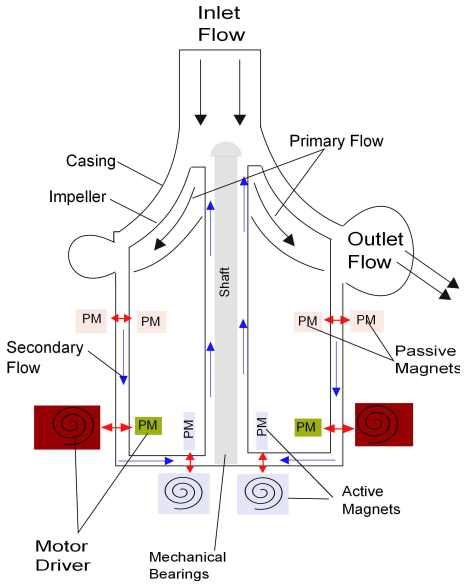

Figure 2.23: Schematic diagram of an centrifugal MCS device implementing combination of active and passive magnets.

2.6 In-Vitro Test of Pump A and B

A single loop test-rig which will be called O-loop hereafter was developed for initial testing of pump A and B to find the characteristics of each pump (flow-rate versus pressure difference at various rotor speeds). The O-loop consists of a place for the pump installation, a valve to change the resistance of the loop, a flow meter to measure flow and two pressure transducers for pressure measurement. Figures 2.24 and 2.27 show the installation of pump A and B in the O-loop test-rig respectively.

2.6.1 Pump A

Rotary pump A is a centrifugal pump with a maximum pressure difference of 105 mmHg and a maximum flow-rate of 9.5 lt/min at the rotor speed of 2400 rpm. The pump pressure difference was defined by the inlet and outlet pressure ($\Delta P = P_0 - P_i$). The pressure difference versus flow-rate was recorded while the circuit resistance was increasing. Figure 2.25 shows the pressure difference versus flow-rate characteristics of the pump A at nominal impeller speed of 2400 rpm. The results of pump A implanted in parallel configurations, both connected from the left ventricle to the descending and the ascending aorta, will be discussed in Chapter 3.

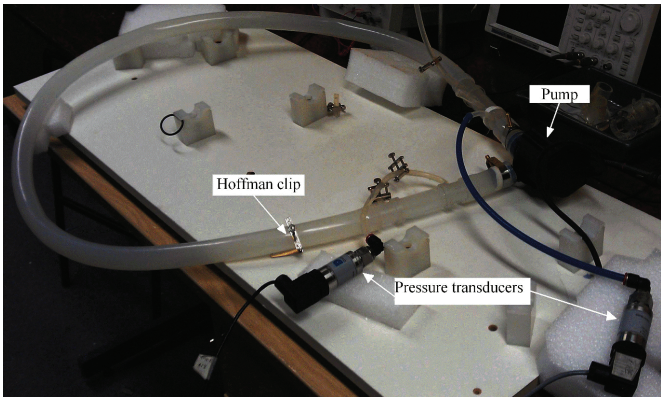

Figure 2.24: Photograph of centrifugal pump A in the O-loop test bench.

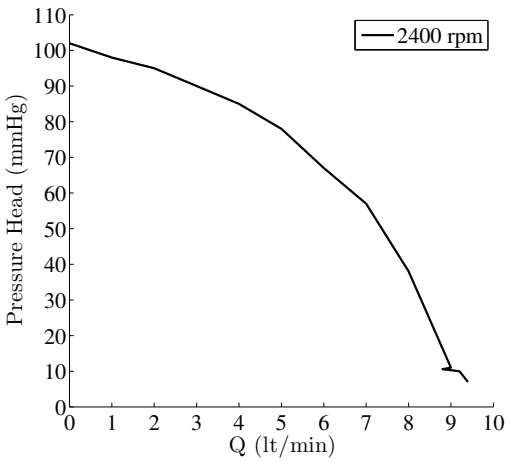

Figure 2.25: Pressure difference (mmHg) verses flow-rate (lt/min) for pump A.

2.6.2 Pump B

Rotary pump B is an axial pump which has been designed and developed for an earlier CHF stage III and possibly CHF stage II to slow down and prevent the progression from stage II to IV with less possible invasive surgery. This pump produces a maximum pressure difference of 35 mmHg and maximum flow-rate of 10 lt/min at the highest rotor speed.

As shown in Figure 2.26, pump B consists of a high speed BrushLess DC (BLDC) motor, a controller designed to control the motor speed and a coupling mechanism to directly drive the rotor of the pump. The rotational speed of the motor drive has been changed from a low value to a nominal maximum speed (2400-6000 rpm). The pressure difference versus flow-rate characteristics of the pump B was investigated under a static flow condition, in the O-loop, as shown in Figure 2.27.

For monitoring the speed of the motor drive, an oscilloscope device has been integrated into the system. The applied voltage has been kept constant at 24V and the drawn current has been measured at each rotational speed to calculate the electrical input power. At the same time the pressure before and after the blade have been measured at each rotational speed using two pressure transducers

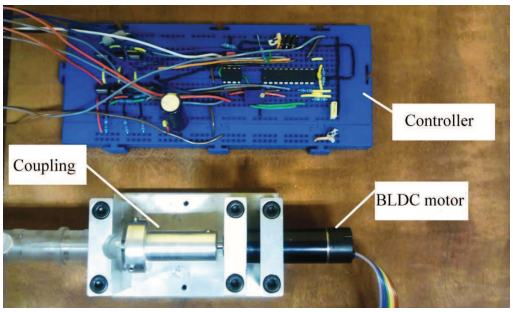

Figure 2.26: Photograph of the components of pump B including the high speed motor, the controller and the coupling.

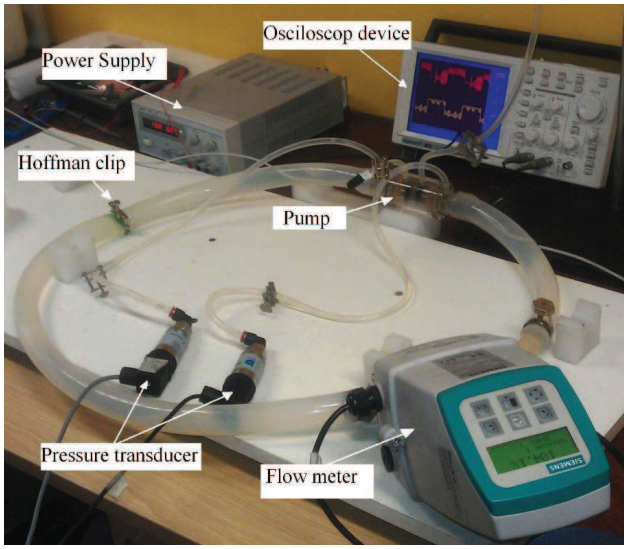

Figure 2.27: Photograph of the axial pump B in the O-loop test bench.

to calculate the inlet and outlet pressures due to the blade ($\Delta P = P_0 - P_i$). The corresponding flow due to the blade rotation has been measured at each rotational speed. All the measurement processes have been repeated for a wide range of resistances from low to high using a set of Hoffman clip. Figure 2.28 shows the graph of pressure difference versus flow-rate for the pump B. The results of pump B implanted in the descending aorta, in series configuration with the heart, will be discussed in Chapter 3 and Chapter 4. In addition, in Chapter 4, the numerical model of pump B integrated in the concentrated lumped parameter model will be examined.

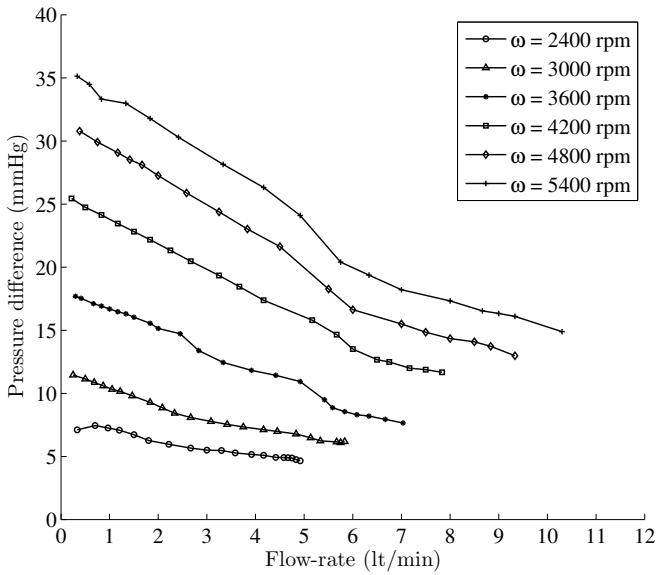

Figure 2.28: Pressure difference (mmHg) verses flow-rate (lt/min) for the prototyped axial pump B.

2.7 Implementation of the SCVL System

This chapter evaluates the performance of the SCVL system with simulation of the physiological and pathological conditions. Three cases have been studied; controlled condition, congestive heart failure (CHF), left ventricular diastolic dysfucntion in hypertension condition (LVDDH). In each case the aortic sinus pressure and the carotid pressure waveforms and Cardiac Output (CO) were recorded as these are the gold standard of cardiac condition assessment [129]. In all four cases,the experimental aortic sinus pressure waveform and the carotid pressure waveform are compared to the numerical data obtained with adaptations of the programs described in previous studies conducted by Korakianitis et al. [98, 99, 100, 101, 102, 103].

2.7.1 Simulation of Controlled Condition

The pressure waveforms at the aortic sinus and carotid artery for controlled condition are demonstrated for two cardiac cycles in Figure 2.29(a) and Figure 2.29(b). In Figure 2.29(a), the dashed line is the clinical aortic pressure waveform extracted from the study conducted by Fischer et al. [2], the dashed-and-dotted line is the numerical data, and the solid line is the measured data from the SCVL. In Figure 2.29(b), the dashed-and-dotted line is the numerical data and the solid line is the measured signal from the SCVL system. It is evident from Figure 2.29(a) and Figure 2.29(b) that the aortic sinus pressure waveform is 125/75 mmHg, and the corresponding carotid pressure waveform is 120/72 mmHg. In both aortic sinus and carotid pressure waveform the dicrotic notch after the aortic valve closure is captured. The P_{mc} (mean circulatory pressure) of the system measured in controlled condition and it is 7 mmHg. The CO is measured in the ascending aorta. In the controlled condition the CO is 5.1 lt/min and the mean aortic pressure (AoP_{mean}) is 91.7 mmHg.

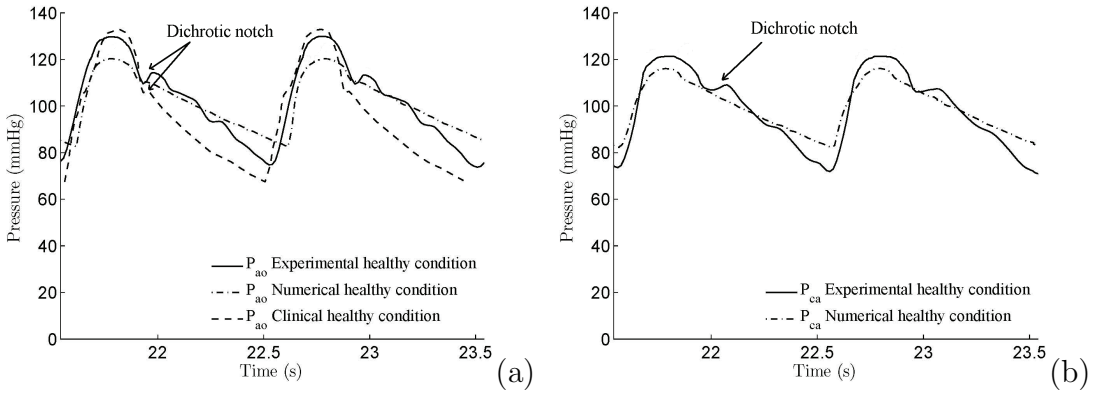

Figure 2.29: Comparison of the aortic and carotid pressure waveforms in controlled conditions. (a) aortic pressure is 125/75 mmHg, (b) carotid pressure is 120/72 mmHg, CO is 5.1 lt/min.

2.7.2 Simulation of Congestive Heart Failure Condition

The condition of Congestive Heart Failure (CHF) can be defined as a heart that becomes severely weakened as a result of cardiovascular disease; mainly my-

ocardiocardial infarction. As a consequence, the pumping action of the heart is severely depressed resulting in two main effects: reduced CO and damming up of blood in the veins leading to an increase in the venous pressure and therefore increase in the right atrial pressure [10]. To reproduce the CHF condition, the circulating volume of water is increased; $\mathrm{Dlv_{min}}$ is increased in order to increase the resting left ventricle volume; $\mathrm{Dlv_{max}}$ is decreased with the purpose of mimicking the reduced left ventricle pumping ability.

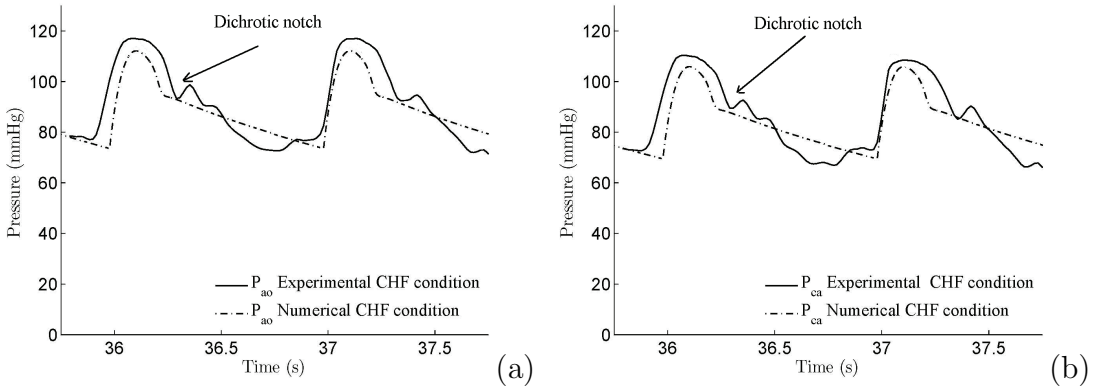

Figure 2.30: Comparison of the aortic and carotid pressure waveforms in CHF condition. (a) aortic pressure is 115/70 mmHg, (b) carotid pressure is 112/68 mmHg, CO is 2.5 lt/min.

In Figures 2.30(a) and 2.30(b), the dashed-and-dotted line is the numerical data and the solid line is the measured data from the SCVL. This is evident in Figure 2.30(a) and 2.30(b), where for both the aortic sinus and the carotid pressure waveform there is a drop in the end diastolic pressure and the end systolic pressure, when compared to the controlled condition. The aortic sinus pressure waveform drops down to 115/70 mmHg and the carotid pressure waveform drops down to 112/68 mmHg. The $\mathrm{AoP_{mean}}$ is 85.5 mmHg. In both the aortic sinus and carotid pressure waveform the dicrotic notch after the aortic valve closure is captured. For the CHF condition the CO drops from 5.1 lt/min, in a control condition, to 2.5 lt/min.

2.7.3 Simulation of Left Ventricular Diastolic Dysfunction in Hypertension Condition

In the clinical setting, hypertension is defined as a systolic blood pressure of 140 mmHg or greater and/or a diastolic blood pressure of 90 mmHg or greater [130]. Most hypertensive patients undergo co-existing impaired diastolic relaxation and therefore impaired left ventricle diastolic filling [131, 132, 133]. Zhou et al. [134] reported aortic stiffening as the main factor for developing increased left ventricle afterload and consequent Left Ventricle Hypertrophy and Left Ventricle Dysfunction (LVDDH).

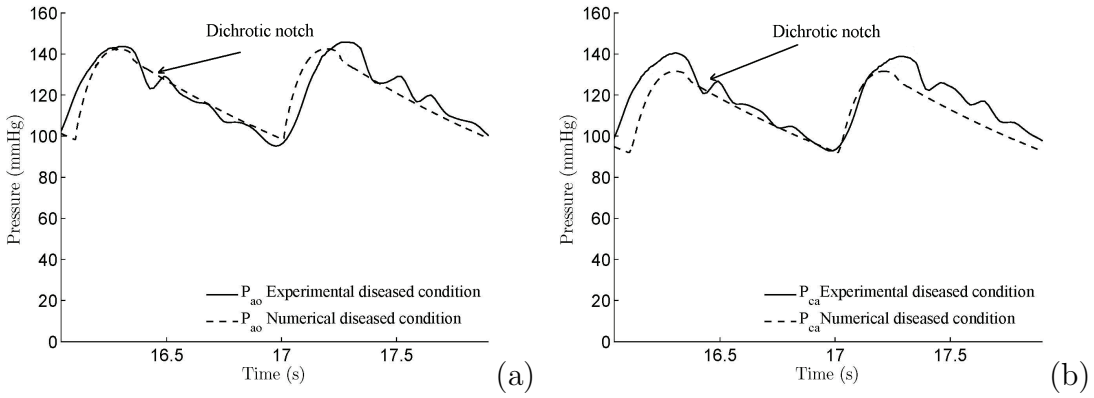

Figure 2.31: Comparison of aortic and carotid pressure waveforms in LVDDH condition. (a) aortic pressure is 145/95 mmHg, (b) carotid pressure is 140/90 mmHg, CO is 3.1 lt/min.

To mimic left ventricular disfunction , the aortic compliance, the left ventricular elastance and the left ventricular resting volume are reduced whereas the total peripheral resistance is increased. This is achieved by decreasing displacement of the the left ventricle actuator. In Figures 2.31(a) and 2.31(b), the dashed-and-dotted line is the numerical data and the solid line is the measured data from the SCVL system. As it is evident from Figure 2.31(a), there is an increase in both the end diastolic pressure and the end systolic pressure of the aortic sinus and the carotid pressure waveform in comparison to the controlled condition. The aortic sinus pressure waveform has increased to 145/95 mmHg and the carotid pressure waveform has increased to 140/90 mmHg. The AoP_{mean} is 111.7 mmHg. In both the aortic sinus and the carotid pressure waveforms the dicrotic notch after the

aortic valve closure is captured. For the LVDDH condition, cardiac output drops down from 5.1 lt/min in a controlled condition to 3.1 lt/min.

The results show the capability of the multi-chambers SCVL to reproduce the aortic sinus and the carotid pressure waveform in control, CHF and LVDDH. Table 2.2 shows the hemodynamic variables as found with the multi-chamber SCVL. Using four tubular permanent magnet linear motors working according to prescribed elastance function of the native ventricles and atria shows the high success of this technique in emulating the contraction phase and filling phases as found in the native cardiac muscle.

Table 2.2: Hemodynamic variables for the different modelled cases.

Parameter	Control	CHF	LVDD	Unit
AoP_{sys}	125	115	145	mmHg
AoP_{dia}	75	70	95	mmHg
AoP_{mean}	91.7	85.5	117	mmHg
CaP_{sys}	120	112	140	mmHg
CaP_{dia}	72	68	90	mmHg
CaP_{mean}	92	82.7	106.7	mmHg
PaP_{mean}	18	29	28	mmHg
P_{mc}	7	20	15	mmHg
CO	5.1	2.5	3.1	lt/min

In all replicated physiological cases the dicrotic notch is captured on the aortic sinus and the carotid pressure waveforms. In comparison to a native pressure waveform, the dicrotic notch on the experimental results seems slightly bigger. This can be justified due to the implementation of glass in the aorta artery segment of the SCVL as the mechanical properties of this material are far from what is found in native vasculature [4].

2.8 Summary

This chapter presents a new device designed to simulate in-vitro flow rates, pressures and other parameters representing normal and diseased conditions of the human cardiovascular system. Such devices are sometimes called bioreactors or "mock" simulators of the cardio-vascular blood-flow loop (SCVL) in the literature. Most SCVL systems only simulate the systemic circulation only and have inherent limitations in studying the interaction of left and right sides of circulation. Those SCVL systems that include both left and right sides of the circulation utilize header reservoirs simulating cycles with constant atrial pressures.

The SCVL described in this paper includes models for all four chambers of the heart, and the systemic and pulmonary circulation loops. Each heart chamber is accurately activated by a separate linear motor to simulate the suction and ejection stages, thus capturing important features in the pressure waveforms. Four mechanical heart valves corresponding to the mitral, pulmonary, tricuspid and aortic are used to control the desired unidirectional flow. This SCVL can emulate different physiological and pathological conditions of the human cardiovascular system by controlling the different parameters of blood circulation through the vascular tree (mainly the resistance, compliance and elastance of the heart chambers). In this study four cases were simulated; control, congestive heart failure and left ventricular diastolic dysfunction in hypertension conditions. The aortic sinus and carotid artery pressure waveforms as well as cardiac output have been investigated. In all cases the experimental results are compared with human physiology and numerical simulations. The results show the capability of the SCVL to replicate various physiological and pathological conditions.

Chapter 3

In-vitro Comparison of Two Different MCS Devices Installed In Series and In Parallel

3.1 Motivation

Congestive Heart Failure (CHF) is the leading cause of death in western countries. More than seven million people in both North America and Europe are diagnosed with a condition of heart failure, among whom nearly 6% are categorised as New York Heart Association (NYHA) class IV heart failure [8]. For end-stage CHF, two conventional solutions are palliative treatment and cardiac transplantation. For the former, the patient is hospital-bound under considerable costly pharmacological treatment and sadly he/she dies after a short period [135]. The latter solution is known as the gold standard for end-stage CHF patients. Nevertheless, with a limited number of heart donors (≈2500 donor annually) there remains a considerable rate of mortality (8-10%) in waiting list patients for cardiac transplant [17]. As a result, the role of Mechanical Circulatory Support (MCS) devices as a bridge to transplantation and destination therapy has become vital for patients on and off the waiting list [9, 23, 27].

There are two traditional approaches for MCS device implantation and for both the pump operates in parallel configuration with the heart. Implantation of an MCS device between the apex of the left ventricle and the ascending aorta

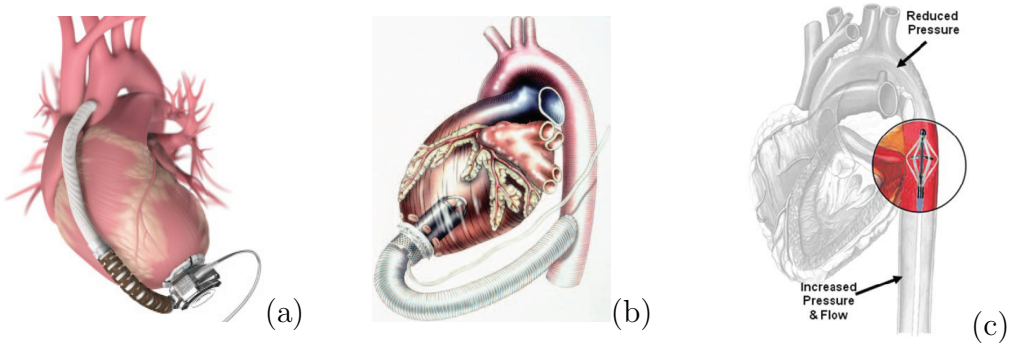

(a) (b) (c)

Figure 3.1: (a) Heartware pump in LV-AA configuration. *From: M. S. Slaughter et al. [45], Heartware miniature axial-flow ventricular assist device design and initial feasibility test, 2009.*, (b) Jarvik pump in LV-DA configuration. *From: O. H. Frazier [23], Research and development of an implantable, axial-flow left ventricular assist device: the jarvik 2000 heart, 2001.*, (c) Reitan Catheter Pump (RCP) in the descending aorta (DA). *From: O. Reitan et al. [53], Hemodynamic effects of a new percutaneous circulatory support device in a left ventricular failure model, 2003*

(LV-AA), occurs using the median sternotomy and implantation of an MCS device between the apex of the left ventricle and the descending aorta (LV-DA), occurs using the left thoracotomy. The former results in a promising hemodynamic improvement in the blood circulation system. However, due to the deep dissection process, the operation is prolonged and may cause severe postoperative complications in critically ill patients [48, 55, 56]. The latter is less invasive and may not necessitate the use of Cardio-Pulmonary Bypass (CPB) during the operation [24]. However, the LV-DA configuration is not an optimal technique in a wide range of MCS supports and may lead to a formation of stagnant and subsequent retrograde flows in the arterial system [54, 58, 59].

Increasing the number of old and sick patients who are no longer eligible for a prolonged invasive implantation surgery has attracted the attention of most researchers to investigate the development of an MCS device with more reliability and less possible invasive complications that would benefit the majority of patients.

Recent studies on the Reitan Catheter Pump (RCP), a short-term percutaneous circulatory assistant device, implanted in the descending aorta after cardiogenic shock, suggest that this technique is less invasive than the traditional

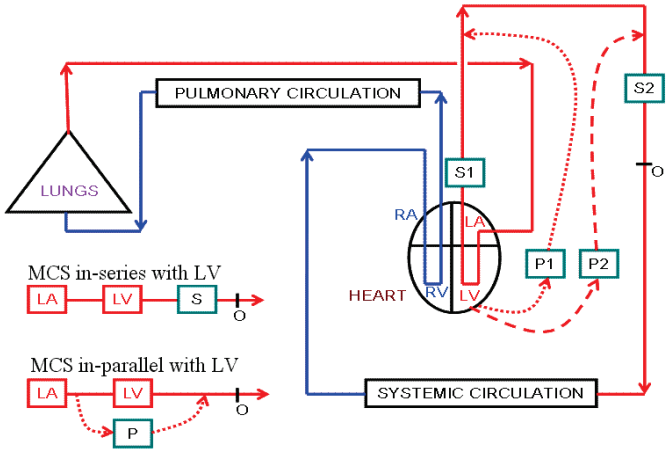

Figure 3.2: Schematic diagram of both in-series and in-parallel configurations.

in-parallel configurations and may have the potential to be employed for the permanent implantation [53, 60, 61, 107].

Figures 3.1(a-c) compares three different existing configurations. Figure 3.1(a) shows the Heartware pump in LV-AA configuration [45]. Figure 3.1(b) shows the Jarvik pump in LV-DA configuration [23]. Figure 3.1(c) shows the RCP in the descending aorta [53].

Figure 3.2 presents the schematic diagram of MCS device in two series configurations (S1 and S2) and MCS device in two parallel configurations (P1 and P2) with the left ventricle. It is evident that S1 is installed in the ascending aorta whereas S2 is installed in the descending aorta in series with the heart. The inlet of both P1 and P2 is connected to the apex of the native left ventricle and the outlet is connected to the ascending aorta and the descending aorta respectively.

The aim of this chapter is to evaluate the previous findings of the existing in-parallel deployments [55, 56, 57]. In addition, since currently there is no comprehensive in-vitro investigation on in-series deployment, the new technique of inserting an MCS device in the descending aorta has been investigated and the results have been compared to in-parallel techniques and the advantages and disadvantages of each have been discussed.

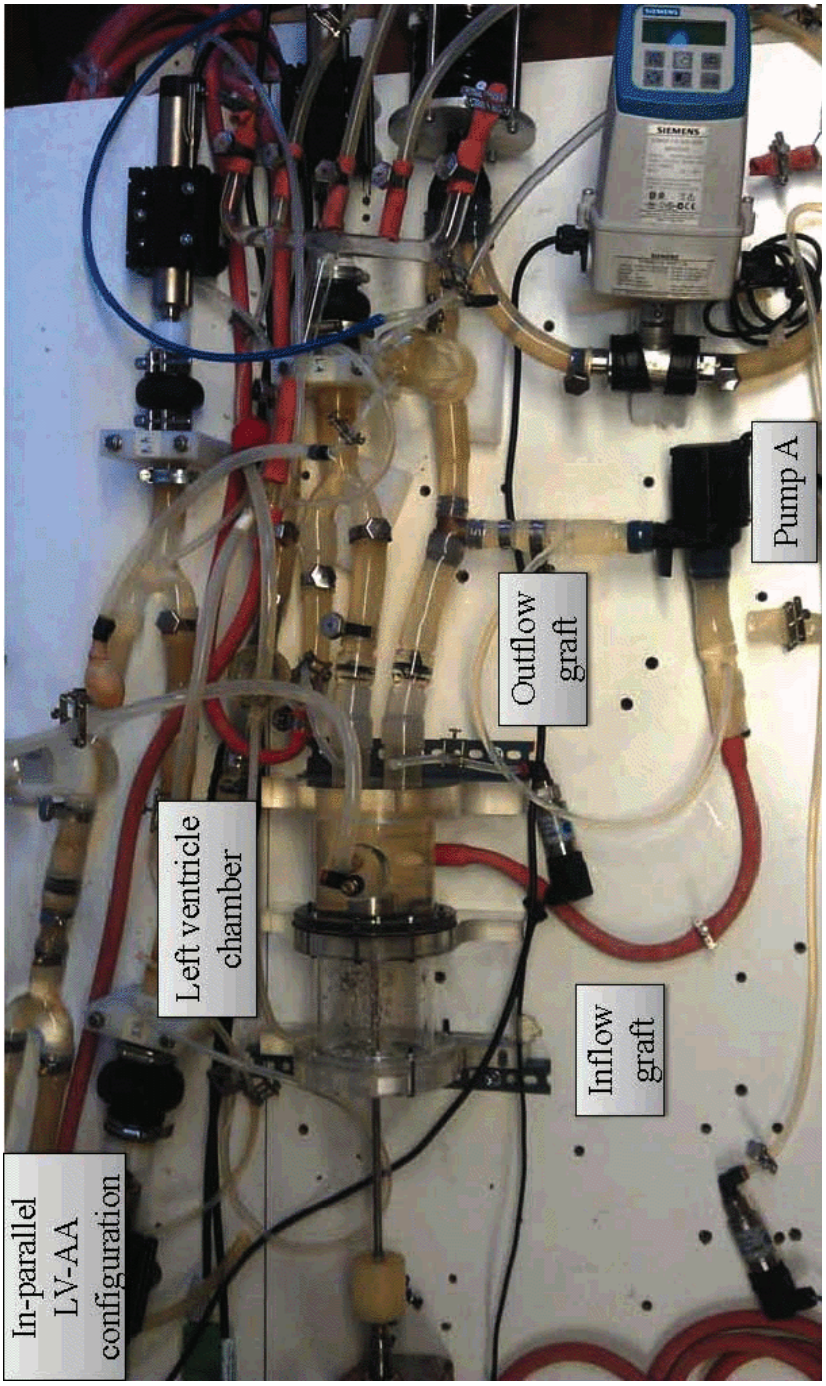

Figure 3.3: Photograph of the SCVL system with the pump A simulating the LV-AA in-parallel configuration.

Due to the fact that there are a significant number of numerical studies on the hemodynamic responses of the cardiovascular system to a rotary pump deployed in parallel with the heart (LV-AA or LV-DA) [81, 102, 103, 136, 137, 138, 139], within this chapter we just focus on the in-vitro comparison of the in-parallel and in-series configurations. Further, in **Chapter 4** the focus will be on the numerical and experimental studies on the hemodynamic responses of the cardiovascular system to a rotary pump deployed in the descending aorta, in-series configuration.

The objectives of the in-vitro test are met by using our in-house multi-chamber Simulator of the Cardiovascular Blood flow Loop (SCVL) which has been described elaborately in **Chapter 2** as well as our previous report [140]. The main purpose of the SCVL sytem is to simulate the pressure waveform features, closer to a controlled and diseased condition as that found in the clinical setting. This includes the close replication of all four phases of the cardiac cycle which is achieved by using individual actuation of four heart chambers through the implementation of linear motors.

3.2 Methodology

First, the CHF condition was simulated in the SCVL system. Following tasks were performed to reproduce the diseased condition.

- The circulating volume of water is increased.
- $\mathrm{Dlv_{min}}$ is increased in order to increase the resting left ventricle volume.
- $\mathrm{Dlv_{max}}$ is decreased with the purpose of mimicking the reduced left ventricle pumping ability.

Figure 3.4 represents a comparison between the slider's maximum and minimum displacement while simulating a healthy and diseased condition.

The experimental measurements for the desired CHF were validated with the corresponding clinical data [2, 4, 10, 141]. In each case, the aortic pressure, left

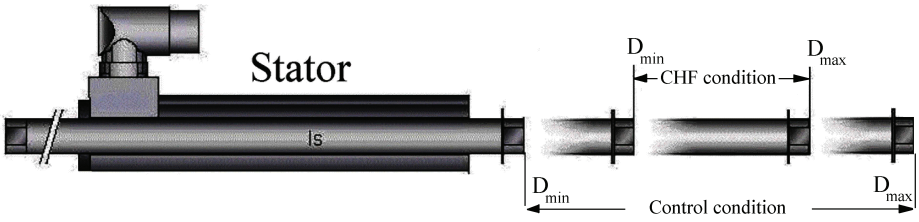

Figure 3.4: Schematic representation of the linear motor, actuating the left ventricle chamber.

ventricle pressure, carotid pressure waveforms as well as the average systemic and pulmonic flow-rate were recorded. These variables are the gold standard of cardiac condition assessment [129].

Due to the narrow size of the carotid artery, the carotid flow couldn't be measured directly using the flow-meter, instead the relative change of the carotid flow (QR_{ca}) has been evaluated by measuring the pressure difference across the carotid artery. According to Poiseuille's law [142], for a circular pipe, the pressure difference across the pipe is proportional to the flow past the pipe. As a result, the QR_{ca} has been defined as a function of the carotid pressure difference measured before and after the pump deployment:

$$QR_{ca} = \frac{Q_{ca,on} - Q_{ca,off}}{Q_{ca,off}} \times 100 = \frac{\Delta P_{ca,on} - \Delta P_{ca,off}}{\Delta P_{ca,off}} \times 100 \tag{3.1}$$

where $\Delta P_{(ca)}$ and $Q_{(ca)}$ are the pressure difference and the volumetric flow rate in the carotid artery respectively. The subscript 'on' belongs to the condition where the pump is in operation and 'off' is when the pump is absent.

In this study, two rotary pumps simulating MCS devices were employed. Pump A is a centrifugal pump with the rotor diameter of 45 mm producing the maximum pressure difference of 102 mmHg and maximum flow-rate of 12 L/min and is used for the in-parallel configurations and pump B is an in-house percutaneous axial pump with the rotor diameter of 22 mm producing the maximum pressure difference of 35 mmHg and maximum flow-rate of 10 L/min and is used for the in-series configuration.

3.2.1 Configurations

The replication of in-parallel LV-AA and LV-DA techniques were conducted by connecting the inflow graft to the connulation port, placed at the bottom of the left ventricle chamber and connecting the outflow graft to the ascending and descending aorta, respectively. Figure 3.5 and Figure 3.6 represent the schematic diagram of LV-AA and LV-DA techniques, respectively. The outflow graft diameter is 22 mm and the ratio of outflow graft to the aortic artery is nearly 1:1. For in-parallel techniques (LV-AA and LV-DA), three experiments were conducted in which the hemodynamic responses of the SCVL system were investigated when the pump A was operating at three examined Pump Settings (PS), as presented in Table 3.1.

Table 3.1: Pressure and flow parameters of pump A at examined pump settings.

PS	ΔP_{pump} (mmHg)	Q_{pump} (L/min)
0 (off)	0	0
1	98	2.5
2	95	4.5
3	90	5.5

Table 3.2: Pressure and flow parameters of pump B at examined pump settings.

PS	ΔP_{pump} (mmHg)	Q_{pump} (L/min)
0 (off)	0	0
1	25	3
2	28	4

The replication of the in-series DA configuration was conducted by placing the pump B in the proximal descending aorta, below the left subclavian artery and above the renal arteries, as shown in Figure 3.7. Two experiments were conducted in which the hemodynamic responses of the SCVL system were investigated when the pump B was operating at two examined PS, as presented in Table 3.2.

3.3 Results and Discussion

First, the CHF condition similar to what is found in our previous publication [140] was reproduced. The experimental measurements for the desired CHF were validated with the corresponding clinical data [2, 4, 10, 141, 143]. In each case, the aortic pressure, left ventricle pressure, carotid pressure waveforms as well as the average systemic and pulmonic flow-rate were recorded. These variables are the gold standard of cardiac condition assessment [129].

3.3.1 In-parallel LV-AA configuration

As shown in Figures 3.8(a-d), the aortic pressure (AoP) and the left ventricular pressure (LVP) waveforms are demonstrated for two consecutive cardiac cycles. The dashed lines in all figures represent the clinical data [4]. The solid line is the measured aortic pressure waveform and the dashed-and-dotted line is the measured left ventricle pressure waveform from the SCVL system.

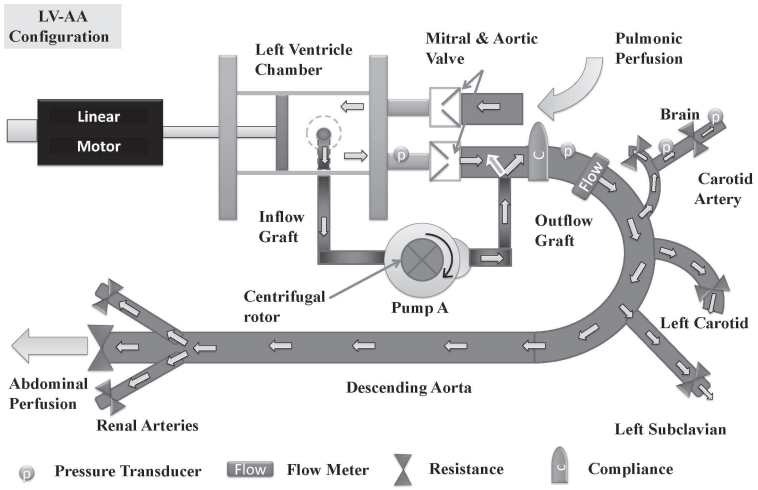

Figure 3.5: Schematic diagram of the left ventricle chamber with pump A in-parallel (LV-AA) configuration.

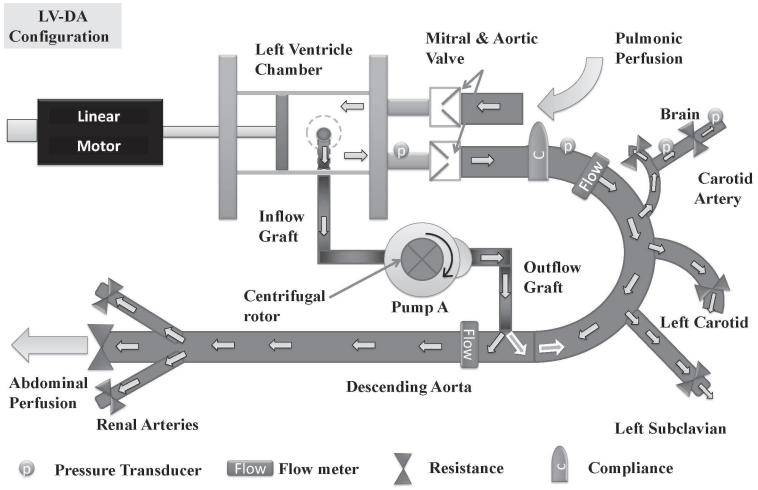

Figure 3.6: Schematic diagram of the left ventricle chamber with pump A in-parallel (LV-DA) configuration.

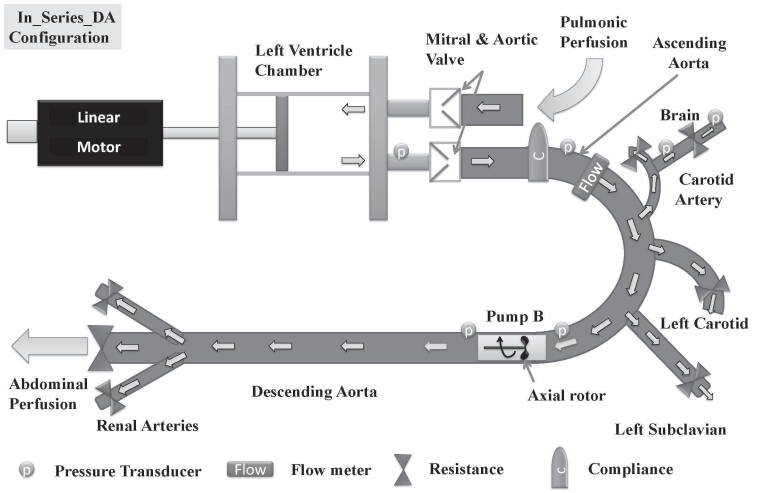

Figure 3.7: Schematic diagram of pump B installed in the descending aorta, in series configuration with the left ventricle.

Figure 3.8(a) shows the AoP and LVP waveforms for the CHF condition when the pump is off and the outflow graft is fully clamped. The AoP and LVP waveforms are 104/81 and 104/30 mmHg, respectively. It can be observed that the experimental AoP is in good agreement to the corresponding clinical data [4]. The use of four tubular permanent magnet linear motors, working according to the prescribed elastance function of the native ventricles and atria shows the high success of this technique in emulating pressure waveform features in very close agreement to the clinical setting. The small bump reflected on the descending limb of the aortic pressure waveform is the dicrotic notch (Incisura) and the small pressure bump reflected just before the ascending limb of the LVP waveform represents the systolic atruim contraction.

Figure 3.8(b-d) show the AoP and LVP waveforms at PS 1, 2 and 3, respectively. It is evident that, at PS 1, the AoP and LVP waveforms are 102/89 and 102/25 mmHg, at PS 2, the AoP and LVP waveforms are 97/95 and 92/15 mmHg and at PS 3, the AoP and LVP waveforms are 107/105 and 85/8 mmHg, respectively.

At PS 0 and 1, the aortic end-systolic pressure (AoP_{sys}) is equal to the left ventricle end-systolic pressure (LVP_{sys}) implying that at these levels, the aortic valve is still active and thus the left ventricle pumping action contributes part of the cardiac circulation. However, at PS 2 and 3, AoP_{sys} is no longer equal to LVP_{sys} implying that the continuous flow from the pump is taking over the left ventricle pulsatile flow, leading to the closure of the aortic valve. Referring to Figure 3.8(a-d), it can be observed that by increasing the pump setting from 1 to 3, the end-diastolic left ventricle pressure LVP_{dia} drops by 83%. A drop in LVP_{dia} leads to a lower volume expansion and thus lower ventricular wall stress during the filling phase. This may assist with the recovery of the damaged myocardial cells in a native system, as indicated by Frazier et al. [144].

Figures 3.9(a-d) show the carotid pressure (CaP) waveforms for two consecutive cardiac cycles. The dashed line in all figures represent the the clinical data for the CHF condition [141]. The solid line is the measured CaP waveform from the SCVL system. As shown in Figure 3.9(a) at PS 0, the CaP waveform is 110/77

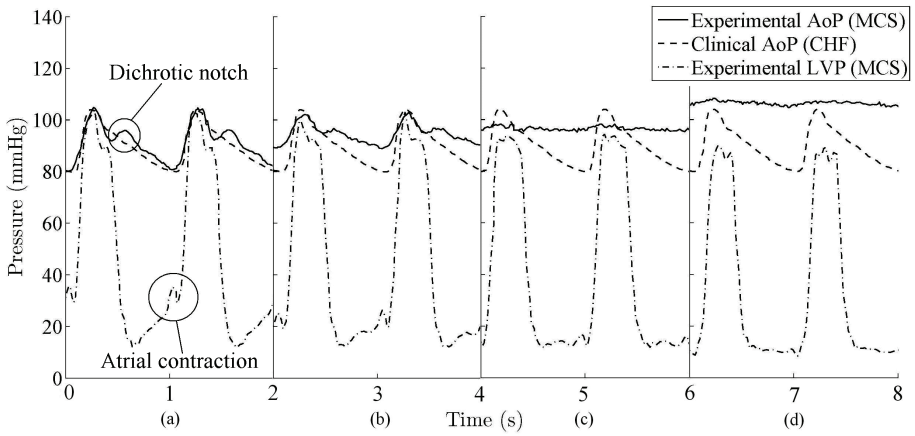

Figure 3.8: (a) AoP and LVP for the CHF condition, $Q_{ao,mean}$=2.5 L/min (b) AoP and LVP at PS 1, $Q_{ao,mean}$=3.5 L/min (c) AoP and LVP at PS 2, $Q_{ao,mean}$=4.3 L/min (d) AoP and LVP at PS 3, $Q_{ao,mean}$=5.4 L/min. The clinical AoP waveforms under CHF condition [4] are shown in all plots for clearer comparison.

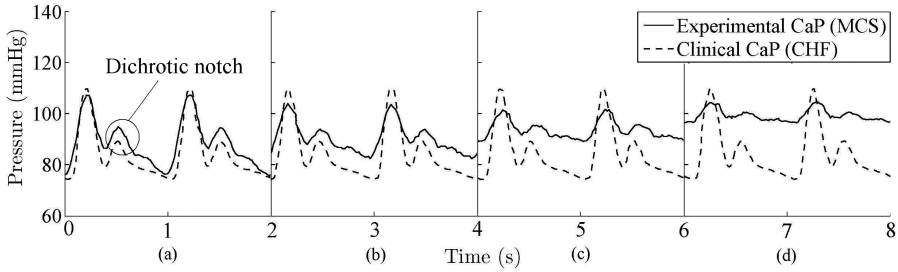

Figure 3.9: (a) CaP for the CHF condition, (b) CaP at PS 1, (c) CaP at PS 2, (d) CaP at PS 3. The clinical CaP waveforms under CHF condition [141] are shown in all plots for clearer comparison.

mmHg which is in good agreement with the clinical data. As the pump setting is increased from 1 to 3, the end diastolic carotid pressure (CaP_{dia}) increases considerably while the end systolic carotid pressure (CaP_{sys}) decreases slightly.

The Pulse Pressure (PP) is determined by subtracting the end-diastolic pressure from the end-systolic pressure [10]. Figure 3.10 compares the aortic and carotid PP with and without the pump. The dashed lines are the aortic and carotid PP in a healthy condition (control) [2, 143] and the solid lines are the measured aortic and carotid PP for the CHF condition at different pump settings. Considering the aortic and carotid PP of 40 and 46 mmHg, respectively

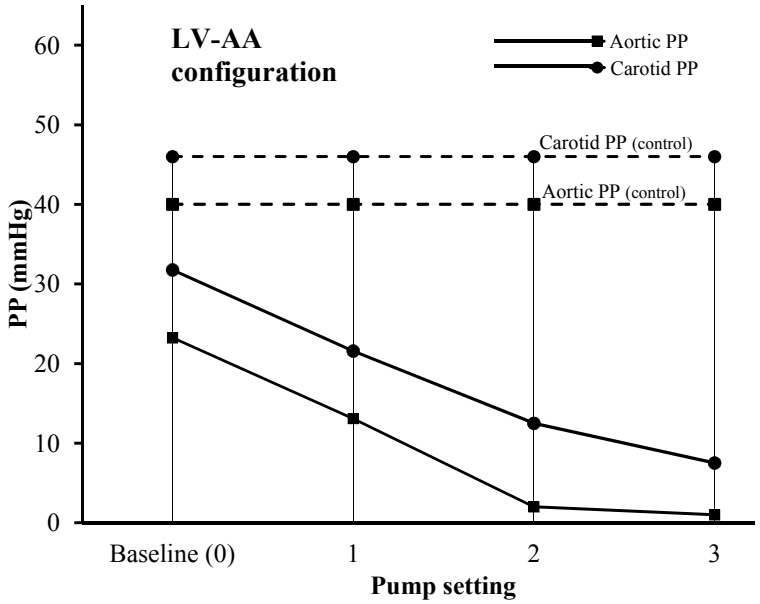

Figure 3.10: The aortic and carotid PP for the CHF condition without the pump and with the pump A at PS 1, 2 and 3. The aortic PP [2] and carotid PP [143] under a healthy condition (control) are plotted as the reference lines.

for the healthy condition, the aortic and carotid PP under the CHF condition drops by 41 and 30%, respectively. When the pump setting is changed from 1 to 3, the aortic PP drops further from 13.1 to 1 mmHg. The carotid PP follows the trend and drops from 21.58 to 7.52 mmHg. It is concluded that increasing the level of continuous flow into the ascending aorta leads to a substantial reduction in pulsatility which may cause some disturbances for end-organ functionality as indicated by Kim et al. [40].

The mean aortic flow ($Q_{ao,mean}$) was measured, downstream of the outflow graft, in the ascending aorta, as shown in Figure 3.5. The $Q_{ao,mean}$ for the replicated CHF condition was recorded as 2.5 L/min. When the pump setting was increased from 1 to 3, it was observed that the $Q_{ao,mean}$ improved from 3.4 to 5.4 L/min at 100% contribution of the pump A. As the pump setting was increased from 1 to 3, the relative change of the carotid flow (QR_{ca}) increased from 3.5 to 8.5%. The positive QR_{ca} indicates that for the LV-AA configuration, regardless of the level of pump support, there will be no carotid perfusion drop. The average Pulmonic

artery Pressure (PaP_{mean}) and the average pulmonic flow ($Q_{pa,mean}$) were recorded at each pump setting. For the CHF condition, PaP_{mean} and $Q_{pa,mean}$ were recorded as 30 mmHg and 2 L/min, respectively. When the pump setting was increased from 1 to 3, PaP_{mean} dropped to 8 mmHg and $Q_{pa,mean}$ improved to 4.6 L/min. Table 3.4 represents the hemodynamic results for in-parallel LV-AA configuration.

It is found that the implementation of the in-parallel LV-AA configuration leads to significant improvement in the systemic and the pulmonic perfusion when the pump contribution is increased. No stagnant region was observed in the aortic arch region over the whole cardiac cycle for the examined pump settings. However one of the adverse effects which was observed after employing the LV-AA configuration was the presence of irregular flow patterns in vicinity of the aortic valve. At PS 1, the interaction between the cardiac pulsatile flow and the pump continuous flow at their junction produced a lot of irregular flow patterns in this region. Hence it was concluded that the flow regime is of the turbulent type. At PS 2 and 3, although the pulsatile flow was absent in the case, the calculated Reynolds number in the outflow graft was higher than the critical Reynolds number (i.e. Re$\simeq$4000 for the pipe flows [142]) which was an indication of the flow being turbulent. Table 3.3, illustrates the calculated Reynolds number in the outflow graft for the examined pump settings.

Although the turbulent regime may have some adverse affect on the aortic valve opening-closing mechanism, it can prevent the complete stagnant flow near the coronary arteries that otherwise would have occurred in the sinus artery upon the valve closure at higher pump settings. In addition, at higher pump settings, the turbulent flow may cause some disturbances in blood properties in a native cardiovascular system [55].

Table 3.3: Reynolds number in the outflow graft for the examined pump settings.

PS	Reynolds number
1	2408
2	4340
3	5308

Table 3.4: Hemodynamic results for the in-parallel LV-AA configuration.

Parameters	Baseline	PS 1	PS 2	PS 3	Unit
LVP_{sys}	104	102	92	85	mmHg
LVP_{dia}	30	25	15	5	mmHg
AoP_{sys}	104	102	97	107	mmHg
AoP_{dia}	81	89	95	105	mmHg
AoP_{mean}	88.7	93.3	95.7	105.7	mmHg
PP_{ao}	23.25	13.1	2	1	mmHg
CaP_{sys}	107.5	104	101.5	104.5	mmHg
CaP_{dia}	75.5	82.5	89	97	mmHg
CaP_{mean}	86.2	89.7	93.2	99.5	mmHg
PP_{ca}	31.5	21.5	12.5	7.5	mmHg
PaP_{mean}	30	26	22	19	mmHg
$Q_{po,mean}$	2	3	3.6	4.6	L/min
$Q_{ao,mean}$	2.5	3.4	4.3	5.4	L/min
QR_{ca}	-	3.5	6	8.5	%

3.3.2 In-parallel LV-DA configuration

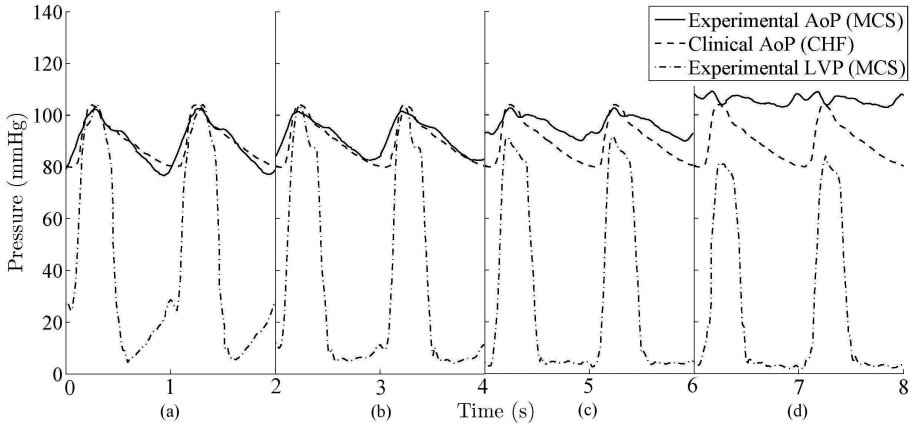

Figure 3.11: (a) AoP and LVP for the CHF condition, (b) AoP and LVP at PS 1, (c) AoP and LVP at PS 2, (d) AoP and LVP at PS 3. The clinical AoP waveforms under CHF condition [4] are shown in all plots for clearer comparison.

Figure 3.11(a) shows the AoP and LVP waveforms for the CHF condition with the same characteristics found in Section 3.3.1. Figure 3.11(b) shows that at PS 1, the AoP and LVP waveforms are 102/80 and 102/10 mmHg, respectively. Figure 3.11(c) shows that at PS 2, the AoP and LVP waveforms are 102/92 and 92/7 mmHg, respectively. Figure 3.11(d) shows that at PS 3, the AoP and LVP are 108/105 and 80/4 mmHg, respectively.

It is evident that at PS 0 and 1, AoP_{sys} is equal to LVP_{sys} implying that at

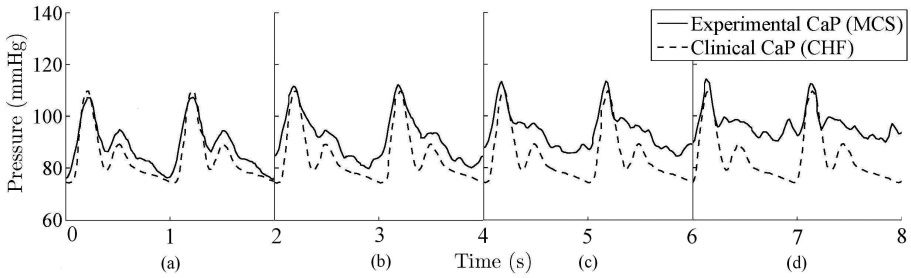

Figure 3.12: (a) CaP at the CHF condition, (b) CaP at PS 1, (c) CaP at PS 2, (d) CaP at PS 3. The clinical CaP waveforms under CHF condition [141] are shown in all plots for clearer comparison.

these levels the aortic valve is still active and thus the left ventricle pumping action contributes a part of the cardiac circulation. However, at PS 2 and 3, AoP_{sys} is no longer equal to LVP_{sys} implying that the continuous flow from the pump is taking over the left ventricle pulsatile flow leading to the closure of the aortic valve. It is observed that as the pump setting is increased from 1 to 3, the LVP_{dia} drops by 85% leading to a lower ventricular wall stress during the filling phase.

Figures 3.12(a-d) show the CaP waveforms for two consecutive cardiac cycles. As the pump setting is increased from 1 to 3, similar to LV-DA configuration, the carotid PP drops substantially.

Figure 3.13 compares the aortic and carotid PP for the CHF condition without the pump and with the pump in LV-DA configuration. When the pump setting is changed from 1 to 3, the aortic PP drops from 18.5 to 6.2 mmHg. The carotid PP follows the trend and drops from 32 to 23 mmHg. Comparing Figure 3.10 and Figure 3.13, it is found that as the pump support level is increased into the SCVL system, both the aortic and carotid PP gradient falls with slower rate in LV-DA than LV-AA configuration. This can be as a result of the adverse pressure occurring due to the continuous retrograde flow from the pump and thus prevent the AoP_{sys} and CaP_{sys} from dropping considerably [23].

As shown in Figure 3.6, for the LV-DA configuration in the systemic loop, two flow measurement tests were conducted. One at the downstream of the

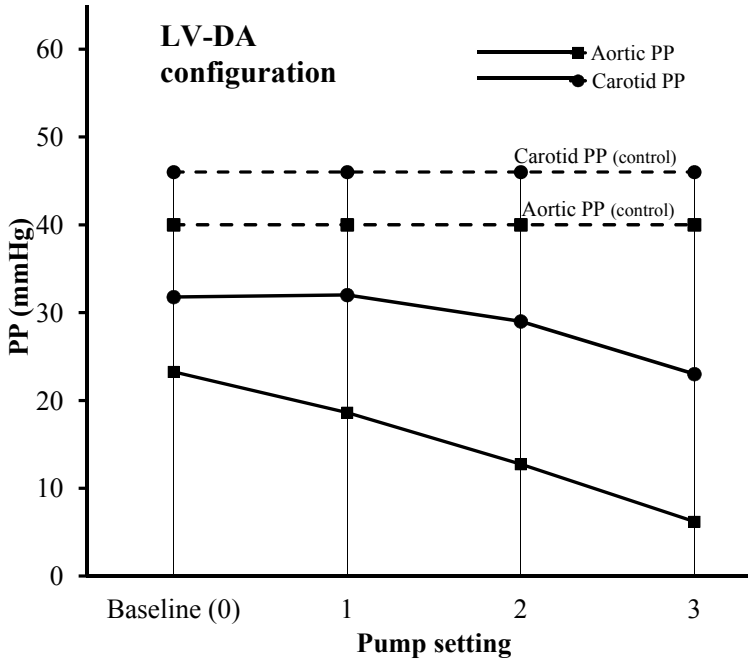

Figure 3.13: The aortic and carotid PP for the CHF condition without the pump and with the pump A at PS 1, 2 and 3. The aortic PP [2] and carotid PP [143] under a healthy condition (control) are plotted as the reference lines.

aortic valve to record the ascending aortic flow-rate ($Q_{ao,asc}$) and the other one in the descending aorta, downstream of the pump outflow graft, to record the abdominal perfusion ($Q_{ao,des}$). The results showed that as the pump setting was increased, $Q_{ao,asc}$ dropped whereas the $Q_{ao,des}$ increased. At PS 3, $Q_{ao,asc}$ dropped to 0 L/min whereas $Q_{ao,asc}$ increased to 4.9 L/min. Having stationary flow in the ascending aorta ($Q_{ao,asc}$=0 L/min) indicate that the retrograde flow from the pump is taking over the aortic arch and prevents the cardiac flow to move forward. As the pump setting was increased from 1 to 3, the QR_{ca} increased from 4.5 to 10.5% implying that, similar to the LV-AA configuration, there is no carotid perfusion drop. Table 3.5 represents the hemodynamic results for the in-parallel LV-DA configuration at various pump settings.

Using the in-parallel LV-DA configuration has shown a significant flow improvement in the descending aorta and other abdominal extremities as the pump setting was increased. It was observed that for PS 0 and 1, the left ventricle

Table 3.5: Hemodynamic results for the in-parallel LV-DA configuration.

Parameters	Baseline	PS 1	PS 2	PS 3	Unit
LVP_{sys}	104	102	92	80	mmHg
LVP_{dia}	30	10	7	4	mmHg
AoP_{sys}	104	101	100	109	mmHg
AoP_{dia}	81	82	90	103	mmHg
AoP_{mean}	88.7	88.3	93.3	105	mmHg
PP_{ao}	23	19	10	6	mmHg
CaP_{sys}	107.5	112	113	112	mmHg
CaP_{dia}	75.5	80	84	89	mmHg
CaP_{mean}	86.2	90.7	93.7	96.7	mmHg
PP_{ca}	32	32	29	23	mmHg
PaP_{mean}	30	28	24	20	mmHg
$Q_{po,mean}$	1.5	2.4	3.5	4.1	L/min
$Q_{ao,des}$	2.4	3.3	4.1	4.9	L/min
$Q_{ao,asc}$	2.5	1.8	0.7	0	L/min
QR_{ca}	-	4.5	7	10.5	%

chamber is contributing considerable pulsatile normograde flow into the aortic arch region, the carotid artery and other upstream branches. At PS 2, there is a combination of normograde flow produced by the left ventricle and retrograde flow produced by the pump into the descending aorta. From PS 1 to 2, the retrograde flow gradually overtake the normograde flow in the aortic arch. Consequently, at PS 3, the aortic arch has a region with the stagnant flow in which the aortic valve remains closed. This may lead to a thrombogenesis condition in the vicinity of the aortic valve in a native cardiovascular system and ultimately may lead to some aortic valvular abnormality [40].

3.3.3 In-Series DA configuration

Figure 3.14(a) shows the measured AoP and LVP for the CHF condition. The AoP and LVP waveforms are 101/79 and 101/25 mmHg, respectively. Figure 3.14(b-c) show the AoP and LVP waveforms at PS 1 and 2 of pump B, respectively. It is evident that at PS 1, the AoP and LVP waveforms drop to 94/66 and 94/17 mmHg and at PS 2, the AoP and LVP waveforms drop further to 84/53 and 84/10 mmHg, respectively.

It is evident that at PS 1 and 2 of pump B, the AoP_{sys} is equal to the LVP_{sys} waveform, indicating that for in-series DA configuration, regardless of the level

of pump support the aortic valve is active, hence the left ventricle delivers the Cardiac Output (CO) into the systemic circulation. The presence of the pulsatile CO reduces the risk of clotting and thrombus formation in vicinity of the aortic valve in a native system [41].

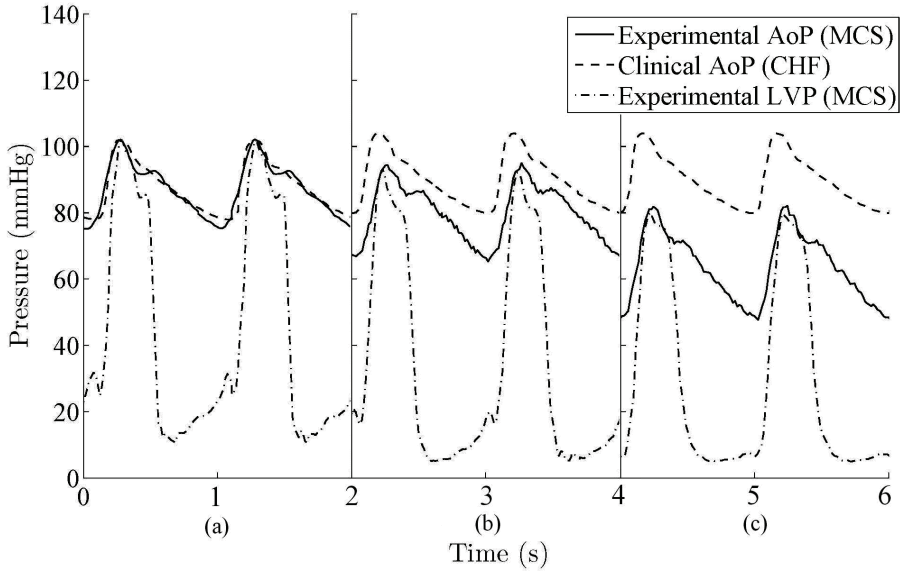

Figure 3.14: (a) Experimental and clinical AoP and LVP waveforms for the CHF condition (b) Experimental AoP and LVP waveforms with the pump B at PS 1, (c) Experimental AoP and LVP waveforms with the pump B at PS 2. The clinical AoP waveforms under CHF condition [4] are shown in all plots for clearer comparison.

Figure 3.15(a) shows the experimental and clinical CaP for the CHF condition. It is evident that the experiment CaP waveforms is 110/76 mmHg. Figure 3.15(b) and Figure 3.15(c) show the CaP waveforms at PS 1 and 2 of pump B in which the CaP drops to 108/58 and 105/45 mmHg, respectively.

Figure 3.16 compares the aortic and carotid PP with and without the pump. It is observed that when the pump B is introduced into the system at PS 1, the aortic and carotid PP improve by 10 and 57%, respectively. At PS 2 the aortic and the carotid PP increase by 26 and 69%, respectively. It is concluded that an increase in the pump support level results in an improved pulsatility of the pressure waveforms. This is in contrast to the in-parallel configurations where an increase in the level of pump support alleviates the pulsatility. It has been

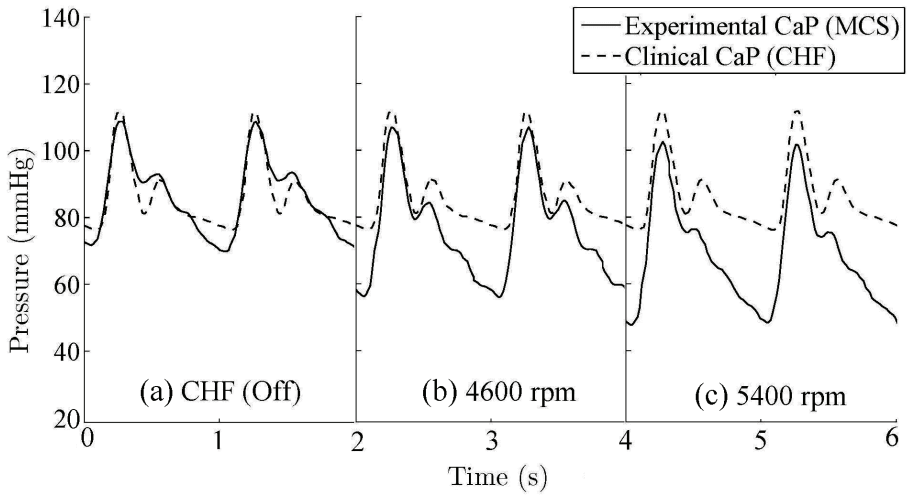

Figure 3.15: (a) Experimental and clinical CaP waveforms for the CHF condition (b) Experimental CaP waveforms with the pump B at PS 1, (c) Experimental CaP waveforms with the pump B at PS 2. The clinical CaP waveforms under CHF condition [141] are shown in all plots for clearer comparison.

reported that pulsatility has a crucial effect on recovery of the cerebral, renal and myocardial blood perfusion [40, 41, 42]. As a result, using the in-series configuration may have better influence on end-organ functionality due to an improved PP in comparison with the in-parallel configurations.

Figure 3.17(a) and Figure 3.17(b) show the pressure difference waveforms across the pump B, in the descending aorta, while the SCVL system is in operation. The solid line represents the measured pressure waveform in the descending aorta for the CHF condition when the pump is not active. The dashed line and dashed-dotted line represent the pressure waveforms at the downstream and the upstream of the pump, respectively. At PS 1, the average pressure difference across the pump and the average flow-rate past the pump were recorded as 25 mmHg and 3 L/min, respectively. When the pump support level was switched to PS 2 the average pressure difference was 28 mmHg and the average flow-rate past the pump was improved to 3.6 L/min.

It is evident in Figure 3.17(a) and Figure 3.17(b), where the difference between the pressure drop is lower than the difference between the pressure rise. Peripheral resistance and the pump rotor speed are two main factors affecting

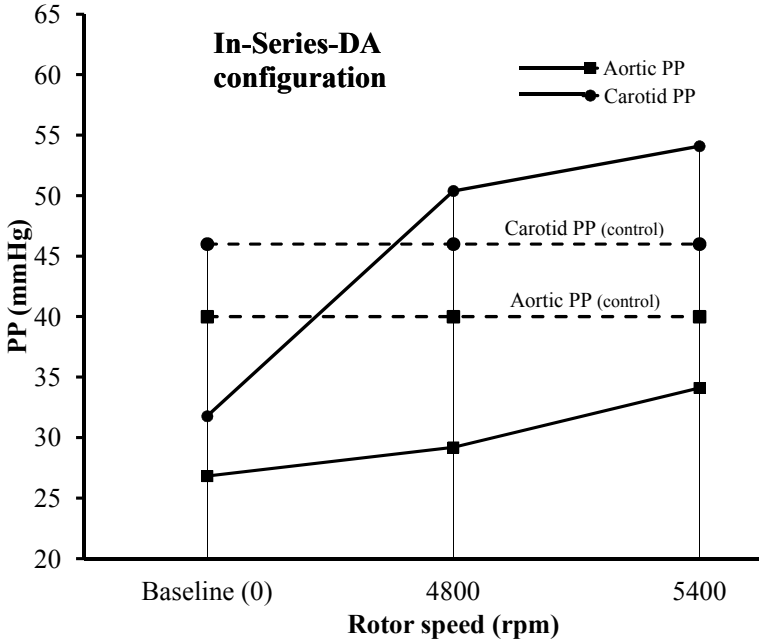

Figure 3.16: Aortic and carotid PP for the CHF condition without and with the pump B at PS 1 and 2. The aortic PP [2] and carotid PP [143] under a healthy condition (control) are plotted as the reference lines.

the pressure difference across the pump. Peripheral resistance is auto-regulated in a native body whereas the rotor speed is a controllable variable. So, depending on the stage of the disease, both pressure drop and pressure rise are beneficial. Pressure drop, at the upstream of the pump, reduces the after-load pressure in the arterial system and hence minimises the ventricular wall stress. This leads to more convenient unloading of the chamber and may also assist with the recovery of the damaged myocardial cells [144]. Also, the pressure rise, at the downstream of the pump may improve the renal function in patients suffering from the renal impairment, as demonstrated by Zanardo et al. [145].

The CO for the replicated CHF condition was recorded as 2.8 L/min. When the pump setting was switched from 1 to 2, it was observed that the CO improved from 3.4 to 4 L/min. Table 3.6 represents the experimental results of the SCVL with the pump B operating in the descending aorta.

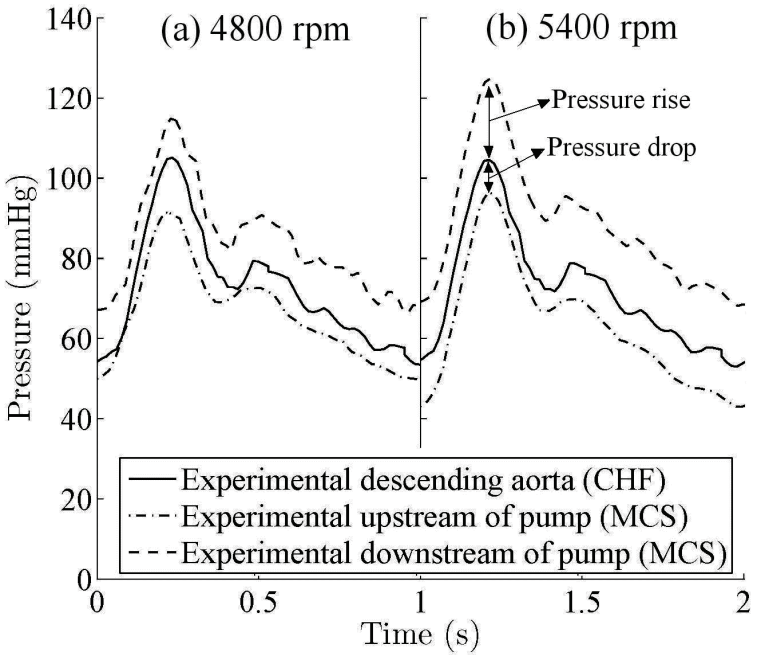

Figure 3.17: (a) Experimental descending aortic pressure without the pump and with the pump B at PS 1 (b) Experimental descending aortic pressure without the pump and with the pump B at PS 2.

One of the crucial concerns of implantation in the descending aorta is the blood perfusion disturbances in the brain that may occur due to the pressure drop generated by the pump. A comparison between the measured QR_{ca} with and without the pump shows a drop of 12.5 to 16.6% at PS 1 and 2, respectively. However, it must be noted that in a native human cardiovascular system, cerebral blood flow is well autoregulated within 60-140 mmHg of AoP_{mean} and the local blood flow feedback control provides enough blood perfusion within this limit [53, 107, 60, 61]. In addition, there is a concern that pressure drop in the aortic sinus may reduce the coronary flow perfusion. It must be noted that the coronary perfusion is controlled via a complex autoregulation mechanism and is dependent on the myocardial oxygen demand [10]. This study has shown that with the pump in series, the left ventricular internal pressure decreases dramatically implying that the myocardial oxygen demand to overcome the after load pressure may drop subsequently. It is evident that a declined heart oxygen demand will have a significant effect on the coronary autoregulation mechanism

Table 3.6: Experimental results from the SCVL with the pump B in the descending aorta

Parameters	Baseline	PS 1	PS 2	Unit
LVP_{sys}	104	94	84	mmHg
LVP_{dia}	25	17	10	mmHg
AoP_{sys}	104	94	84	mmHg
AoP_{dia}	79	66	53	mmHg
AoP_{mean}	87.3	75.3	63.3	mmHg
PP_{ao}	25	28	31	mmHg
CaP_{sys}	110	108	105	mmHg
CaP_{dia}	76	58	48	mmHg
CaP_{mean}	87.3	74.7	67	mmHg
PP_{ca}	34	52	59	mmHg
PaP_{mean}	25	22	19	mmHg
$Q_{po,mean}$	2	2.2	2.9	L/min
ΔP_{pump}	-	25	28	mmHg
CO_{mean}	2.8	3.4	4	L/min
QR_{ca}	-	-12.5	-16.6	%

which may compensate the coronary perfusion in a native system. These are the questions needs to be addressed through an *in vivo* test.

3.4 Summary

The objective of this study is to investigate the novel approach of placement of the pump in the descending aorta and compare it with the traditional approaches of the Left Ventricle to Ascending Aorta (LV-AA) and the Left Ventricle to Descending Aorta (LV-DA). Tests were conducted by using the in-house Simulator of the Cardio-Vascular blood-flow Loop (SCVL). The results indicate that the use of in-parallel LV-AA configuration leads to a significant improvement in the systemic and the pulmonic flow as the level of continuous flow is increased. The use of LV-DA in-parallel technique leads to an improvement in the systemic and pulmonic flow at lower level of continuous flow but at higher level of support leads to a flow retrogradation. In both in-parallel approaches (LV-AA and LV-DA), increasing the level of MCS continuous flow leads to a decrease in the aortic and the carotid pulse pressures to a certain extent. The results of the in-series configuration show that the pressure drop upstream of the pump facilitates the cardiac output as a result of the after-load reduction. Also the pressure rise downstream of the pump may assist the renal perfusion. At the same time the generated pressure drop at the proximal part of the descending aorta induces a slight drop in the carotid perfusion which will be autoregulated by the brain in a native cardiovascular system. The pulse wave analysis shows that the placement of the pump in the descending aorta, in series with the heart, leads to improved pulsatility which is beneficial for end-organ functionality in the native cardiovascular system.

Chapter 4

Numerical and in-vitro Investigation of a Novel MCS Device Installed in the Descending Aorta

4.1 Motivation

Congestive Heart Failure (CHF) as a result of different heart diseases is one of the leading cause of death in men and women alike. Patients with severe heart failure suffer from renal impairment and pulmonary hypertension [11]. Cardiac transplantation is the most established solution for end-stage CHF patients. However, among 4,200,000 patients suffering from end-stage heart failure in North America and Europe, only a minority of young patients ($\leq$50 year old) are eligible for cardiac transplantation and the rest are not able to meet the risk criteria. Donor heart supply meets less than 2% of the demand for eligible patients and leaves the great majority of patients under palliative treatment [17]. As a result, the role of Mechanical Circulatory Support (MCS) devices as a bridge to transplantation for patients on the waiting list and as a bridge to destination for patients off the waiting list has become vital [9, 23, 27].

The implantation of an MCS device between the left ventricle and the ascending aorta or between the left ventricle and the descending aorta is prolonged and highly invasive [24, 48, 55, 58, 59]. A significant number of patients with a critical physiological or pathological condition are not eligible for a long invasive

implantation surgery. It is also reported that those patients experiencing long invasive surgery may suffer from postoperative complications such as infection, end-organ injury or internal bleeding [9, 54, 56]. As a result, looking for a less invasive implantation technique which can be utilized in a variety of patients has become a recent area of interest.

Recent studies on the Reitan Catheter Pump (RCP), a temporary paracorporeal MCS device, inserted percutaneously into the descending aorta to prevent cardiogenic shock, suggests that the descending aorta can be a promising location to install a long-term implantable MCS device with minimally invasive surgery [53, 60, 61]. However, there is a theoretical concern that as the pump is operating in the descending aorta, there may be a "steal" phenomenon of blood flow from the brain and upper extremities.

In addition, there is a question associated with the effect of the pressure rise on renal perfusion. Renal impairment has been known as a high risk factor of mortality in end-stage CHF patients. The heart and kidneys are two interdependent organs. So, any heart dysregulation may cause the renal function to deteriorate and in contrast any pharmacological therapy to alleviate the condition of CHF may have further adverse effects on renal function [146].

The aim of this study is to conduct numerical and experimental investigations on the hemodynamic responses of the cardiovascular system aided with an MCS device operating in the descending aorta.

The numerical simulations of the cardiovascular system allow for the investigation into the hemodynamic parameters of the whole circulatory system which is not feasible in a native human body due to the complexity of the system. In general, the numerical models are classified as distributed parameter models and concentrated parameter models. The distributed parameter models are employed to investigate the local dynamics in certain parts of the cardiovascular system, such as for simulation of the heart [147]. The general distributed parameter model includes computational fluid dynamics, finite elements and the transmission line method [98]. In contrast, the concentrated parameter models are used for investigation of the global response of the cardiovascular system [136].

In this study, the objectives of the numerical study are met using the modified version of the Concentrated Lumped Parameter (CLP) model, adapted from the programs described in different studies conducted by Korakianitis et al. [98, 99, 100, 101, 102, 103]. As an improvement from previous studies, the original CLP model has been updated from C language into the Simulink environment of the MATLAB program. In addition, to study the hemodynamic responses of the upper and lower extremities to the pump operating in the descending aorta, the carotid circulation and the renal circulation compartments have been added to the systemic loop.

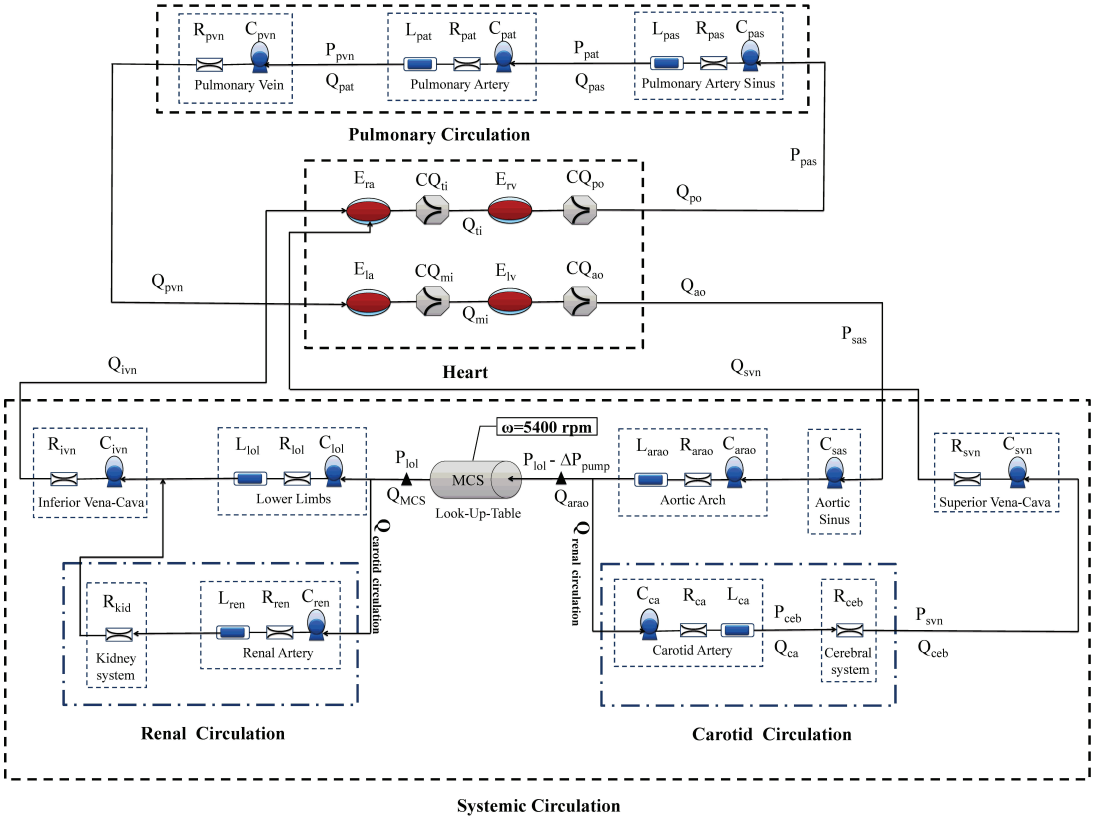

Figure 4.1: Schematic diagram of the CLP model with the pump integrated in the descending aorta.

The design and implementation of mechanical cardiovascular simulators has been motivated by the necessity and significance of in-vitro tests of various artificial devices such as heart valves, ventricular assist devices (VAD), MCS devices

etc. prior to in-vivo tests.

In general, cardiovascular simulators are classified into three main categories based on the number of actuators replicating the heart chambers. Single-chamber SCVL systems are used for the investigation of newly developed time-varying elastance functions of the left ventricle [148]. Twin-chamber SCVL systems are used for the investigation of the hemodynamic responses of the heart to implanted various prosthetic devices [84] and multi-chamber SCVL are used for the investigation of the central and peripheral hemodynamic variables of the systemic and the pulmonary circulations simultaneously [83]. In this study, the objectives of the experimental study are met using our in-house multi-chamber Simulator of Cardio-Vascular Loops (SCVL) described in Chapter 2. The main purpose of our multi-chamber SCVL is to simulate the pressure waveform features, closer to a controlled and diseased condition as that found in the clinical setting. This includes the close replication of all four phases of the cardiac cycle which is achieved by using individual actuation of four heart chambers through the implementation of linear motors.

4.2 Numerical Study

Figure 4.1 shows the schematic diagram of the CLP model with the MCS device integrated in the descending aorta. The CLP model is classified into two sections: the heart and the blood circulation loop. The heart chambers are modelled with the time-varying elastance concept originally described by Suga et al. [93]. The local effects of the systemic and the pulmonic loops are modelled with the resistance, capacitance and inductance (RCL) components based on the modified version of the Windkessel model [149]. Figure 4.2 shows the Simulink environment of the cardiovascular system with the pump integrated in the descending aorta.

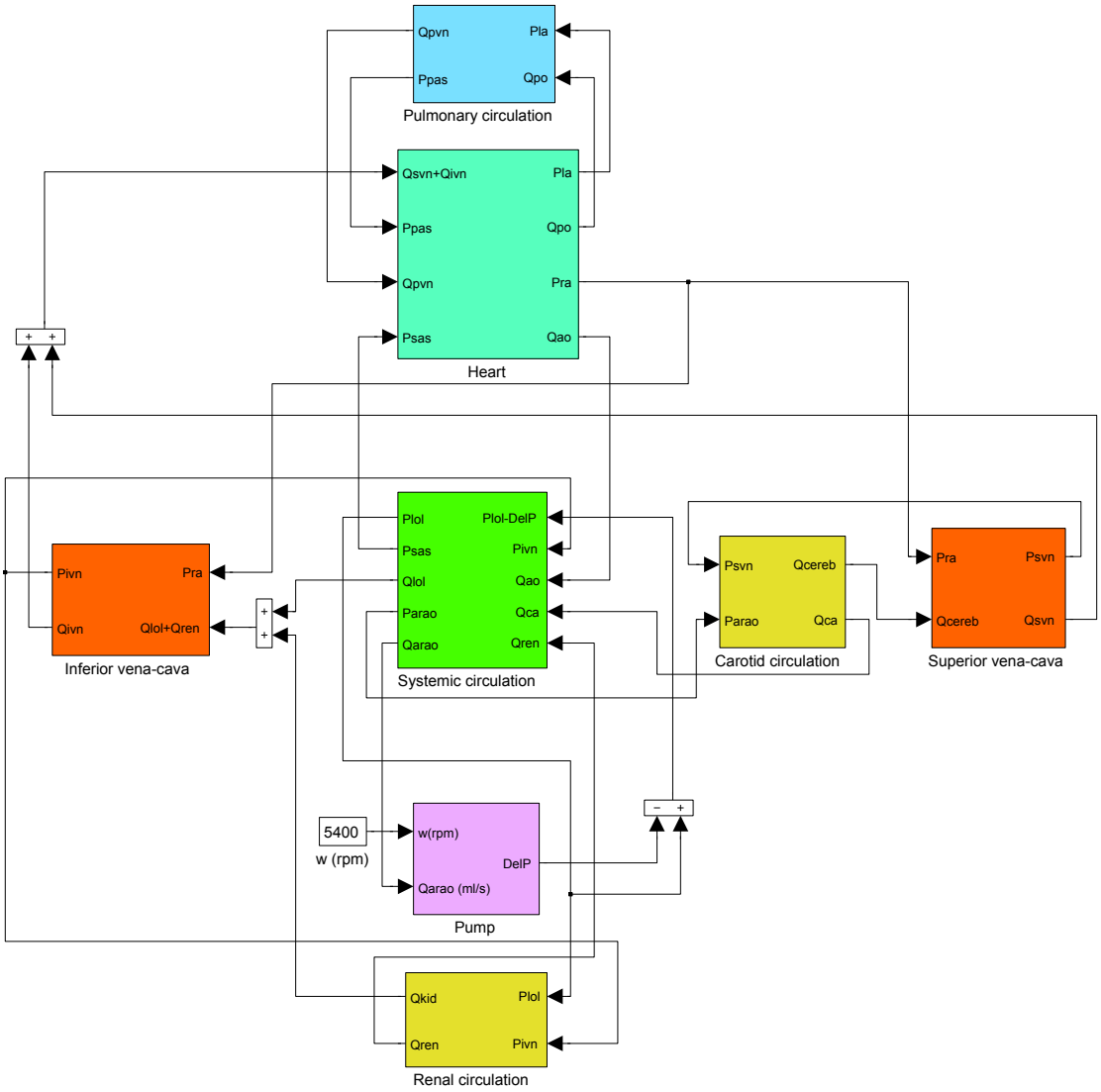

Figure 4.2: Simulink environment of the CLP model with the numerical model of pump B integrated in series with the heart.

4.2.1 Heart Model

The heart is modelled by four chambers. Each chamber is activated separately according to the corresponding time-varying elastance model, originally described by Suga et al. [93]. The volume of each chamber is evaluated through the flow-rate difference between the outlet and the inlet of the chamber. The pressure variation inside the chamber is a linear function of the volume and the corresponding elastance model. Considering the left ventricle for instance, the instantaneous left ventricle volume variation is described as the flow-rate difference between the mitral and aortic valves:

$$\frac{\mathrm{dV_{lv}}}{\mathrm{dt}} = \mathrm{Q_{mi}} - \mathrm{Q_{ao}} \tag{4.1}$$

The time-varying elastance model of the left ventricular chamber is a function of the left ventricular characteristics and the activation function.

$$\mathrm{E_{lv}(t)} = \mathrm{E_{lv_{min}}} + \frac{\mathrm{E_{lv_{max}}} - \mathrm{E_{lv_{min}}}}{2} e_{\mathrm{lv}}(t) \tag{4.2}$$

where $\mathrm{E_{lv}}(t)$ represents the time-varying elastance as a function of the maximum and the minimum elastance of the chamber ($\mathrm{E_{max}}$ and $\mathrm{E_{min}}$) and $\mathrm{e_{lv}}(t)$ represents the activation function as adopted from different studies conducted by Korakianitis et al. [98, 99, 100, 101, 102, 103].

$$e_{\mathrm{lv}}(t) = \begin{cases} 1 - \cos\left(\dfrac{t}{\mathrm{T_{vc}}}\pi\right) & : \quad 0 \leq t < \mathrm{T_{vc}} \\ 1 + \cos\left(\dfrac{t - \mathrm{T_{vc}}}{\mathrm{T_{vf}} - \mathrm{T_{vc}}}\pi\right) & : \quad \mathrm{T_{vc}} \leq t < \mathrm{T_{vf}} \\ 0 & : \quad \mathrm{T_{vf}} \leq t < \mathrm{T} \end{cases} \tag{4.3}$$

where $\mathrm{T_{vc}}$ and $\mathrm{T_{vf}}$ are related to the time to reach the maximum contraction and that to initiate chamber filling of the ventricle, respectively. Subsequently,

the pressure in the left ventricle is evaluated through the linear relation between instantaneous volume and time-varying elastance value.

$$\mathrm{P_{lv}}(t) = \mathrm{E_{lv}}(\mathrm{V_{lv}}(t) - \mathrm{V_{lv,0}}) \tag{4.4}$$

where $\mathrm{P_{lv}}(t)$ and $\mathrm{V_{lv}}(t)$ are the left ventricular pressure and volume respectively and $\mathrm{V_{lv,0}}$ is the fixed volume-axis intercept, described by Suga et al. [93]. The model for the right ventricle is similar to that for the left ventricle, apart from the values of parameters.

The atrium model is in close agreement with the ventricle model with different values. Also the form of activation function is derived based on the atrium dynamic action. Considering the left atrium for instance, the time-varying elastance model of the atrium chamber is a function of the atrium characteristic and activation function.

$$\mathrm{E_{la}}(t) = \mathrm{E_{la_{min}}} + \frac{\mathrm{E_{la_{max}}} - \mathrm{E_{la_{min}}}}{2} e_{\mathrm{la}}(t) \tag{4.5}$$

where $\mathrm{E_{la}}(t)$ represents the time-varying elastance as a function of the maximum and the minimum elastance of the chamber ($\mathrm{E_{max}}$ and $\mathrm{E_{min}}$) and $\mathrm{e_{la}}(t)$ represents the activation function as adopted from studies conducted by Korakianitis et al. [98, 99, 100, 101, 102, 103].

$$e_{\mathrm{la}}(t) = \begin{cases} 0 & : \quad 0 \leq t < \mathrm{T_{ac}} \\ 1 - \cos\left(\dfrac{t - \mathrm{T_{ac}}}{\mathrm{T_{af}} - \mathrm{T_{ac}}} 2\pi\right) & : \quad \mathrm{T_{ac}} \leq t < \mathrm{T_{af}} \\ 0 & : \quad \mathrm{T_{af}} \leq t < \mathrm{T} \end{cases} \tag{4.6}$$

where $\mathrm{T_{ac}}$ and $\mathrm{T_{af}}$ are related to the time to reach the maximum contraction and that to initiate chamber filling of the atrium, respectively. The model for the right atrium is similar to that for the left atrium with different parameter values. Figure 4.3 represents the elastance change in both the ventricles as well as the

atriums simulating the desired CHF condition during a typical heart cycle.

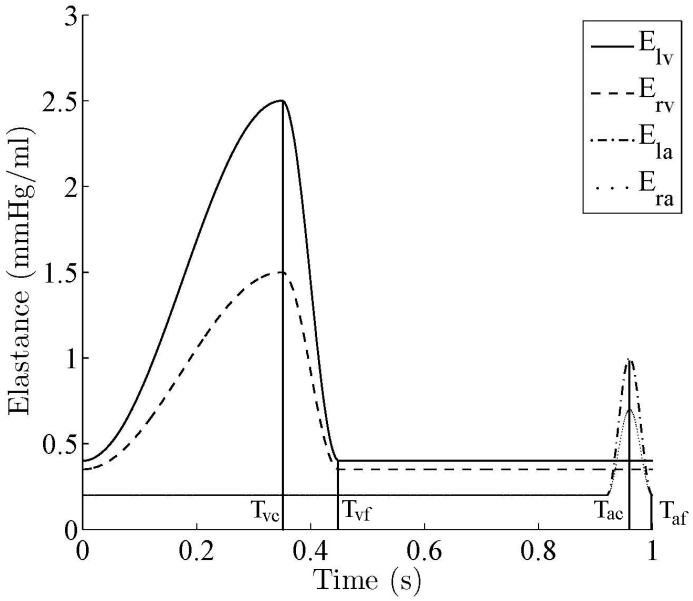

Figure 4.3: Elastance change in the left and right ventricles and the left and right atriums during a typical heart cycle modelling the desired CHF condition.

Figure 4.4 represents the heart block diagram in the Simulink environment. The heart block diagram is divided into two block diagrams for each side. Figure 4.5 represents the left side of the heart which is further subdivided into four block diagrams including the left atrium, the mitral valve, the left ventricle and the aortic valve. The left ventricle block diagram is modelled according to Equations (4.1), (4.2), (4.3) and (4.4) and the left atrium block diagram is modelled according to Equations (4.1), (4.4), (4.5) and (4.6). Figure 4.6 represents the right side of the heart which is further divided into four block diagrams including the right atrium, the tricuspid valve, the right ventricle and the pulmonic valve. The model for the right ventricle and the right atrium are similar to that for the left ventricle and the left atrium, respectively apart from the values of parameters.

The opening-closing mechanism of each valve is a function of the angular position of the valve leaflets. Considering the aortic valve for instance, the pressure-flow relation in the aortic valve can be evaluated by the orifice model adopted

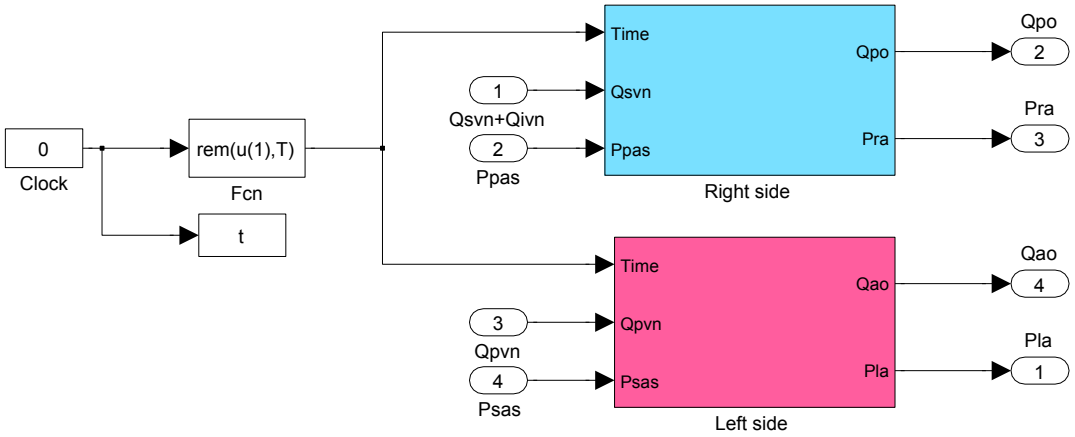

Figure 4.4: Block diagram of the heart.

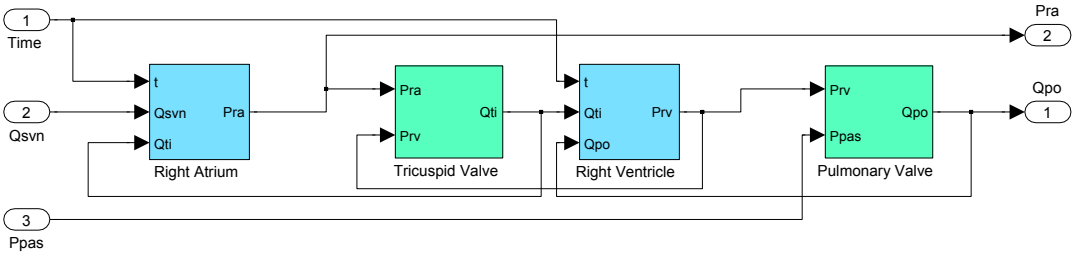

Figure 4.5: Right side of the heart block diagrams including the right atrium, the tricuspid valve, the right ventricle and the pulmonic valve.

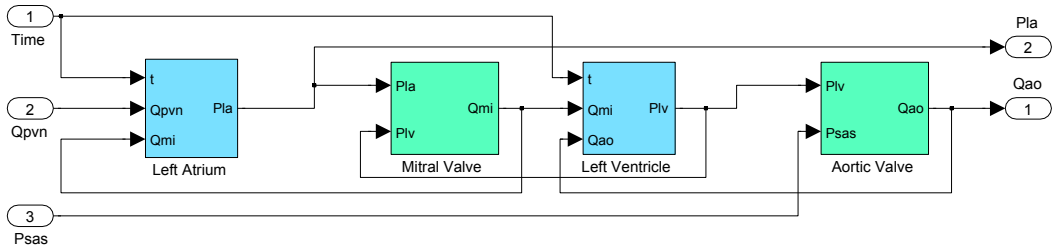

Figure 4.6: Left side of the heart block diagrams including the left atrium, the mitral valve, the left ventricle and the aortic valve.

from Granet et al. [142].

$$Q_{ao} = \begin{cases} CQ_{ao}.AR_{ao}.\sqrt{P_{lv} - P_{sas}} & : \quad P_{lv} \geq P_{sas} \\ CQ_{ao}.AR_{ao}.\sqrt{P_{sas} - P_{lv}} & : \quad P_{lv} < P_{sas} \end{cases} \tag{4.7}$$

where CQ_{ao} is the aortic flow coefficient and AR_{ao} is the area ratio of the aortic valve. According to Equation (4.8), the AR_{ao} is a function of the aortic leaflet opening angle (θ) as well as the aortic valve radius (r_{ao}):

$$AR_{ao} = \frac{\pi[r_{ao}(1 - \cos\theta)]^2}{\pi[r_{ao}(1 - \cos\theta_{max})]^2} = \frac{(1 - \cos\theta)^2}{(1 - \cos\theta_{max})^2} \tag{4.8}$$

The θ is evaluated by considering various factors that affect the leaflet motion. These include the moment due to the pressure difference across the valve, the moment generated by the shear stress on the leaflet due to fluid flow, the moment produced by the frictional force and the moment generated by the vortex near the valve leaflet surface. Here, the θ is computed using Equation (4.9) described by Korakianitis et al. [98, 99, 100, 101, 102, 103]:

$$I_{ao}\frac{d^2\theta}{dt^2} = k_{p,ao}(P_{lv} - P_{sas})A_{ao}\cos\theta - k_{f,ao}\frac{d\theta}{dt} \tag{4.9}$$

where I_{ao} is the inertial moment of rotating and A_{ao} is the sectional area of the aortic valve. $k_{p,ao}$ and $k_{f,ao}$ are the coefficients corresponding to the effect of the pressure force and frictional action, respectively. The models for the other three valves are similar to that for the aortic valve with different values.

In this study, most of the hemodynamic variables for a desired CHF condition are assigned values based on the studies conducted by Korakianitis et al. [98, 99, 100, 101, 102, 103] and the rest are based on the clinical data [2, 4, 10, 141]. The time parameters are listed in Table 4.1. The input parameters for the right and the left side of the heart to simulate the prescribed CHF are presented in Tables 4.2. The input coefficients for the valves are presented in Table 4.3.

Table 4.1: List of time parameters.

Parameter	Value	Unit
HR	70	bpm
T	1.0	s
T_{vc}	0.3	s
T_{vf}	0.45	s
T_{ac}	0.85	s
T_{af}	1.0	s

Table 4.2: Parameter of the heart for the CHF condition.

Part	Parameter	Value
Left heart	CQ_{ao}(ml/(s mm $Hg^{0.5}$))	350
	CQ_{mi}(ml/(s mm $Hg^{0.5}$))	400
	$E_{lv,max}$(mmHg/ml)	2.5
	$E_{lv,min}$(mmHg/ml)	0.4
	$V_{lv,0}$(ml)	5
	$E_{la,max}$(mmHg/ml)	1
	$E_{la,min}$(mmHg/ml)	0.2
	$V_{la,0}$(ml)	4
Right heart	CQ_{po}(ml/(s mm $Hg^{0.5}$))	350
	CQ_{ti}(ml/(s mm $Hg^{0.5}$))	400
	$E_{rv,max}$(mmHg/ml)	1.5
	$E_{rv,min}$(mmHg/ml)	0.35
	$V_{rv,0}$(ml)	1
	$E_{ra,max}$(mmHg/ml)	0.7
	$E_{ra,min}$(mmHg/ml)	0.2
	$V_{ra,0}$(ml)	1

4.2.2 Blood Circulation Loop

The blood circulation loop has been divided into the systemic and the pulmonary loops. Each loop consists of a number of components representing the artery, arteriole, capillary and vein. Each component is modelled by a series of resistance, compliance and inductance (RCL) similar to the fashion described by Lim et al. [137, 150]. Each RCL component has been tuned based on the local effects

Table 4.3: Coefficients for variable valve opening modeling.

Part	Parameter	Value
Left side	$K_{p,ao}$(m/(s^2mmHg))	5500
	$K_{f,ao}$(s^{-1})	50
	$K_{p,mi}$(m/(s^2mmHg))	5500
	$K_{f,mi}$(s^{-1})	50
Right side	$K_{p,po}$(m/(s^2mmHg))	5500
	$K_{f,ppo}$(s^{-1})	50
	$K_{p,ti}$(m/(s^2mmHg))	5500
	$K_{f,ti}$(s^{-1})	50

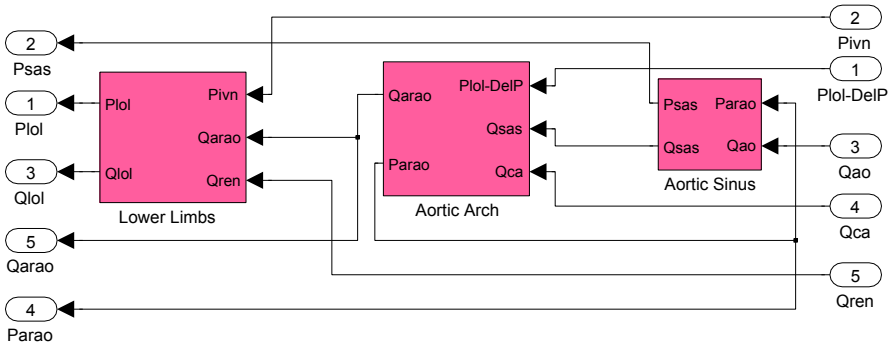

Figure 4.7: Aortic sinus, aortic arch and lower limbs block diagrams.

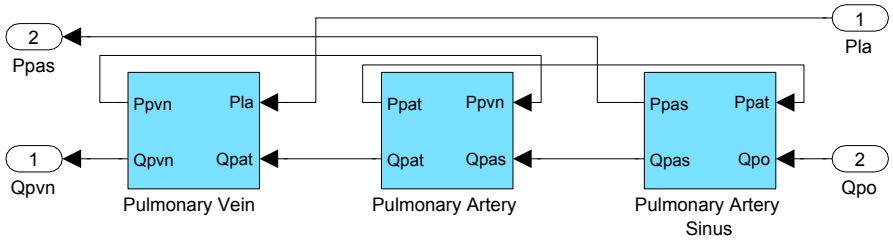

Figure 4.8: Pulmonary artery sinus, pulmonary artery and pulmonary vein block diagrams.

of friction, elasticity and inertia of the blood. Considering the pulmonary artery compartment from Figure 4.1 as an example, the dynamic pressure and the dynamic flow have been obtained from the following equations:

$$\frac{dP_{pat}}{dt} = \frac{Q_{pas} - Q_{pat}}{C_{pat}} \tag{4.10}$$

$$\frac{dQ_{pat}}{dt} = \frac{P_{pat} - P_{pvn} - (R_{pat})Q_{pat}}{L_{pat}} \tag{4.11}$$

where R_{pat}, L_{pat} and C_{pat} are the resistance, inductance and the compliance of the pulmonary artery compartment, respectively. P_{pat} and P_{pvn} represent the pressure of the pulmonary artery and pulmonary vein compartment, respectively.

Figure 4.7 represents the systemic block diagram. The systemic block diagram is further divided into three block diagrams including the aortic sinus, the

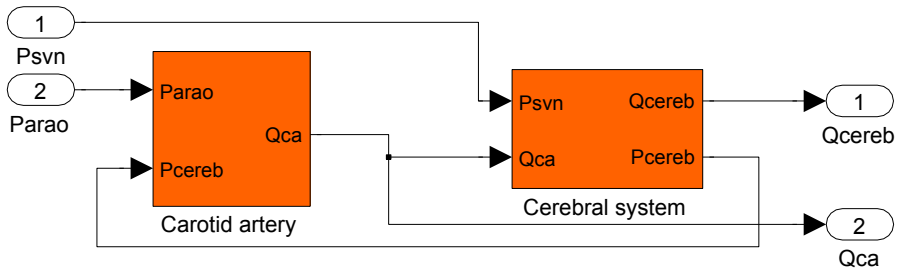

Figure 4.9: Carotid circulation compartments.

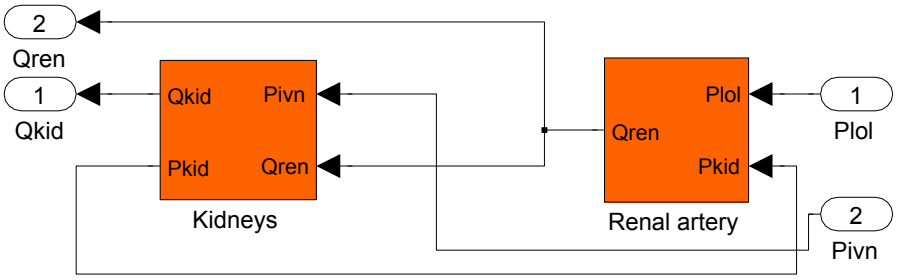

Figure 4.10: Renal circulation compartments.

aortic arch and the lower limbs compartments. Figure 4.8 shows the pulmonic circulation. The pulmonic diagram is divided into three block diagrams including the pulmonary sinus, the pulmonary artery and the pulmonary vein. In this study, in order to investigate the hemodynamic responses of the upper and the lower extremities to the pump, the carotid circulation and the renal circulation compartments have been added to the systemic loop, as shown in Figure 4.1.

Each block diagram in the systemic, pulmonic, renal and the carotid circulations is modelled according to Equations (4.10) and (4.11). However the input parameters vary depending on the dynamics of each compartment in the native cardiovascular system. The input parameters for the systemic, pulmonic, renal and the carotid circulations are presented in Table 4.4.

4.2.3 Numerical Model of the MCS Device

The typical operating condition for an MCS device in the descending aorta, in series with the heart, is 24 ± 10 mmHg against 10 lt/min [53, 60, 61]. Here, the prototyped rotary pump B simulating an MCS device with a wide range of rotor speeds (2400-5400 rpm) was employed. More details on the pump description can be found in **Chapter 2** of this thesis. Figure 4.11 shows the graph of pressure flow-rate relationship of the prototype MCS device at different rotor speeds.

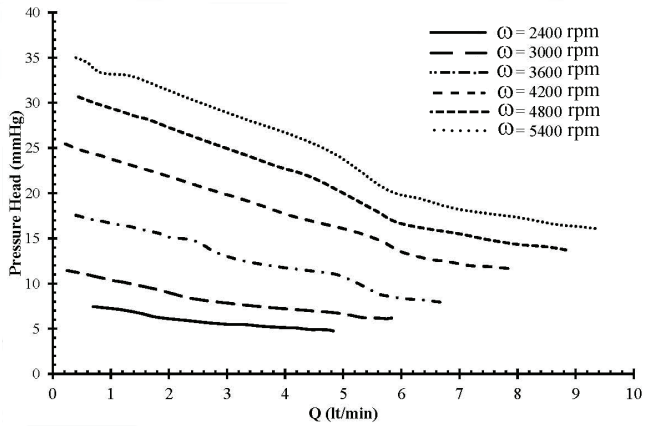

Figure 4.11: Pressure gradient (mmHg) verses flow-rate (lt/min) for the prototyped pump B. The pressure gradient against flow-rate were recorded in a non-pulsatile loop at each pump rotor speed, while the circuit resistance was increasing.

For the numerical study, the MCS device is modelled by fitting the pressure flow-rate curves into the Look-Up-Table function integrated in Simulink envi-

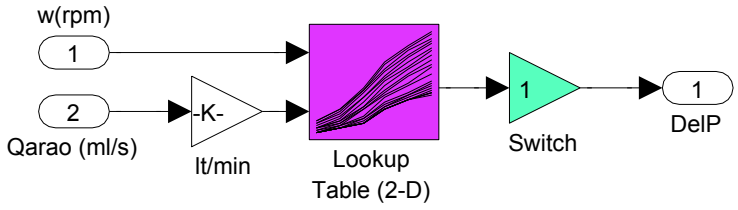

Figure 4.12: Block diagram of the pump in the Simulink environment.

ronment of the MATLAB program. Referring to the electric-fluid analogy, with the pump in series configuration, the aortic arch flow-rate (Q_{arao}) is taken as the input value to the pump and the pressure difference across the pump is the output. This is in contrast with modelling of the in-parallel configurations where the pressure difference was taken as the input parameter and the flow-rate was the output [81, 102, 103, 136, 137, 138, 139].

$$Q_{MCS} = Q_{arao} \tag{4.12}$$

The pressure difference across the pump is calculated simultaneously in terms of Q_{arao} and the rotor speed (ω) value using an in-built interpolation-extrapolation process of Look-Up-Table function, as shown in Figure 4.12. The output pressure across the pump is incorporated into the system, as shown in Figure 4.1, and ultimately induces the flow throughout the whole CLP model.

Table 4.4: Parameter of the blood vessels for the CHF condition.

Part	Parameter	Value
Systemic circulation	C_{sas}(ml/mmHg)	400
	C_{arao}(ml/mmHg)	0.1
	R_{arao}(mmHg s/ml)	0.8
	L_{arao}(mmHg $s^{0.5}$/ml)	0.0017
	V_{arao}(ml)	41.6667
	C_{lol}(ml/mmHg)	400
	R_{lol}(mmHg s/ml)	2.5
	L_{lol}(mmHg $s^{0.5}$/ml)	0.1
	R_{sar}(mmHg s/ml)	2.5
	R_{scp}(mmHg s/ml)	2.5
	V_{lv0}(ml)	5
Pulmonary circulation	C_{pas}(ml/mmHg)	400
	R_{pas}(mmHg s/ml)	2.5
	L_{pas}(mmHg $s^{0.5}$/ml)	0.1
	C_{pat}(ml/mmHg)	400
	R_{pat}(mmHg s/ml)	2.5
	L_{pat}(mmHg $s^{0.5}$/ml)	0.1
	R_{par}(mmHg s/ml)	2.5
	R_{pcp}(mmHg s/ml)	2.5
	R_{pvn}(mmHg s/ml)	2.5
	C_{pvn}(ml/mmHg)	400
	C_{pvc}(ml/mmHg)	400
	V_{rv0}(ml)	5
Carotid circulation (Carotid artery and Brain)	C_{ca}(ml/mmHg)	0.01
	R_{ca}(mmHg s/ml)	0.8
	L_{ca}(mmHg $s^{0.5}$/ml)	0.0017
	V_{ca}(ml)	57.9150
	R_{cereb}(mmHg s/ml)	0.8
	C_{svn}(ml/mmHg)	11.8196
	R_{svn}(mmHg s/ml)	1.0100
	L_{svn}(mmHg $s^{0.5}$/ml)	0.0017
	V_{svn}(ml)	100
Renal circulation (Renal artery and Kidneys)	C_{ren}(ml/mmHg)	11.8196
	R_{ren}(mmHg s/ml)	0.1422
	L_{ren}(mmHg $s^{0.5}$/ml)	0.0033
	V_{ren}(ml)	100
	R_{kid}(mmHg s/ml)	0.1422
	R_{ivn}(mmHg s/ml)	2.5
	C_{ivn}(ml/mmHg)	400
	C_{ivc}(ml/mmHg)	400

4.3 Experimental study

The objectives of experimental test are met by using our in-house multi-chamber simulator of the cardiovascular blood flow loop (SCVL). Figure 4.14 shows the photograph of the multi-chamber SCVL which has been elaborated in **Chapter 2**.

Following tasks were performed to reproduce the diseased condition.

- The circulating volume of water is increased.
- $\mathrm{Dlv_{min}}$ is increased by 20% in order to increase the resting left ventricle volume.
- $\mathrm{Dlv_{max}}$ is decreased by 20% with the purpose of mimicking the reduced left ventricle pumping ability.

Figure 4.13 represents a comparison between the slider's maximum and minimum displacement while simulating a healthy and diseased condition.

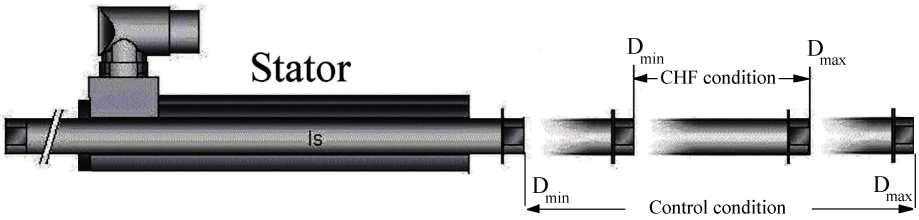

Figure 4.13: Schematic representation of the linear motor, actuating the left ventricle chamber.

The experimental measurements for the CHF condition were validated with the corresponding clinical data [2, 4, 141]. In each case, the aortic pressure, left ventricle pressure, carotid pressure waveforms as well as the average CO were recorded.

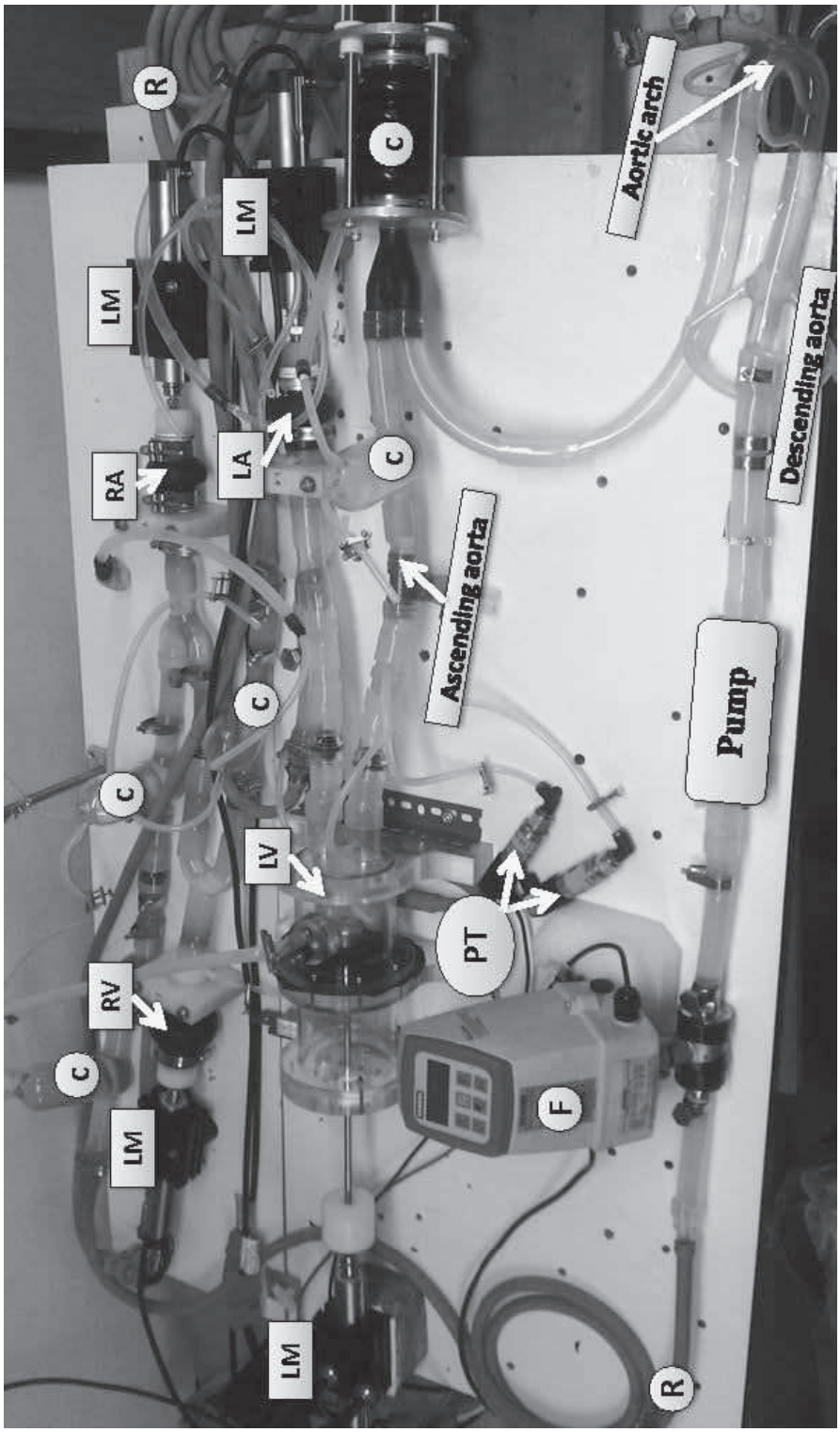

Figure 4.14: Photograph of the SCVL system with the pump in the descending aorta, LM: Linear Motor, LA: Left Atrium, LV: Left Ventricle, RA: Right Atrium, RV: Right Ventricle, C: Compliance, R: Resistance, F: Flow meter, PT: Pressure Transducer.

4.4 Results and Discussion

For the experimental test, the replication of the in-series configuration was conducted by placing the pump in the proximal descending aorta, below the Subclavian artery and above the renal arteries, as shown in Figure 4.14. Subsequently, for the numerical test, the Look-Up-Table function was incorporated into the CLP model as shown in Figure 4.1. In this experiment, to observe the ultimate hemodynamic responses of the SCVL system in the presence of the MCS device, the pump was run at its maximum rotor speed of 5400 rpm.

Figure 4.15 shows two consecutive cycles of the experimental and numerical differential pressure (ΔP) of pump B operating in the descending aorta, while the SCVL system is in operation. It is shown that the maximum differential pressure across the pump (ΔP_{max}=32 mmHg) occurs at the end-diastolic pressure (points 1), whereas the minimum differential pressure (ΔP_{min}=25 mmHg) occurs at the end-systolic pressure (point 2) of the first cardiac cycle.

It is evident that after point 1, upon the opening of the aortic valve, the experimental and numerical pressure traces fall down sharply with a good agreement until they reach to point 2 where the aortic valve closes. From point 2 toward point 3, where the second cardiac cycle begins, the numerical trace rises smoothly whereas the experimental trace does not follow the numerical trend accurately. This discrepancy can be interpreted due to the implementation of the air/water compliance units replicating viscoelastic feature of the cardiovascular system. It is also evident that as a result of the pump vibration, a number of high frequent oscillations are appearing during each cardiac cycle. Although the presence of the transient oscillations is not a major concern in our in-vitro test, in future studies it will be significantly reduced with the application of a higher grade bearing system. Considering the pressure flow-rate relationship of the pump in Figure 4.11, for the pump differential pressure changing from 32 to 25 mmHg, the corresponding flow-rates of 1.8 and 4.5 lt/min can be extracted resulting in an improved averaged flow-rate of 3.5 lt/min of the cardiac output.

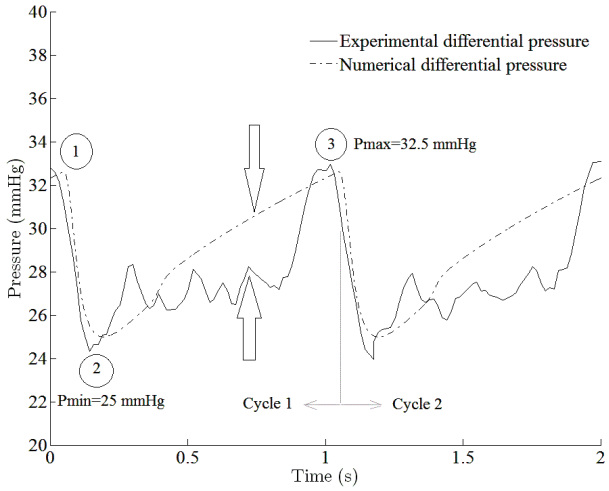

Figure 4.15: Experimental and numerical dynamic differential pressure of the MCS device operating in the descending aorta.

Figure 4.16(a) and Figure 4.16(b) show the experimental and numerical simulation as well as the corresponding clinical data [4] of the Aortic Pressure (AoP) waveforms for the CHF condition before and after the MCS device insertion in the descending aorta. It is evident that for the CHF condition the AoP is 102/79 mmHg and with the pump in operation the AoP has lowered to 80/50 mmHg. It is observed that with the pump in operation the aortic pulse pressure (Ao_{PP}) has improved from 24 mmHg for the CHF condition to 29 mmHg with the pump in operation. The improved pulse pressure is in agreement with those studies [40, 41, 42] that emphasize on the pulsatility as a beneficial aspect for end-organ functionality.

As shown in Figure 4.16(a), during the systolic and diastolic phases of the cardiac cycles the numerical and experimental simulations are in fair agreement with the corresponding clinical data [4]. The small bump reflected on the descending limb of the AoP waveform is known as dicrotic notch (Incisura) occurring due to the aortic valve closure at the pressure of 93 mmHg. It is evident that the dicrotic notch on the experimental trace is slightly larger compared to the one appearing on the clinical as well as numerical traces. This can be justified due to the inherent rigidity of the replicated aortic valve leaflets which responses slightly different from the biological valves in a native system.

In Figure 4.16(b), the small transient pressure oscillations appearing on the AoP waveform are due to the vibration occurring during the pump operation. It is also evident that the dicrotic notch is less obvious than the one for the CHF condition. This is mainly due to the pressure drop generated upstream of the MCS device that avoids the aortic valve of being fully closed.

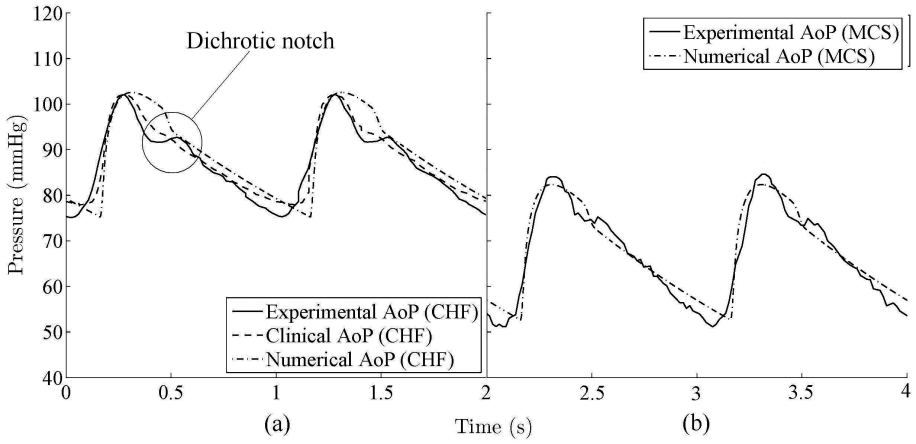

Figure 4.16: (a) Experimental, numerical and clinical [4] AoP for the CHF condition. (b) Experimental and numerical AoP with the pump in the descending aorta.

Figure 4.17(a) and Figure 4.17(b) show the experimental as well as the numerical simulation of the Left Ventricle Pressure (LVP) waveforms for the CHF condition before and after the MCS device insertion in the descending aorta, respectively. It is evident that for the CHF condition the LVP is 104/28 mmHg and with the pump in operation the LVP has lowered to 80/10 mmHg.

In Figure 4.17(a), the small pressure bump reflected just before the ascending limb of the LVP waveform represents the systolic atria contraction occurring at the end of the cardiac filling phase in a native system. It is evident that at the LVP of 100 mmHg, a significant oscillation is appearing on the experimental trace. This is regarded as the hammer effect which is due to the sudden closure of the rigid leaflets of the mechanical valve [86].

As shown in Figure 4.17(b), due to the pressure drop generated upstream of the pump, the end-diastolic pressure of the left ventricle (LVP_{dia}) has dropped to the level of 10 mmHg. A drop in LVP_{dia} leads to a lower volume expansion

and thus lower ventricular wall stress during the filling phase in a native system. This may assist with the recovery of the damaged myocardial cells in an impaired heart [144].

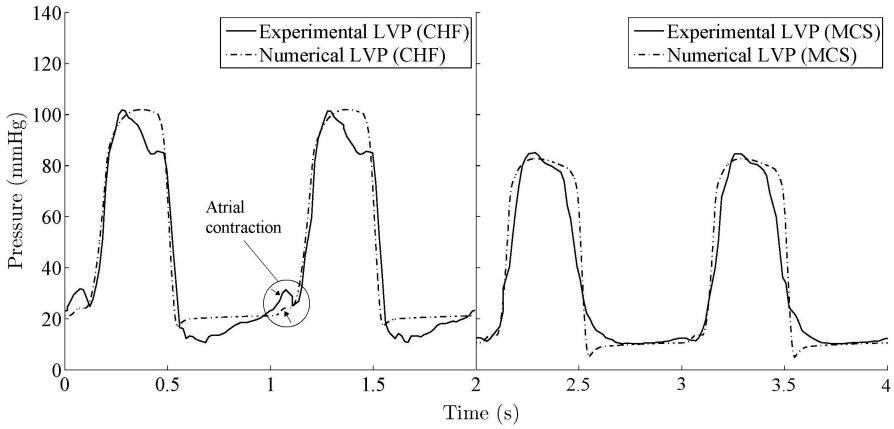

Figure 4.17: (a) Experimental and numerical LVP for the CHF condition, (b) Experimental and numerical LVP with the pump in the descending aorta.

Figure 4.18(a) and Figure 4.18(b) show the experimental and numerical simulations as well as the clinical data [141] of the Carotid Pressure (CaP) waveforms for the CHF condition before and after the MCS device insertion in the descending aorta. Figure 4.18(a) shows that for the CHF condition the CaP is 110/76 mmHg and with the pump in operation, as shown in Figure 4.18(b), it has lowered

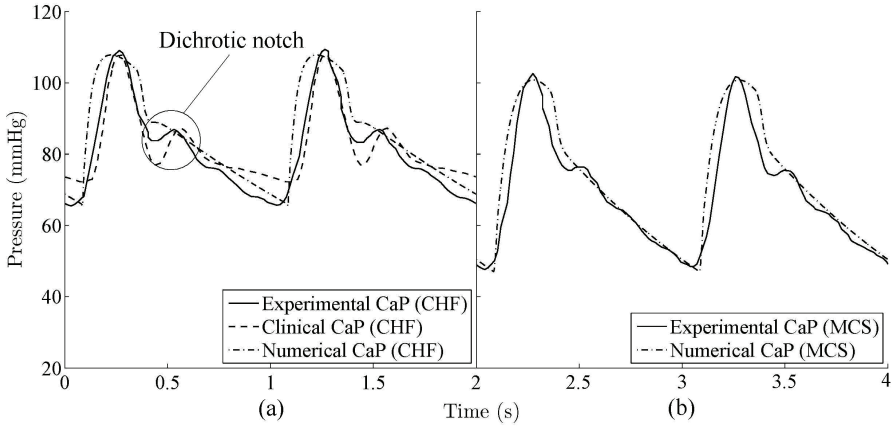

Figure 4.18: (a) Experimental, numerical, clinical [141] CaP for the CHF condition, (b) Experimental and numerical CaP with the pump in the descending aorta.

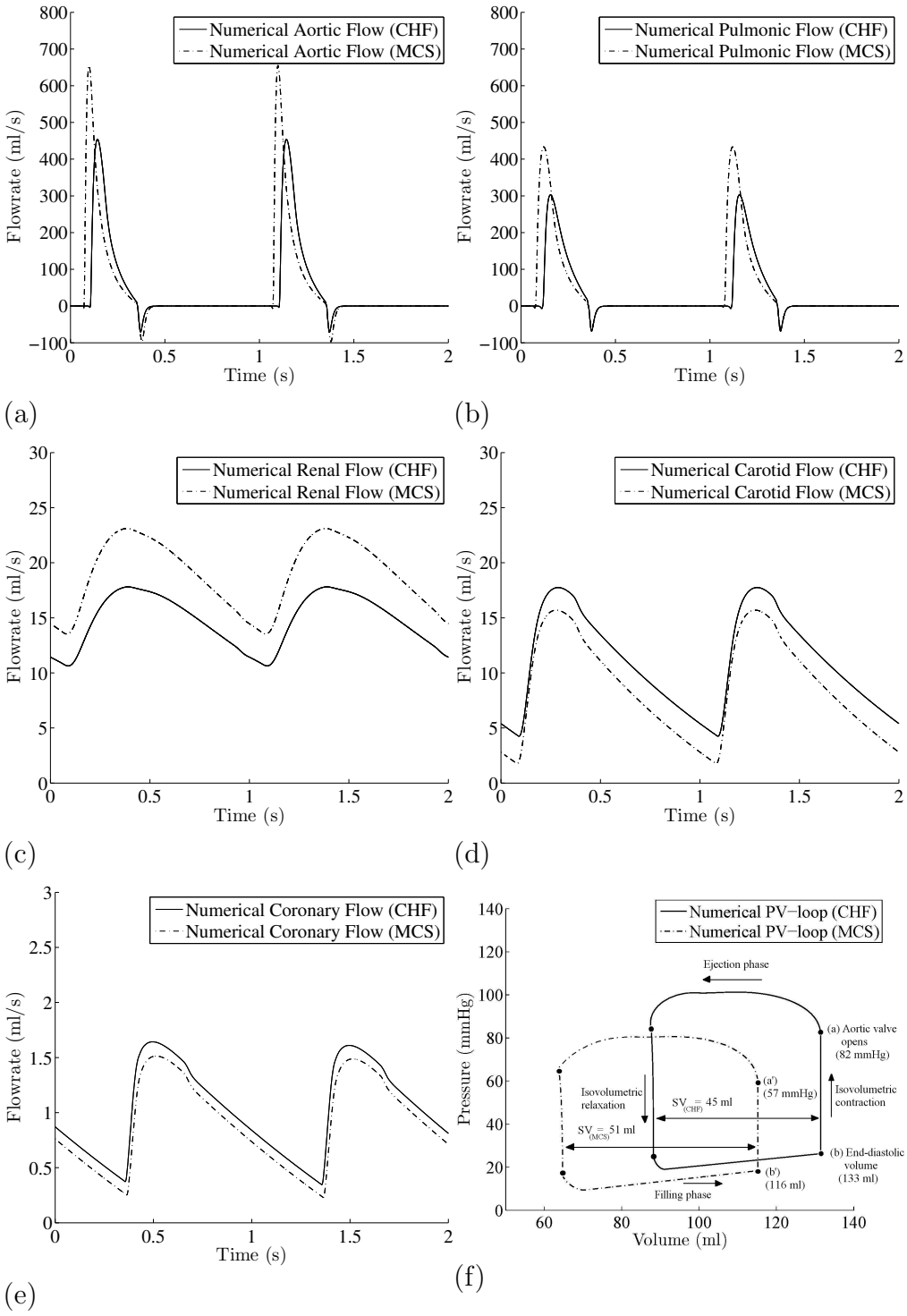

Figure 4.19: (a) Numerical time histories of the left ventricle output flow with and without the pump, (b) Numerical time histories of the right ventricle output flow with and without the pump, (c) Numerical time histories of the renal artery flow with and without the pump, (d) Numerical time histories of the carotid artery flow with and without the pump. (e) Numerical time histories of the coronary artery flow with and without the pump. (f) Numerical diagram of the pressure-volume loop with and without the pump.

to 105/48 mmHg. It is evident that the pressure drop generated upstream of the pump alleviates the end-diastolic carotid pressure (CaP_{dia}) substantially from 76 mmHg for the CHF condition to 48 mmHg, leading to a rise in the carotid pulse pressure (Ca_{PP}) from 40 to 54 mmHg.

Figures 4.19(a-f) show the numerical flow-rate past the aortic valve, the pulmonic valve, the renal arteries, the carotid artery and the coronary arteries in the presence of the pump in the descending aorta. As shown in Figure 4.19(a), with the pump in operation, the peak flows past the aortic valve ($Q_{ao,peak}$) has increased from 450 to 650 ml/s. Similarly, as shown in Figure 4.19(b), there is an improvement in the peak flows past the pulmonic valve ($Q_{po,peak}$) from 290 to 420 ml/s. In both Figures 4.19(a-b), a slight aortic and pulmonic back flow can be appreciated by negative value of the flow occurring during the aortic and the pulmonic valve closure, respectively.

The experimental flow records are in good agreement with the numerical results. It has been shown that with the pump operating at 5400 rpm in the descending aorta of the SCVL system, the average cardiac output and the average pulmonic flow have increased by about 40 and 50%, respectively.

Figure 4.19(c) shows that the renal artery flow-rate (Q_{ren}) has increased by 28% with the pump operating in the descending aorta. The mean renal artery pressure (P_{ren}) was recorded on the SCVL system. It was observed that the P_{ren} improved from 76 mmHg for the CHF condition to 90 mmHg with the pump in operation. In a native system, the renal perfusion is not autoregulated unless the P_{ren} is greater than 85 mmHg [10]. It is further demonstrated by Zanardo et al. [145] that the pressure rise in the renal artery may improve the renal function in patients suffering from the kidney failure.

Figure 4.19(d) shows that with the pump operating in the descending aorta, the carotid artery flow-rate (Q_{ca}) has dropped by 14.3% and the experimental result showed a drop of 16.6% in QR_{ca} with the pump operating at 5400 rpm. However, it must be noted that in a native human cardiovascular system, cerebral blood flow is well auto-regulated within 60-140 mmHg of AoP_{mean} and the local blood flow feedback control provides enough blood perfusion within this limit [53,

60, 61].

Figure 4.19(e) shows that the coronary artery flow-rate (Q_{cor}) has decreased by 12% with the pump operating in the descending aorta. Similar to the carotid perfusion, it must be noted that in a native system the coronary perfusion is controlled via a complex auto regulation mechanism that is dependent on the myocardial oxygen demand [10]. As indicated in the present study, with the pump operating in the descending aorta, the left ventricular internal pressure decreases dramatically implying that the myocardial oxygen demand to overcome the after load pressure may drop subsequently. It is evident that a declined heart oxygen demand will have a significant effect on the coronary autoregulation which may compensate the coronary perfusion in a native system.

Figure 4.19(f) represents the numerical diagram of the left ventricular Pressure versus Volume (PV-loop) for the CHF condition with and without the pump. The PV-loop is a useful approach of representing the cardiac performance [10]. By referring to the CHF PV-loop, it is observed that during the iso-volumetric contraction phase the maximum ventricular pressure, just before opening of the aortic valve, is 82 mmHg (point (a)), implying that the impaired heart needs to consumes a lot of energy for increasing the ventricular pressure to overcome the elevated after-load pressure, so less energy remains for the ejection phase. With the pump in operation, the MCS PV-loop shows that the maximum pressure has dropped to 57 mmHg (point (á)), indicating that more energy is consumed for the ejection phase. During the ejection phase, with the pump in operation the stroke volume has increased from 45 to 51 ml. During the iso-volumetric relaxation with the pump in operation the ventricular pressure has dropped subsequently. This may help with the elastic recoil of the ventricle in a native system [10]. Finally, during the filling phase, it is evident that the end diastolic volume has decreased from 133 ml (point (b)) to 116 ml (point (b́)) with the pump in operation.

Table 4.5 represents the hemodymanmic responses of the CLP model as well as the SCVL system to the pump operating in the descending aorta.

Table 4.5: Hemodynamic results of the cardiovascular system with the MCS device integrated in the descending aorta.

Parameters	Baseline	MCS	Units
LVP_{sys}	102	82	mmHg
LVP_{dia}	25	17	mmHg
$LVP_{valve,open}$	82	57	mmHg
AoP_{sys}	102	82	mmHg
AoP_{dia}	76	53	mmHg
AoP_{mean}	84.7	62.7	mmHg
Ao_{PP}	26	29	mmHg
CaP_{sys}	108	102	mmHg
CaP_{dia}	68	48	mmHg
CaP_{mean}	81.3	66	mmHg
Ca_{PP}	40	54	mmHg
$P_{ren,exp}$	76	90	mmHg
LVV_{sys}	88	65	ml
LVV_{dia}	133	116	ml
SV	45	51	ml
$Q_{ao\text{-}peak}$	540	650	ml/s
$Q_{po\text{-}peak}$	430	525	ml/s
$Q_{ren\text{-}peak}$	18	23	ml/s
$Q_{ca\text{-}peak}$	17.8	15.5	ml/s
$Q_{co\text{-}peak}$	1.75	1.6	ml/s
$Q_{po,exp}$	2	3.1	lt/min
$Q_{ao,exp}$	2.5	3.5	lt/min
ΔP_{max}	-	32	mmHg
ΔP_{min}	-	25	mmHg
$QR_{ca,exp}$	-	-16.6	%

4.5 Summary

Traditional implantation techniques from the apex of left ventricle to the ascending or descending aorta are highly invasive and carry substantial complications for end-stage heart failure patients. This study has shown that the descending aorta can be a promising location to install a long-term implantable mechanical circulatory support with minimally invasive surgery. Herein, the hemodynamic effect of an in-house prototyped pump implanted in the descending aorta was investigated numerically as well as experimentally. The objective of the experimental study is met by using the in-house simulator of the cardiovascular loop replicating congestive heart failure condition. The objective of the numerical study was met by using the modified version of the concentrated lumped parameter model developed by the same team. The results show that the pump placement in the descending aorta can lead to an improvement in pulsatility. The pressure drop, generated at the upstream of the pump, facilitates the cardiac output as a result of after-load reduction but at the same time, it induces a slight drop in the carotid perfusion. The pressure rise, generated at the downstream of the pump, improves the blood perfusion in the renal circulation.

Chapter 5

Conclusions and Future Work

5.1 Conclusions

Despite a significant improvement in long-term results, the use of MCS devices is still associated with considerable post-operational complications such as infection, bleeding and end-organ failure. It is reported that many of these physiological complications are due to prolonged invasive implantation procedures in critically ill patients. Therefore, less invasive alternative techniques have become an area of research interest.

Although an in-vivo test has been recognised as the most reliable approach to investigate the hemodynamic responses of cardiovascular systems, the uncontrollable environment of an in-vivo experiment results in significant uncertainties and complications. In contrast, an in-vitro simulation of the cardiovascular system which can emulate the characteristics of the native cardiovascular system not only simulates the required hemodynamic response but also avoids a number of complications that can occur in an in-vivo test. These in-vitro simulations can be classified as numerical or experimental. This thesis investigated the feasibility of MCS device implantation in the descending aorta using both experimental and numerical approaches.

As presented in Chapter 2, for the experimental investigation a Simulator of CardioVascular Loop (SCVL) was designed and developed. This system included models for all four chambers of the heart, and the systemic and pulmonary circulation loops. Each heart chamber was accurately activated by a separate linear motor to simulate the suction and ejection stages, thus capturing important features of the perfusion waveforms. Four mechanical heart valves corresponding to the mitral, pulmonary, tricuspid and aortic were used to control the desired unidirectional flow. The experimental results showed the feasibility of emulating different physiological and pathological conditions of the human cardiovascular system with this SCVL system. This was achieved by controlling the different parameters of blood circulation through the vascular tree, mainly the resistance, compliance and elastance of the heart chambers.

The experimental test on the feasibility of MCS implantation into the descending aorta in series with the heart and a comparison with two in-parallel configurations of LV-AA and LV-DA was presented in Chapter 3. It was concluded that the implementation of the LV-AA configuration results in the most significant improvement in the systemic and pulmonic flow perfusion. However, this approach requires more invasive surgery than other configurations. The LV-DA configuration is less invasive compared to the LV-AA configuration, but the LV-DA configuration was not considered as optimal due to the flow retrogradations in the aortic arch at high levels of MCS support. In both in-parallel approaches (LV-AA and LV-DA), increasing the level of MCS support led to a decrease in the aortic and the carotid pulse pressures to a certain extent. Finally, the use of an MCS device in the descending aorta showed an improvement in the systemic and pulmonic flow perfusion. In addition, it could lead to an improved haemodynamic pulsatility which is beneficial for end-organ functionality in a native cardiovascular system.

In Chapter 4, a numerical study on the in-series configuration was conducted using a modified version of the Concentrated Lumped Parameter (CLP) model. It was evident from the numerical results that the pressure drop upstream of the pump facilitated the cardiac output as a result of afterload reduction. Further, the pressure rise downstream of the pump improves the blood perfusion in the

renal circulation. In addition, similar to the experimental results, numerical studies showed that the generated pressure drop at the proximal part of the descending aorta induced a slight drop in the carotid perfusion. However, in a native cardiovascular system, the carotid perfusion drop may be autoregulated by the brain.

In conclusion, the experimental and numerical results from this study suggested that the in-series technique which is a less invasive procedure than the traditional in-parallel approaches of LV-AA and LV-DA, could be considered as a feasible configuration for long-term MCS devices. This technique can be considered for implantation of miniatured long-term MCS devices in human body in near future. However, extensive research is required to address the issues discussed in this thesis, and further analysis is needed through an in vivo test.

5.2 Future Goals

In order to achieve more reliable results from the in-vitro testing as well as the numerical simulation, a number of modifications are recommended for future studies.

- In the present study, the SCVL represents a simplified model of a patient suffering from CHF condition in a supine position only. Any changes in posture will impose additional hydrostatic pressure on the upper limbs which may lead to the risk of morbidity or mortality. For future studies, it is recommended that the pump will be equipped with a control system which responds accordingly to any sudden change of local variables including the flow and pressure. In addition, the effect of reflex mechanisms needs to be integrated into both numerical and experimental models.

- In this investigation, an open-loop control system is employed to control the position of the linear motors. This open-loop control system is capable of accurately and independently controlling the displacement of each slider

according to the predefined time-varying elastance functions. Nevertheless, simulation of desired pressure or flow signals through an open-loop control system is not an easy task and it is mainly calibrated manually using a trial and error process. As a result, the open-loop control system is not the best option. For future studies, it is recommended to integrate a closed-loop proportional-integral control system. The closed-loop control system is more accurate than the open-loop control system and it performs well for multi-variable systems.

- In the present study, the systemic and pulmonic resistances are replicated using a number of clips, adjusted manually to simulate different physiological and pathological conditions. In future studies, the clips can be replaced by proportional control pinch valves for a more adaptable system.

- The current multi-chamber SCVL system as well as our numerical model do not include the auto-regulation mechanism for the cerebral and kidney components. The numerical simulation and the in-vitro testing could eventually be extended to include these mechanisms.

- During this experiment our cardiovascular simulator was under development, so the use of animal blood or blood analog fluids (mixtures of water and glycerine) was not feasible at this stage. It is evident that the viscosity is considered as a profound parameter for the design of a rotary blood pump, however it may not have a significant impact on the hemodynamic responses of the SCVL system in the presence of the MCS device. For future studies, it is recommended that a blood analogue fluid should be employed to investigate haematological and thrombological blood complications.

Appendices

Publications:

Publications extracted from this research and my previous area of research are listed as follow:

- Design of high-efficiency turbomachinery blades for energy conversion devices with the three dimensional prescribed surface curvature distribution blade design (CIRCLE) method. T. Korakianitis, I. Hamakhan, **M. A. Rezaienia**, A. P. S. Wheeler, E. Avital and J. J. R. Williams. Applied Energy, Vol 89, pp. 215-227, 2012.

- Aerodynamic improvements of wind-turbine airfoil geometries with the prescribed surface curvature distribution (CIRCLE) blade design method, T. Korakianitis, **M. A. Rezaienia**, I. Hamakhan, E. Avital and J. J. R. Williams, Journal of Engineering for Gas Turbines and Power, Transactions of the ASME, Vol 134, Issue 8, 2012.

- Two- and three-dimensional prescribed surface curvature distribution (CIRCLE) blade design method for the design of high-efficiency turbines, compressors and isolated airfoils. T. Korakianitis, I. Hamakhan, **M. A. Rezaienia** and A. P. S. Wheeler, Journal of Turbomachinery, Transaction of the ASME, Vol 135, Issue 3, 2013.

- In vitro cardiovascular system emulator (bioreactor) for the simulation of normal and diseased conditions with and without mechanical circulatory support, P. Ruiz, **M. A. Rezaienia**, A. Rahideh, T. R. Keeble, M. T. Rothman, T. Korakianatis, Artificial organs, 37(6):549-560, Jun 2013.

- In-vitro comparison of two different mechanical circulatory support devices installed in series and in Parallel **M. A. Rezaienia**, A. Rahideh, M. T. Rothman, S. A. Sell, K. Mitchell, T. Korakianitis, accepted for published in the Artificial Organs Journal.

- Numerical and in-vitro investigation of a novel mechanical circulatory support device installed in the descending aorta. **M. A. Rezaienia**, A. Rahideh, B. Alhosseini ,S. P. Zustiak, D. E. M. Bosak, T. Korakianitis, accepted for published in the Artificial Organs Journal.

Bibliography

[1] R.J. Levick. *An Introduction to Cardiovascular Physiology*. Hodder Arnold, 4th edition, 2003.

[2] E. I. Cabrera Fischer, R. L. Armentano, F. M. Pessana, S. Graf, L. Romero, A. I. Christen, A. Simon, and J. Levenson. Endothelium-dependent arterial wall tone elasticity modulated by blood viscosity. *American Journal of Physiology-Heart and Circulatory Physiology*, 282(2):H389–394, 2002.

[3] M. Starling. Left ventricular-arterial coupling relations in the normal human heart. *American Heart Journal*, 125:1659–1666, 1993.

[4] S. J. Denardo, R. Nandyala, G. L. Freeman, G. L. Pierce, and W. W. Nichols. Pulse wave analysis of the aortic pressure waveform in severe left ventricular systolic dysfunction. *Circulation-Heart Failure*, 3(1):149–156, 2010.

[5] K. Swedberg, J. Cleland, H. Dargie, H. Drexler, F. Follath, M. Komajda, L. Tavazzi, O. A. Smiseth, A. Gavazzi, A. Haverich, A. Hoes, T. Jaarsma, J. Korewicki, S. Levy, C. Linde, J. L. Lopez-Sendon, M. S. Nieminen, L. Pierard, W. J. Remme, and Diagnosis Chronic Heart Euro Soc. Guidelines for the diagnosis and treatment of chronic heart failure: executive summary (update 2005). *European Heart Journal*, 26(11):1115–1140, Jun. 2005.

[6] W.J. Remme and K. Swedberg. Comprehensive guidelines for the diagnosis and treatment of chronic heart failure - task force for the diagnosis and

treatment of chronic heart failure of the european society of cardiology. *Euorpean Journal of Heart Failure*, 4(1):11–22, Jan. 2002.

[7] R. M. Califf and J. R. Bengtson. Current concepts - cardiogenic-shock. *New England Journal of Medicine*, 330(24):1724–1730, 16th Jun. 1994.

[8] J Lloyd. Heart disease and stroke statistics-2009 update: A report from the american heart association statistics committee and stroke statistics subcommittee (vol 119, pg e21, 2009). *Circulation*, 124(16):E424, Oct 18 2011.

[9] C. Christiansen, A. Klocke, and R Autschbach. Past, present, and future of long-term mechanical cardiac support in adults. *Journal of Cardiac Surgery*, 23(6):664–676, Nov-Dec 2008.

[10] A. C. Guyton and J. E. Hall. *Textbook of Medical Physiology*. Elsevier Saunders, 2006.

[11] P. J. Hauptman, S. J. Goodlin, M Lopatin, M. R Costanzo, G. C. Fonarow, C. W. Yancy, ADHERE Sci Advisory Study Grp, and ADHERE Study Grp. Characteristics of patients hospitalized with acute decompensated heart failure who are referred for hospice care. *Archives of internal medicine*, 167(18):1990–1997, Oct 2007.

[12] T. G. Ganiats, D. K. Browner, and H. C. Dittrich. Comparison of quality of well-being scale and nyha functional status classification in patients with atrial fibrillation. *American Heart Journal*, 135(5):819–824, 1998.

[13] N. H. Guiha, J. N. Cohn, E. Mikulic, J. A. Francios, and C. J. Limas. Treatment of refractory heart-failure with infusion of nitroprusside. *New England Journal of Medicine*, 291(12):587–592, 1974.

[14] D. A. Macgregor, J. F. Butterworth, G. P. Zaloga, R. C. Prielipp, R. James, and R. L. Royster. Hemodynamic and renal effects of dopexamine and dobutamine in patients with reduced cardiac-output following coronary-artery bypass-grafting. *Chest*, 106(3):835–841, Sep. 1994.

[15] Sharon A. Hunt. Taking heart - cardiac transplantation past, present, and future. *New England Journal of Medicine*, 355(3):231–235, Jul 20 2006.

[16] S Westaby and M Deng. Continuous flow blood pumps: the new gold standard for advanced heart failure? *Europen Journal of Cardio-Thoracic Surgery*, 44:4–8, 2013.

[17] J Stehlik, L. B. Edwards, A. Y. Kucheryavaya, P Aurora, J. D. Christie, R Kirk, F Dobbels, A. O. Rahmel, and M. I. Hertz. The registry of theinternational society for heart and lung transplantation: twenty-seventh official adult heart transplant report-2010. *Journal of Heart and Lung Transplantation*, 29(10):1089–1103, OCT 2010.

[18] L. E. Barker. The total artificial heart. *AACN Clin Issues Crit Care Nurs*, 2(3):587–97, 1991.

[19] M. J Slepian, Y Alemu, J. S Soares, Smith R. G, S Einav, and D Bluestein. The syncardia (tm) total artificial heart: in vivo, in vitro, and computational modeling studies. *Journal of Biomechanical*, 46:266–75, Jan 2013.

[20] R. D. Dowling, L. A. Gray, S. W. Etoch, H. Laks, D. Marelli, L. Samuels, J. Ebtwhistle, G. Couper, G. J. Vlahakes, and O. H. Frazier. The abiocor implantable replacement heart. *Annals of Thoracic Surgery*, 75(6, S):S93–S99, Jun. 2003.

[21] S. D. Moulopoulos, S. Topaz, and W. J. Kolff. Diastolic balloon pumping(with carbon dioxide) in the aorta–a mechanical assistance to the failing circulation. *American Heart Journal*, 63:669–75, 1962.

[22] R.W. Smalling, M. Sweeney, B. Lachterman, M.J. Hess, R. Morris, H.V. Anderson, J. Heibig, G. Li, J.T. Willerson, O.H. Frazier, and R.K. Wampler. Transvalvular left-ventricular assistance in cardiogenic-shock secondary to acute myocardial-infarction - evidence for recovery from near-fatal myocardial stunning. *Journal of The American College of Cardiology*, 23(3):637–644, 1st Mar. 1994.

[23] O. H. Frazier, T. J. Myers, R. K. Jarvik, S. Westaby, D. W. Pigott, I. D. Gregoric, T. Khan, D. W. Tamez, J. L. Conger, and M. P. Macris. Research and development of an implantable, axial-flow left ventricular assist device: the jarvik 2000 heart. *Annals of Thoracic Surgery*, 71:125–132, 2001.

[24] R. Hetzer, Y. G. Weng, E. V. Potapov, M. Pasic, T. Drews, M. Jurmann, E. Hennig, and J. Muller. First experiences with a novel magnetically suspended axial flow left ventricular assist device. *European Journal of Cardio-Thoracic Surgery*, 25(6):964–970, Jun. 2004.

[25] D. D. Schocken, M. I. Arrieta, P. E. Leaverton, and E. A. Ross. Prevalence and mortality-rate of congnsive-heart-failure in the united-states. *Journal of The American College of Cardiology*, 20(2):301–306, Aug. 1992.

[26] O. H. Frazier. First use of an untethered, vented electric left-ventricular assist device for long-term support. *Circulation*, 89(6):2908–2914, Jun. 1994.

[27] B. P. Griffith, R. L. Kormos, H. S. Borovetz, K. Litwak, J. F. Antaki, V. L. Poirier, and K. C. Butler. Heartmate ii left ventricular assist system: From concept to first clinical use. *Annals of Thoracic Surgery*, 71(3, S):S116–S120, Mar. 2001.

[28] K. D. Aaronson, M. J. Eppinger, D. B. Dyke, S. Wright, and F. D. Pagani. Left ventricular assist device therapy improves utilization of donor hearts. *Journal of the American College Of Cardiology*, 39(8):1247–1254, 17th Apr. 2002.

[29] T. Drews, M. Jurmann, D. Michael, P. Miralem, Y. Weng, and R. Hetzer. Differences in pulsatile and non-pulsatile mechanical circulatory support in long-term use. *Journal of Heart and Lung Transplantation*, 27(10):1096–1101, Oct. 2008.

[30] E. Tuzun, K. Eya, H. K. Chee, J. L. Conger, N. K. Bruno, O. H. Frazier, and K. A. Kadipasaoglu. Myocardial hemodynamics, physiology, and perfusion with an axial flow left ventricular assist device in the calf. *ASAIO Journal*, 50(1):47–53, Jan.-Feb. 2004.

[31] T. J. Myers, T. Khan, and O. H. Frazier. Infectious complications associated with ventricular assist systems. *ASAIO Journal*, 46(6):S28–S36, Nov.-Dec. 2000.

[32] M. Macris, T. J. Myers, and R. Jarvik. In vivo revolutation of an electri intraventricular axial flow pump assist device. *Asaio Journal*, 40:719–722, 1994.

[33] D. J. Farrar, S. H. Reichenbach, S. A. Rossi, and J. R. Weidman. Development of an intracorporeal thoratec ventricular assist device for univentricular or biventricular support. *ASAIO Journal*, 46(3):351–353, May-Jun. 2000.

[34] Y. Nose and K. Furukawa. Current status of the gyro centrifugal blood pump-development of the permanently implantable centrifugal blood pump as a biventricular assist device (nedo project). *Artificial Organs*, 28(10):953–958, Oct. 2004.

[35] D. Liotta, C. W. Hall, D. A. Cooley, and M. E. De Bakey. Prolonged ventricular bypass with intrathoracic pumps. *Transactions - American Society for Artificial Internal Organs*, 10:154–156, 1964.

[36] L. E. Samuels, J. C. Entwistle, E. C. Holmes, T. Parris, and A. S. Wechsler. Mechanical support of the unrepaired postinfarction ventricular septal defect with the abiomed bvs 5000 ventricular assist device. *Journal of Thoracic and Cardiovascular Surgery*, 126(6):2100–2101, Dec. 2003.

[37] D. J. Farrar, W. R. Holman, L. R. McBride, R. L. Kormos, T. B. Icenogle, P. J. Hendry, C. H. Moore, D. Y. Loisance, A. El-Banayosy, and H. Frazier. Long-term follow-up of thoratec ventricular assist device bridge-to-recovery patients successfully removed from support after recovery of ventricular function. *Journal of Heart and Lung Transplantation*, 21(5):516–521, May 2002.

[38] E. A. Farkas and J. A. Elefteriades. Assisted circulation: experience with the novacor (r) left ventricular assist system. *Expert Review of Medical Devices*, 4(6):769–774, Nov. 2007.

[39] S. M. Mehta, W. E. Pae, C. Rosenberg, A. J. Snyder, W. J. Weiss, J. P. Lewis, M. Eng, D. J. Frank, M. Eng, J. J. Thompson, and W. S. Pierce. The lionheart lvd-2000: A completely implanted left ventricular assist device for chronic circulatory support. *Annals of Thoracic Surgery*, 71(3, S):S156–S161, Mar. 2001.

[40] H. K. Kim, H. S. Son, Y. H. Fang, S. Y. Park, C. M. Hwang, and K. Sun. The effects of pulsatile flow upon renal tissue perfusion during cardiopulmonary bypass: A comparative study of pulsatile and nonpulsatile flow. *ASAIO Journal*, 51(1):30–36, Jan.-Feb. 2005.

[41] A. Undar. Myths and truths of pulsatile and nonpulsatile perfusion during acute and chronic cardiac support. *Artificial Organs*, 28(5):439–443, May 2004.

[42] A. Sezai, M. Shiono, Y. Orime, K. Nakata, M. Hata, M. Iida, S. Kashiwazaki, J. Kinoshita, M. Nemoto, T. Koujima, M. Furuichi, K. Eda, H. Hirose, T. Yoshino, A. Saitoh, T. Taniguchi, and Y. Sezai. Major organ function under mechanical support: Comparative studies of pulsatile and nonpulsatile circulation. *Artificial Organs*, 23(3):280–285, Mar. 1999.

[43] G. S. Allen, K. D. Murray, and D. B. Olsen. The importance of pulsatile and nonpulsatile flow in the design of blood pumps. *Artificial Organs*, 21(8):922–928, Aug. 1997.

[44] L. R. Golding, G. Jacobs, T. Murakami, S. Takatani, F. Valdes, H. Harasaki, and Y. Nose. Chronic non-pulsatile blood-flow in an alive, awake animal 34-day survival. *Transactions American Society for Artificial Internal Organs*, 26:251–255, 1980.

[45] M. S. Slaughter, M. A. Sobieski, D. Tamez, T. Horrell, J. Graham, P. S. Pappas, A. J. Tatooles, and J. LaRose. Heartware miniature axial-flow ventricular assist device design and initial feasibility test. *Texas Heart Institute Journal*, 36(1):12–16, Feb. 2009.

[46] A. G. Rose, S. J. Park, A. J. Bank, and L. W. Miller. Partial aortic valve fusion induced by left ventricular assist device. *Annals of Thoracic Surgery*, 70(4):1270–1274, Oct. 2000.

[47] J.D. Hill and O. Reinhartz. Clinical outcomes in pediatric patients implanted with thoratec ventricular assist device. *Seminars in Thoracic and Cardiovascular Surgery: Pediatric Cardiac Surgery Annual*, 9(1):115–122, 2006.

[48] T. Komoda, Y. Weng, C. Nojiri, and R. Hetzer. Implantation technique for the duraheart left ventricular assist system. *Journal of Artificial Organs*, 10(2):124–127, 2007.

[49] K. Bourque, D. B. Gernes, H. M. Loree, J. S. Richardson, V. L. Poirier, N. Barletta, A. Fleischli, G. Foiera, T. M. Gempp, R. Schoeb, K. N. Litwak, T. Akimoto, M. J. Watach, and P. Litwak. Heartmate iii: Pump design for a centrifugal lvad with a magnetically levitated rotor. *ASAIO Journal*, 47(4):401–405, Jul.-Aug. 2001.

[50] D. J. Burke, E. Burke, F. Parsaie, V. Poirier, K. Butler, D. Thomas, L. Taylor, and T. Maher. The heartmate ii: Design and development of a fully sealed axial flow left ventricular assist system. *Artificial Organs*, 25(5):380–385, May 2001.

[51] R. Hetzer, E. V. Potapov, Y. G. Weng, H. Sinawski, F. Knollmann, T. Komoda, E. Hennig, and M. Pasic. Implantation of micromed debakey vad through left thoracotomy after previous median sternotomy operations. *Annals of Thoracic Surgery*, 77(1):347–350, Jan. 2004.

[52] M. Goldowsky. Magnevad - the world's smallest magnetic-bearing turbo pump. *Artificial Organs*, 28(10):945–952, Oct. 2004.

[53] O. Reitan, S. Steen, and H. Ohlin. Hemodynamic effects of a new percutaneous circulatory support device in a left ventricular failure model. *ASAIO Journal*, 49:731–736, 2003.

[54] B. Kar, R. M. Delgado, O. H. Frazier, I. D. Gregoric, M. T. Harting, Y. Wadia, T. J. Myers, R. D. Moser, and J. Freund. The effect of lvad investigation aortic outflow-graft placement on hemodynamics and flow - implantation technique and computer flow modeling. *Texas Heart Institute Journal*, 32(3):294–298, 2005.

[55] K. N. Litwak, S. C. Koenig, R. C. Cheng, G. A. Giridharan, K. J. Gillars, and G. M. Pantalos. Ascending aorta outflow graft location and pulsatile ventricular assist provide optimal hemodynamic support in an adult mock circulation. *Artificial Organs*, 29(8):629–635, Aug. 2005.

[56] C. H. Selzman and B. C. Sheridan. Off-pump insertion of continuous flow left ventricular assist devices. *Journal of Cardiac Surgery*, 22(4):320–322, Jul.-Aug. 2007.

[57] I. D. Gregoric, S. La Francesca, T. Myers, W. Cohn, P. Loyalka, B. Kar, C. Gemmato, and O. H. Frazier. A less invasive approach to axial flow pump insertion. *Journal of Heart and Lung Transplantation*, 27(4):423–426, Apr. 2008.

[58] M. Pasic, P. Bergs, E. Hennig, M. Loebe, Y. G. Weng, and R. Hetzer. Simplified technique for implantation of a left ventricular assist system after previous cardiac operations. *Annals of Thoracic Surgery*, 67(2):562–564, Feb. 1999.

[59] L. A. Baloa, J. R. Boston, and J. F. Antaki. Elastance-based control of a mock circulatory system. *Annals of Biomedical Engineering*, 29(3):244–251, 2001.

[60] O. Reitan, J. Sternby, and H. Ohlin. Hydrodynamic properties of a new percutaneous intra-aortic axial flow pump. *ASAIO Journal*, 46:323–329, 2000.

[61] E. J. Smith, O. Reitan, T. Keeble, K. Dixon, and M. T. Rothman. A first-in-man study of the reitan catheter pump for circulatory support in patients undergoing high-risk percutaneous coronary intervention. *Catheterization and Cardiovascular Interventions*, 73:859–865, 2009.

[62] J. F. Cornhill. Aortic left ventricular pulse duplicator used in testing prosthetic aortic heart-valves. *Journal of Thoracic and Cardiovascular Surgery*, 73(4):550–558, 1977.

[63] L. N. Scotten, D. K. Walker, and R. T. Brownlee. Construction and evaluation of a hydromechanical simulation facility for the assesment of mitral-valve prostheses. *Journal of Medical Engineering & Technology*, 3(1):11–18, 1979.

[64] D. K. Walker, L. N. Scotten, V. J. Modi, and R. T. Brownlee. Invitro assessment of mitral-valve protheses. *Journal of Thoracic and Cardiovascular Surgery*, 79:680–688, 1980.

[65] H. Schima, S. Tsangaris, P. Zilla, M. Kadletz, and E. Wolner. Mechanical simulation of shear-stress on the walls of peripheral arteries. *Journal of Biomechanics*, 23(8):845–851, 1990.

[66] P. Sipkema, R. D. Latham, N. Westerhof, B. J. Rubal, and D. M. Slife. Isolated aorta setup for hemodynamic-studies. *Annals of Biomedical Engineering*, 18(5):491–503, 1990.

[67] H. Schima, H. Baumgartner, F. Spitaler, P. Kuhn, and E. Wolner. A modular mock circulation for hydromechanical studies on valves, stenoses, vascular grafts and cardiac devices. *International Journal of Artificial Organs*, 15(7):417–421, 1992.

[68] L. A. Garrison, J. A. Frangos, D. B. Geselowitz, T. C. Lamson, and J. M. Tarbell. A new mock circulatory loop and its application to the study of chemical additive and aortic pressure effects on hemolysis in the penn state electric ventricular assist device. *Artificial Organs*, 18(5):397–407, 1994.

[69] M. A. Helal, K. C. Watts, and A. E. Marble. Hydrodynamic simulation of arterial networks which include compliant and rigid bypass grafts. *Journal of Biomechanics*, 27(3):277–287, 1994.

[70] S. Vandenberghe, P. Segers, B. Meyns, and P. Verdonck. Hydrodynamic characterisation of ventricular assist devices. *International Journal of Artificial Organs*, 24(7):470–477, 2001.

[71] B. Knierbein, H. Reul, R. Eilers, M. Lange, R. Kaufmann, and G. Rau. Compact mock loops of the systemic and pulmonary circulation for blood pump testings. *International Journal of Artificial Organs*, 15(1):40–48, 1992.

[72] G. Ferrari, C. Delazzari, R. Mimmo, D. Ambrosi, and G. Tosti. Mock circulatory-system for in-vitro reproduction of the left-ventricle, the arterial tree and their interaction with a left-ventricular assist device. *Journal of Medical Engineering & Technology*, 18(3):87–95, 1994.

[73] P. Vermette, J. Thibault, and G. Laroche. A continuous and pulsatile flow circulation system for evaluation of cardiovascular devices. *Artificial Organs*, 22(9):746–752, 1998.

[74] M. K. Sharp and R. K. Dharmalingam. Development of a hydraulic model of the human systemic circulation. *ASAIO Journal*, 45:535–540, 1999.

[75] J. D. Schaub, S. C. Koenig, M. J. Schroeder, D. L. Ewert, G. A. Drew, and R. D. Swope. Development of a flow feedback pulse duplicator system with rhesus monkey arterial input impedance characteristics. *ASAIO Journal*, 45(4):334–338, 1999.

[76] G. Ferrari, A. Nicoletti, C. De Lazzari, F. Clemente, G. Tosti, M. Guaragno, R. Mimmo, D. Ambrosi, and K. Gorczynska. A physical model of the human systemic arterial tree. *International Journal of Artificial Organs*, 23(9):647–657, 2000.

[77] G. Ferrari, M. Kozarski, C. De Lazzari, F. Clemente, M. Merolli, G. Tosti, M. Guaragno, R. Mimmo, D. Ambrosi, and J. Glapinski. A hybrid (numerical-physical) model of the left ventricle. *International Journal of Artificial Organs*, 24(7):456–462, 2001.

[78] F. M. Colacino, F. Moscato, F. Piedimonte, G. Danieli, S. Nicosia, and M. Arabia. A modified elastance model to control mock ventricles in real-time: Numerical and experimental validation. *ASAIO Journal*, 54(6):563–573, 2008.

[79] K. Sagawa, L. Maughan, H. Suga, and K. Sunagawa. *Cardiac contraction and thepressure volume relationship*. Oxford University Press, 1988.

[80] A.C. Guyton. *Textbook of Medical Physiology*. W.B. Saunders Company, 1986.

[81] G. Ferrari, C. D. Lazzari, M. Kozarski, F. Clemente, K. Gorczynska, R. Mimmo, E. Monnanni, G. Tosti, and M. Guaragno. A hybrid mock circulatory system: Testing a prototype under physiologic and pathological conditions. *ASAIO Journal*, 48(5):487–494, 2002.

[82] N. Westerhof, J. W. Lankhaar, and B. E. Westerhof. The arterial windkessel. *Medical & Biological Engineering & Computing*, 47(2):131–141, 2009.

[83] D. Timms, M. Hayne, K. McNeil, and A. Galbraith. A complete mock circulation loop for the evaluation of left, right, and biventricular assist devices. *Artificial Organs*, 29(7):564–572, 2005.

[84] M. A. Z. Garcia, L. A. Enriquez, W. Dembitsky, and K. May-Newman. The effect of aortic valve incompetence on the hemodynamics of a continuous flow, ventricular assist device in a mock circulation. *ASAIO Journal*, 54(3):237–244, 2008.

[85] D. Legendre, J. Fonseca, A. Andrade, J. F. Biscegli, R. Manrique, D. Guerrino, A. K. Prakasan, J. P. Ortiz, and J. C. Lucchi. Mock circulatory system for the evaluation of left ventricular assist devices, endoluminal prostheses, and vascular diseases. *Artificial Organs*, 32(6):461–467, 2008.

[86] M. K. Sharp, C. M. Richards, K. J. Gillars, G. Giridharan, and G. M. Pantalos. The influence of mock circulation input impedance on valve accelera-

tion during in vitro cardiac device testing. *ASAIO Journal*, 54(4):341–346, 2008.

[87] R. Zannoli, I. Corazza, and A. Branzi. Mechanical simulator of the cardiovascular system. *Physica Medica*, 25(2):94–100, 2009.

[88] G. M. Pantalos, C. Ionan, S. C. Koenig, K. J. Gillars, T. Horrell, S. Sahetya, J. Colyer, and L. A. Gray. Expanded pediatric cardiovascular simulator for research and training. *ASAIO Journal*, 56(1):67–72, 2010.

[89] Y. Liu, P. J. Allaire, H. Wood, and D. Olsen. Design and initial testing of a mock human circulatory loop for left ventricular assist device performance testing. *Artificial Organs*, 29(4):341–345, 2005.

[90] Daniel L. Timms, Shaun D. Gregory, Nicholas A. Greatrex, Mark J. Pearcy, John F. Fraser, and Ulrich Steinseifer. A compact mock circulation loop for the in vitro testing of cardiovascular devices. *Artificial Organs*, 35:384–391, 2011.

[91] D. Robinson. Quantitative analysis of cardiac loop for the evaluation of left, right, and biventricular assist devices. *ASAIO Journal*, 29:207–221, 1965.

[92] J. E. W. Beneken. *A mathematical approach to cardiovascular function, the uncontrolled human system.* PhD thesis, University of Utrecht, The Netherlands, 1965.

[93] H. Suga, K. Sagawa, and A. A. Shoukas. Load independence of the instantaneous pressure-volume ratio of the canine left ventricle and effects of epinephrine and heart rate on the ratio. *Circulation Research*, 32:314–322, 1973.

[94] H. Suga and K. Sagawa. Instantaneous pressure-volume relationships and their ratio in the excised supported canine left ventricle. *Circulation Research*, 35:117–126, 1974.

[95] F. Piedimonte, F. M. Colacino, F. Moscato, M. Arabia, G. A. Danieli, and S. Nicosia. A new elastance-based artificial ventricle for mock circulatory systems: Analysis of interaction with a closed-loop hydraulic circulation. *International Journal of Artificial Organs*, 29(5):505–505, 2006.

[96] M. Kozarskia, G. Ferrari, K. Zielinski, K.and Gorczynska, K. J. Palko, A. Tokarz, and M. Darowski. A new hybrid electro-numerical model of the left ventricle. *Computers in Biology and Medicine*, 38(9):979–989, 2008.

[97] J. Fonseca, A. Andrade, D. E. C. Nicolosi, J. F. Biscegli, J. Leme, D. Legendre, E. Bock, and J. C. Lucchi. Cardiovascular simulator improvement: Pressure versus volume loop assessment. *Artificial Organs*, 35(5):454–458, 2011.

[98] T. Korakianitis and Y. Shi. A concentrated parameter model for the human cardiovascular system including heart valve dynamics and atrioventricular interaction. *Medical Engineering & Physics*, 28(7):613–628, Jul. 2006.

[99] T. Korakianitis and Y. Shi. Effects of atrial contraction, atrioventricular interaction, and heart valve dynamics on human cardiovascular system response. *Medical Engineering & Physics*, 28(8):762–779, Aug. 2006.

[100] T. Korakianitis and Y. Shi. Numerical simulation of cardiovascular dynamics with healthy and diseased heart valves. *Journal of Biomechanics*, 39(11):1964–1982, Aug. 2006.

[101] Y. Shi and T. Korakianitis. Numerical simulation of cardiovascular dynamics with left heart failure and in-series pulsatile ventricular assist device. *Artificial Organs*, 30(12):929–948, Dec. 2006.

[102] T. Korakianitis and Y. Shi. Numerical comparison of hemodynamics with atrium to aorta and ventricular apex to aorta vad support. *ASAIO Journal*, 53(5):537–548, Sep.-Oct. 2007.

[103] Y. Shi, T. Korakianitis, and C. Bowles. Numerical simulation of cardiovascular dynamics with different types of VAD assistance. *Journal of Biomechanics*, 40(13):2919–2933, Oct. 2007.

[104] H. Mohammadi and K. Mequanintb. Prosthetic aortic heart valves: Modeling and design. *Medical Engineering & Physics*, 33:131147, 2011.

[105] J. W. Lankhaar, F. A. Rvekamp, P. Steendijk, B. E. Westerhof, T. Kind, A. Vonk-Noordegraaf, and N. Westerhof. Modeling the instantaneous pressurevolume relation of the left ventricle: A comparison of six models. *Annals of Biomedical Engineering*, 37:1710–1726, 2009.

[106] M. Behbahani, M. Behr, M. Hormes, U. Steinseifer, D. Arora, O. Coronado, and M. Pasquali. A review of computational fluid dynamics analysis of blood pumps. *EUROPEAN JOURNAL OF APPLIED MATHEMATICS*, 20(4):363–397, AUG 2009.

[107] O. Reitan, H. Ohlin, B. Peterzen, H. Granfeldt, S. Steen, and H. Emanuelsson. Initial tests with a new cardiac assist device. *ASAIO Journal*, 45:317–321, 1999.

[108] S P Sutera and M H Mehrjardi. Deformation and fragmentation of human red blood cells in turbulent shear flow. *Biophysical journal*, 15(1):1–10, January 1975.

[109] Tao Zhang, M Ertan Taskin, Hong-bin Fang, Adam Pampori, and Robert Jarvik. Study of flow-induced hemolysis using novel couette-type blood-shearing devices. 35(12):1180–1186, 2011.

[110] LJ WURZINGER, R OPITZ, M WOLF, and H SCHMIDSCHONBEIN. Shear induced platelet activation - a critical reappraisal. *BIORHEOLOGY*, 22(5):399–413, 1985.

[111] Katharine H Fraser, M Ertan Taskin, Bartley P Griffith, and Zhongjun J Wu. The use of computational fluid dynamics in the development of ventricular assist devices. *Medical engineering & physics*, 33(3):263–80, April 2011.

[112] Juntao Zhang, Barry Gellman, Andrew Koert, Kurt a Dasse, Richard J Gilbert, Bartley P Griffith, and Zhongjun J Wu. Computational and ex-

perimental evaluation of the fluid dynamics and hemocompatibility of the centrimag blood pump. *Artificial organs*, 30(3):168–77, March 2006.

[113] D. Carswell, D. McBride, T.N. Croft, a.K. Slone, M. Cross, and G. Foster. A cfd model for the prediction of haemolysis in micro axial left ventricular assist devices. *Applied Mathematical Modelling*, 37(6):4199–4207, March 2013.

[114] G HEUSER and R OPITZ. A couette viscometer for short-time shearing of blood. *BIORHEOLOGY*, 17(1-2):17–24, 1980.

[115] M GIERSIEPEN, LJ WURZINGER, R OPITZ, and H REUL. Estimation of shear stress-related blood damage in heart-valve prostheses - invitro comparison of 25 aortic valves. *INTERNATIONAL JOURNAL OF ARTIFICIAL ORGANS*, 13(5):300–306, MAY 1990.

[116] M Ertan Taskin, Katharine H Fraser, Tao Zhang, Changfu Wu, Bartley P Griffith, and Zhongjun J Wu. Evaluation of eulerian and lagrangian models for hemolysis estimation. *ASAIO journal (American Society for Artificial Internal Organs : 1992)*, 58(4):363–72, 2012.

[117] Xinwei Song, Houston G. Wood, and Don Olsen. Computational fluid dynamics (cfd) study of the 4th generation prototype of a continuous flow ventricular assist device (vad). *Journal of Biomechanical Engineering*, 126(2):180, 2004.

[118] Jingchun Wu, James F Antaki, Trevor a Snyder, William R Wagner, Harvey S Borovetz, and Bradley E Paden. Design optimization of blood shearing instrument by computational fluid dynamics. *Artificial organs*, 29(6):482–9, June 2005.

[119] Ryo Kosaka, Osamu Maruyama, Masahiro Nishida, Toru Yada, Sakae Saito, Shusaku Hirai, and Takashi Yamane. Improvement of hemocompatibility in centrifugal blood pump with hydrodynamic bearings and semi-open impeller: in vitro evaluation. *Artificial organs*, 33(10):798–804, October 2009.

[120] S C Yu, B T Ng, W K Chan, and L P Chua. The flow patterns within the impeller passages of a centrifugal blood pump model. *Medical engineering & physics*, 22(6):381–93, July 2000.

[121] W K Chan, Y W Wong, Y Ding, L P Chua, and S C M Yu. Numerical investigation of the effect of blade geometry on blood trauma in a centrifugal blood pump. 26(9):785–793, 2002.

[122] Leok Poh Chua, Guoliang Song, Simon Ching, Man Yu, and Tau Meng Lim. Computational fluid dynamics of gap flow in a biocentrifugal blood pump. 29(8):620–628, 2005.

[123] M Ertan Taskin, Katharine H Fraser, Tao Zhang, Barry Gellman, Andi Fleischli, Kurt a Dasse, Bartley P Griffith, and Zhongjun J Wu. Computational characterization of flow and hemolytic performance of the ultramag blood pump for circulatory support. *Artificial organs*, 34(12):1099–113, December 2010.

[124] Ji-Bin Teo, Weng-Kong Chan, and Yew-Wah Wong. Prediction of leakage flow in a shrouded centrifugal blood pump. *Artificial organs*, 34(9):788–91, September 2010.

[125] h. Hoshi, T. Shinshi, and S. Takatani. Third-generation blood pumps with mechanical noncontact magnetic bearings. *Artificial Organs*, 30(5):324–338, 2006.

[126] Peter A Watterson, John C Woodard, Victor S Ramsden, and John A Reizes. Ventrassist hydrodynamically suspended, open, centrifugal blood pump. 24(6):475–477, 2000.

[127] Tomohiro Nishinaka, Heinrich Schima, Wilfried Roethy, Angela Rajek, Chisato Nojiri, Ernest Wolner, and Georg M Wieselthaler. The duraheart vad, a magnetically levitated centrifugal pump. 70(November):1421–1425, 2006.

[128] Fiete Boehning, Daniel L Timms, Felipe Amaral, Leonardo Oliveira, Roland Graefe, Po-Lin Hsu, Thomas Schmitz-Rode, and Ulrich Steinseifer.

Evaluation of hydraulic radial forces on the impeller by the volute in a centrifugal rotary blood pump. *Artificial organs*, 35(8):818–25, August 2011.

[129] R. Mukkamala and D. Xu. Continuous and less invasive central hemodynamic monitoring by blood pressure waveform analysis. *American Journal of Physiology-Heart and Circulatory Physiology*, 299(3):H584–H599, 2010.

[130] A. V. Chobanian, G. L. Bakris, H. R. Black, W. C. Cushman, L. A. Green, J. L. Izzo Jr., D. W. Jones, B. J. Materson, S. Oparil, J. T. Wright Jr, and E. J. Roccella. The seventh report of the joint national committee on prevention, detection, evaluation, and treatment of high blood pressure: The JNC 7 report. *Journal of the American Medical Association*, 289(219):2560 – 2571, 2003.

[131] G. Schillaci, L. Pasqualini, P. Verdecchia, G. Vaudo, S. Marchesi, C. Porcellati, G. de Simone, and E. Mannarino. Prognostic significance of left ventricular diastolic dysfunction in essential hypertension. *Journal of the American College of Cardiology*, 39(12):2005 – 2011, 2002.

[132] K. Wachtell, V. Palmieri, E. Gerdts, J. N. Bella, G. P. Aurigemma, V. Papademetriou, B. Dahlof, T. Aalto, H. Ibsen, J. E. Rokkedal, and R. B. Devereux. Prognostic significance of left ventricular diastolic dysfunction in patients with left ventricular hypertrophy and systemic hypertension (the life study). *The American Journal of Cardiology*, 106(7):999 – 1005, 2010.

[133] M. T. Lonnebakken, E. Gerdts, K. Boman, K. Wachtell, B. Dahlof, and R. B. Devereux. In-treatment stroke volume predicts cardiovascular risk in hypertension. *Journal of Hypertension*, 29(8):1508–1514, 2011.

[134] R. H. Zhou, A. E. Vendrov, I. Tchivilev, X. L. Niu, K. C. Molnar, M. Rojas, J. D. Carter, H. Tong, G. A. Stouffer, N. R. Madamanchi, and M. S. Runge. Mitochondrial oxidative stress in aortic stiffening with age the role of smooth muscle cell function. *Arteriosclerosis Thrombosis and Vascular Biology*, 32(3):745–U491, 2012.

[135] Merryn Gott, Sarah Barnes, Chris Parker, Sheila Payne, David Seamark, Salah Gariballa, and Neil Small. Dying trajectories in heart failure. *Palliative Medicine*, 21(2):95–99, 2007.

[136] E. Lim, A. H. Alomari, A. V. Savkin, S. Dokos, J. F. Fraser, D. L. Timms, D.G. Mason, and N. H. Lovell. A method for control of an implantable rotary blood pump for heart failure patients using noninvasive measurements. *Artificial Organs*, 35(8), 2011.

[137] E. Lim, S. Dokos, R. F. Salamonsen, F. L. Rosenfeldt, P. J. Ayre, and N. H. Lovell. Numerical optimization studies of cardiovascular-rotary blood pump interaction. *Artificial Organs*, 36(5):E110–E124, May 2012.

[138] Y. Shi, P. V. Lawford, and D. R. Hose. Numerical modeling of hemodynamics with pulsatile impeller pump support. *Annals of Biomedical Engineering*, 38(8):2621–2634, Aug. 2010.

[139] JH Zhou, GP Armstrong, AL Medvedev, WA Smith, LAR Golding, and JD Thomas. Numeric modeling of the cardiovascular system with a left ventricular assist device. *ASAIO Journal*, 45(1):83–89, Jan-Feb 1999.

[140] P. Ruiz, M. A. Rezaienia, A. Rahideh, T. R. Keeble, M. T. Rothman, and T. Korakianitis. In vitro cardiovascular system emulator (bioreactor) for the simulation of normal and diseased conditions with and without mechanical circulatory support. *Artificial Organs*, will be published in 2014.

[141] K. Hirata, T. Yaginuma, M. F. O'Rourke, and M. Kawakami. Age-related changes in carotid artery flow and pressure pulses - possible implications for cerebral microvascular disease. *Stroke*, 37(10):2552–2556, Oct. 2006.

[142] I. Granet. *Fluid Mechanics*. Prentice Hall, 1996.

[143] Stephanie L. Curtis, Andrew Zambanini, Jamil Mayet, Simon A. McG Thom, Rodney Foale, Kim H. Parker, and Alun D. Hughes. Reduced systolic wave generation and increased peripheral wave reflection in chronic heart failure. *American Journal of Physiology-Heart and Circulatory Physiology*, 293(1):557–562, Jul 2007.

[144] O. H. Frazier, C. R. Benedict, B. Radovancevic, R. J. Bick, P. Capek, W. E. Springer, M. P. Macris, R. Delgado, and L. M. Buja. Improved left ventricular function after chronic left ventricular unloading. *Annals of Thoracic Surgery*, 62(3):675–681, Sep. 1996.

[145] G. Zanardo, P. Michielon, A. paccagnella, P. Rosi, M. Calo, V. Salandin, A. Daros, F. Michieletto, and G. Simini. Acute-renal-failure in the patient undergoing cardiac operation-prevalence, mortality-rate, and main risk-factors. *Journal of Thoracic and Cardiovascular Surgery*, 107(6):1489–1495, Jun. 1994.

[146] MG Shlipak, GL Smith, SS Rathore, BM Massie, and HM Krumholz. Renal function, digoxin therapy, and heart failure outcomes: Evidence from the digoxin intervention group trial. *Journal of the American Society of Nephrology*, 15(8):2195–2203, Aug 2004.

[147] Bee Ting Chan, Einly Lim, Kok Han Chee, and Noor Azuan Abu Osman. Review on cfd simulation in heart with dilated cardiomyopathy and myocardial infarction. *Computer in Biology and Medicine*, 43(4):377–385, May 1 2013.

[148] Vanessa Diaz-Zuccarini and Jacques LeFevre. An energetically coherent lumped parameter model of the left ventricle specially developed for educational purposes. *Computational in Biology and Medicine*, 37(6):774–784, Jun 2007.

[149] K . Sagawa, RK . Lie, and J. Schaefer. Translation of frank, otto paper the basic shape of the arterial pulse - 1st treatise - mathematical-analysis - translators introduction. *Journal of molecular and cellular cardiology*, 22:253–254, 1990.

[150] E. Lim, S. Dokos, S. L. Cloherty, R. F. Salamonsen, D. G. Mason, J. A. Reizes, and N. H. Lovell. Parameter-optimized model of cardiovascular-rotary blood pump interactions. *IEEE Transactions on Biomedical Engineering*, 57(2):254–266, 2010.